APPENDIX 3.9.1
DSC SHELL STRUCTURAL ANALYSIS

Table of Contents

List of Tables

List of Figures

3.9.1 DSC SHELL STRUCTURAL ANALYSIS

The purpose of this appendix is to present the structural evaluation of the shell assembly of the EOS-37PTH dry shielded canister (DSC) and the EOS-89BTH DSC under all applicable normal, off-normal and accident loading conditions during storage in the EOS horizontal storage module (HSM) and during transfer in the EOS transfer cask (TC). The EOS system consists of the EOS-HSM, the EOS-TC, the dual-purpose (transportable/storage) EOS-37PTH and EOS-89BTH DSC, and associated ancillary equipment.

The design of the DSC includes five design options: EOS-37PTH (short, medium and long) and EOS-89BTH (short and medium). The longest and heaviest EOS-37PTH DSC, which uses TC135 for transfer operations, is analyzed to bound all DSC design options in the NUHOMS® EOS System.

3.9.1.1 General Description

The DSC consists of a fuel basket and a shell assembly. The DSC pressure boundary consists of DSC shell with two cover plates at each end. Non-pressure boundary shield plugs are included at each end of the assembly. The inner bottom shield (IBS) is confined between the inner bottom cover plate (IBCP) and outer bottom cover plate (OBCP). The top shield plug (TSP) is confined by the inner top cover plate (ITCP) and four lifting lugs, which are welded to the inside of the DSC shell. The grapple ring support is welded to the OBCP using full penetration weld. The ITCP is welded along the top perimeter with partial penetration weld. The IBCP is welded using a full penetration weld. Grapple ring assembly connections are all made using full penetration welds.

The DSC shell thickness is 0.50 inch, and the top and bottom closure assemblies are 10.0 inches and 8.0 inches, respectively. The DSC shell is constructed entirely from stainless steel or duplex steel. There are no penetrations through the pressure boundary. The draining and venting systems are covered by the port plugs. The outer top cover plate (OTCP) and the ITCP are welded to the cylindrical shell with multilayer welds. The DSC cavity is pressurized above atmospheric pressure with helium. The DSC shell assembly geometry and the materials used for its analysis and fabrication are shown on drawings EOS01-1000-SAR, EOS01-1001-SAR, EOS01-1005-SAR and EOS01-1006-SAR included in Chapter 1.

3.9.1.2 DSC Shell Assembly Stress Analysis

An enveloping technique of combining various individual loads in a single analysis is used in this evaluation for several load combinations. This approach reduces the number of computer runs, while remaining conservative. For some load combinations, stress intensities under individual loads are added to obtain resultant stress intensities for the specified combined loads. This addition at the

stress intensity level for the combined loads, instead of at component stress level, is also a conservative method for reducing the number of analysis runs.

The stresses of all components are assessed by means of elastic analysis methodology for all load combinations, except for accident loading conditions. Elastic-plastic analysis methodology is used to assess the stresses for Service Level D load combinations.

A detailed description of each load combination is provided in Section 3.9.1.2.8.

3.9.1.2.1 Material Properties

For elastic analysis, temperature dependent material properties used for each component of DSC shell assembly are obtained from the American Society of Mechanical Engineers (ASME) code [3.9.1-2], and are summarized in Chapter 8. Material properties used for stress evaluations are conservatively taken at 500 °F. For the partial penetration welds and grapple assembly, 350 °F allowable stresses are used for comparison to load induced stresses as these components remain below this lower temperature.

For plastic analysis, a bilinear stress-strain curve with a 5% tangent modulus is used for steel components. The non-linear material properties at 500 °F for side drop analysis are shown in Table 3.9.1-3. Steel material (except shield plugs) is modeled by bilinear kinematic hardening method (TB, BKIN – [3.9.1-9]).

3.9.1.2.2 DSC Shell Stress Criteria

The calculated stresses in the DSC shell assembly structural components are compared with the allowable stresses set forth by ASME Boiler and Pressure Vessel (B&PV) Code, Section III, Subsection NB [3.9.1-3] under normal (Level A), and off-normal (Level B) loading conditions. Appendix F of the ASME B&PV Code is used to evaluate the calculated stresses in the DSC shell assembly under accident (Level D) loading conditions. Allowable stress limits for Levels A, B and D service loading conditions, as appropriate, are summarized in Table 3-1, and the corresponding allowable stress values at different temperatures are summarized in Table 3.9.1-5.

The OTCP-to-DSC shell weld and the ITCP-to-DSC shell weld, which are both partial penetration welds, are to be evaluated using a joint efficiency factor of 0.8. Per NUREG-1536 [3.9.1-7], the minimum inspection requirement for end closure welds is multi-pass dye penetrant testing (PT) using a stress (allowable) reduction factor of 0.8. The allowable weld stresses are summarized in Table 3.9.1-4.

3.9.1.2.3 Finite Element Model Description

The EOS DSC shell assembly is analyzed for the postulated load conditions using a three-dimensional (3D) 180° half- symmetric finite element model (FEM). The FEM is developed using the nominal dimensions of the long cavity DSC.

Each of the DSC shell assembly components is modeled using (ANSYS SOLID185) 3D solid elements. The elements have translational degrees of freedom (DOF) at each of the eight nodes (no rotational DOF). The top end of the DSC is assembled such that no axial gaps initially exist between the OTCP, ITCP, and TSP. Similarly, the bottom end of the DSC is assembled so that no axial gaps initially exist between the OBCP, IBS, and IBCP. The interfaces between the mating surfaces are modeled using (ANSYS CONTA178) 3D node-to-node contact elements that allow the transfer of compressive (bearing) loads.

Contact is not modeled between the cover plates and the shell. This modeling approach is conservative as it forces all loads to be transferred through the welds.

Figure 3.9.1-1 through Figure 3.9.1-4 depict the components and meshed model of the DSC. Table 3.9.1-1 lists the major dimensions of the bounding model and Table 3.9.1-2 lists the material designations of each modeled component.

A description of the FEM for the DSC components is shown below.

DSC Shell

The DSC shell is modeled using 3D solid elements (ANSYS element SOLID185) and has five elements through the thickness of the component. The shell is connected to the OTCP, ITCP, and OBCP with partial penetration welds and is connected to the IBCP using a full penetration weld.

Outer Top Cover Plate

The OTCP is modeled using 3D solid elements (ANSYS element SOLID185) and has 15 elements through the thickness of the component. The plate is connected to the DSC shell with partial penetration welds.

Inner Top Cover Plate

The ITCP is modeled using 3D solid elements (ANSYS element SOLID185) and has 15 elements through the thickness of the component. The plate is connected to the DSC shell with partial penetration welds.

Top Shield Plug

The TSP is modeled using 3D solid elements (ANSYS element SOLID185) and has 11 elements through the thickness of the component. The TSP is confined by the ITCP and four lifting lugs, which are welded to the inside of the DSC shell.

Outer Bottom Cover Plate

The OBCP is modeled using 3D solid elements (ANSYS element SOLID185) and has 15 elements through the thickness of the component. The plate is connected to the DSC shell with partial penetration welds and to the grapple ring assembly (grapple ring and grapple ring support) with full penetration welds.

Inner Bottom Shield

The IBS is modeled using 3D solid elements (ANSYS element SOLID185) and has eight elements through the thickness of the component. The IBS is confined between the IBCP and OBCP.

Inner Bottom Cover Plate

The IBCP is modeled using 3D solid elements (ANSYS element SOLID185) and has six elements through the thickness of the component. The plate is connected to the DSC shell with a full penetration weld.

Grapple Ring

The grapple ring is modeled using 3D solid elements (ANSYS element SOLID185) and has four elements through the thickness of the component. The grapple ring is connected to the grapple ring support with full penetration welds.

Grapple Ring Support

The grapple ring support is modeled using 3D solid elements (ANSYS element SOLID185) and has two elements through the thickness of the component. The grapple ring support is connected to the OBCP with full penetration welds.

Weld Components

Partial penetration welds are used between the DSC shell and the OBCP, OTCP and ITCP and are modeled by merging the nodes of the appropriate components. The OBCP-to-DSC shell weld and OTCP-to-DSC shell weld are 0.5 inch with five elements through the thickness of the weld. The ITCP-to-DSC shell weld is 3/16 inch with five elements through the thickness of the weld.

Full penetration welds are used between the DSC shell and the IBCP; therefore, all nodes through the thickness of the plate along the perimeter are merged with the DSC shell nodes.

Full penetration welds are also used between the grapple ring support and the OBCP. The grapple ring and grapple support plate welds are also full penetration welds. Therefore, for these components, nodes at the interfaces are merged.

3.9.1.2.4 Mesh Sensitivity

Mesh sensitivity studies are a validation that a model produces accurate results by refining a mesh and studying the change in results. A model is shown to be valid when the solution from increasingly refined meshes under a particular set of loadings and boundary conditions results in only negligible differences in relevant output. As one study cannot encompass all general load paths and configurations, multiple studies must be performed with each modeling a particular "archetype" of the overall simulation in order to keep the influence of unintended variables as small as possible. Aspects of the mesh relevant for each archetype are then combined to constitute the base model for the analysis. Figure 3.9.1-21 through Figure 3.9.1-23a show that the chosen model (using the relevant aspects of model 4 in both cases) produces an accurate solution for the foreseeable loads.

Three sensitivity studies were performed. The first studied the impact of mathematical versus geometric/visual gap modeling to represent the interface between the top cover plates and the DSC shell under a side drop loading. The second studied the effect of mesh density in the radial and axial dimensions near the welds between the top cover plates and the DSC shell in an axisymmetric internal pressure loading. The third studied the effect of mesh density (principally) in the circumferential direction under a side drop loading.

Effect of Gap Modeling Methodology upon Results (Study No. 1)

Two models were compared, where all details were identical except for the radial locations of the outer-most five layers of nodes in the top cover plates. These models, shown in Figure 3.9.1-21, used the side drop load case as the basis for comparison.

In the first model, these outer-most nodes were coincident with the adjacent inner-surface nodes of the DSC shell, with the nominal radial gap incorporated as a parameter in the contact elements between the bodies that allows for a specific amount of penetration before contact effects were introduced. In the second model, the above-referenced outer-most nodes of the cover plates were moved inward by the magnitude of the nominal gap.

The modeling methodology of visual versus strictly mathematical representation of the nominal radial gaps has no effect on the results, as shown in Figure 3.9.1-21.

Effect on Results of Mesh Refinement in Axisymmetric Loading (Study No. 2)

Six models were compared, where all details were identical except for the radial lengths of the outer-most elements in the top cover plates, as well as the elements throughout the thickness of the DSC shell. In models four, five, and six, the circumferential length of the elements is halved in order to keep elemental aspect ratios within reasonable limits, although this circumferential sensitivity is explored in Study No. 3. Model five is identical to model four, except that solid185 elements have been replaced with solid186 elements with midside nodes. These models, shown in Figure 3.9.1-22, used the normal internal pressure load case as the basis for comparison.

The model's accuracy is sensitive to radial element length, but only at the largest value tested – 0.69 inches. A radial length of 0.17 inch for the weld between the OTCP and the DSC shell, and a radial length of 0.125 inch for the weld between the ITCP and the DSC shell, produces accurate results as shown in Figure 3.9.1-22. The more refined model (model 6) shows a slight increase in the membrane plus bending stresses, as well a decrease in the membrane stress. The membrane stresses are more critical for this evaluation; therefore, it is concluded that model 4 has adequate mesh characteristics for this study.

Effect of Higher Order Elements with Midside Nodes

The internal pressure load case is evaluated with higher order elements with midside nodes. The results with low order nodes show conservative results as shown in Figure 3.9.1-22.

Effect on Results of Mesh Refinement in Side Drop Loading (Study No. 3)

Five models were compared, where all facets were identical except for the circumferential lengths of the outer-most elements in the top cover plates, as well as the elements throughout the thickness of the DSC shell. These models, shown in Figure 3.9.1-23, used the side drop load case as the basis for comparison.

The model is more sensitive to radial element lengths than circumferential lengths in low gradient areas away from the areas impacted by the presence of boundary conditions, where the 1.4-inch elements from model 2 produce results that are not appreciably different from the highly refined model. In high gradient areas near boundary conditions, a smaller element length of 0.36 inch produces accurate results as shown in Figure 3.9.1-23a.

3.9.1.2.5 Post-Processing

The DSC component stress results were post-processed using the ANSYS LPATH and PRSECT commands, which linearize the stress distribution through the requested section. Stress linearization for the DSC components are performed on all possible paths, both radially and circumferentially, through the thickness of a component or weld as appropriate, using the ANSYS post-processing macro. Stress linearization for weld stresses are performed on stress paths at the throat location of the weld, including the elements adjacent to the weld. Figure 3.9.1-19 shows examples of the stress linearization paths for the components and welds. The methodology employed is location agnostic - reported peak membrane stresses are combined with reported peak membrane + bending stresses even if they occur in disparate locations of a particular component. However, locations are tracked on the basis of proximity to the confinement boundary welds and gross structural discontinuities, or proximity to boundary conditions.

Stress Linearization Method

Stress evaluation on predefined paths and the stress linearization procedure are based on the method employed in the ANSYS code. Stress results are mapped onto a path by first interpolating stress components (σ_x, σ_y, σ_z, σ_{xy}, σ_{yz}, σ_{zx}) at the path location. Then, stress averaging and linearization on the path are done independently for all six stress components.

Principal membrane stresses and membrane stress intensity are then derived from membrane parts of the individual stress components. Similarly, linearized principal stresses and linearized stress intensity at the path section surface are derived from linearized individual stress components of that surface.

The stress path evaluation in ANSYS brings the information about membrane stress intensity across the path, as well as maximum linearized stress membrane plus bending at classification path surface.

ASME NB-3213.2 defines a gross structural discontinuity as a geometric or material discontinuity, which affects the stress or strain distribution through the entire wall thickness of the pressure-retaining member. Examples of gross structural discontinuities are head-to-shell junctions, flange-to-shell junctions, and nozzles. ASME Table NB-3217-1 concludes that at the junction of shell and head, the membrane stresses are P_L and bending stresses are Q, provided that the edge restraint is not required to maintain the bending stress in the middle to acceptable limits. Section NB-3224.4 states that the requirement of primary plus secondary stress intensity does not need to be satisfied for Level C service limits. Appendix F, Section F-1332.3 states that bearing stress does not need to be evaluated for Level D service limits.

Membrane stresses distant from gross structural discontinuities are compared against primary membrane (P_m) allowable stresses. Analogous membrane + bending stresses are compared against primary membrane + bending ($P_m + P_b$) allowable stresses.

Membrane stresses proximate to gross structural discontinuities are compared against primary local membrane (P_L) allowable stresses. Membrane + bending stresses proximate to gross structural discontinuities are compared against secondary allowable stresses.

3.9.1.2.6 Stress Categorization Sensitivity Studies

Limit Load Analysis

Limit load analysis sensitivity studies are performed on the internal pressure and side drop load combination to supplement the stress categorization. The analysis directly relates the gross plastic deformation of primary stresses to failure and removes the stress categorization uncertainties. Limit load analysis is performed per Paragraph NB-3228.1, where the acceptance criterion is that the specified loading does not exceed two-thirds of the lower bound collapse load. The lower bound collapse load is determined using an ideally plastic (non-strain hardening) material model, with a yield stress of $1.5S_m$. This criterion is used for Service Level A and B load cases. For Service Level D load cases, the rules of ASME Section III Appendix F Paragraph F-1341.3 [3.9.1-3] are used, which states that the loads "shall not exceed 90% of the limit analysis collapse load using a yield stress which is the lesser of $2.3S_m$ and $0.7S_u$."

For both the internal pressure and side drop load cases, all materials are modeled as elastic-perfectly plastic with a yield stress based on $1.5S_m$. Elastic-perfectly plastic is described as an idealized material that behaves in a linear-elastic manner up to its yield point, and thereafter is perfectly plastic (i.e., non-strain hardening). Also note that, even though the side drop is a Level D event, the $1.5S_m$ value is conservatively used, which inherently adds an approximate safety factor equal to:

$$\frac{\frac{0.7 \cdot S_U}{1.1}}{\frac{1.5 \cdot S_m}{1.5}} \geq 2$$

Both analyses use small deflection theory (NLGEOM, OFF). This is necessary since deflections are unrealistically high in limit load analysis due to the lower-bound, non-strain-hardening material properties. If large deflections are used, the beneficial effects of membrane action would result in a higher collapse load.

The FEM described in Section 3.9.1.2.3 is used for the internal pressure load case, except that the material properties are changed to an elastic-perfectly plastic model. A reduction factor of 0.8 is used for elements in the partial penetration ITCP to DSC shell and OTCP to DSC shell welds such that the yield stress is equal to:

$$\sigma_{yield} = 0.8 \cdot 1.5 \cdot S_m$$

The internal pressure is linearly increased until the solution fails to converge.

The FEM described in Section 3.9.1.2.3 is used for the internal pressure plus side drop load case, except that the material properties are changed to an elastic-perfectly plastic model. A reduction factor of 0.8 is used as above for elements in the partial penetration ITCP to DSC shell and OTCP to DSC shell welds. Furthermore, contact between the DSC shell and the inner surface of the cask is neglected. The loads (20 psig internal pressure and 1g acceleration) are applied at a time value of 1. The loads are then increased with the time step until the solution fails to converge. *Figure 3.9.1-24 and Figure 3.9.1-25 show the maximum displacement history and indicate the expected plastic instability that occurs as the limit load is approached. The last converged solution was at a pressure of 270 psig for internal pressure load and a deceleration of 217 g for the side drop load case.*

Strain Criteria Analysis

Similar to the limit load analysis sensitivity studies, a strain criteria sensitivity study is performed on the side drop load combination to supplement the stress categorization. The strain criterion directly relates equivalent plastic strain to failure and removes the stress categorization uncertainties. Strain criteria analyses are performed per non-mandatory Appendix FF of the ASME Code [3.9.1-10].

Since the critical areas for the DSC Shell are the partial penetration welds between ITCP and DSC Shell and OTCP and DSC Shell, the average and the maximum equivalent plastic strain, ε_{eq}^{p}, multiplied by the triaxiality factor (TF) at 75g are compared against following criteria:

$$\left[TF \cdot \left(\varepsilon_{eq}^{p}\right)\right]_{avg} \leq \left(0.85 \cdot \varepsilon_{uniform}\right)$$
$$\left[TF \cdot \left(\varepsilon_{eq}^{p}\right)\right]_{max} \leq \left[\varepsilon_{uniform} + 0.25 \cdot \left(\varepsilon_{fracture} - \varepsilon_{uniform}\right)\right]$$

Where:

$$TF = \frac{(\sigma_1 + \sigma_2 + \sigma_3)}{\sqrt{\frac{1}{2} \cdot [(\sigma_1 - \sigma_2)^2 + (\sigma_2 - \sigma_3)^2 + (\sigma_3 - \sigma_1)^2]}}$$

Where σ_1, σ_2, and σ_3 are the principal stresses at the location, and:

ε_{eq}^{p} is equal to the equivalent plastic strain.

$\varepsilon_{uniform}$ is equal to the true strain just prior to the onset of necking in a uniaxial tensile test.

$\varepsilon_{fracture}$ is equal to the true strain at fracture in a uniaxial tensile test.

At this time, ASME standard true stress-strain curves, true uniform strain, and true fracture strain are under development. Therefore, the following assumptions are made for the material properties, which may not be sufficient for a full qualification using strain criteria, but are determined to be sufficient for this sensitivity study:

A bilinear curve is used for the analysis where the material behaves in a linear-elastic manner up to its ASME specified yield point and, thereafter, a slope of 2.59 x 10^4 psi is used (i.e., the tangent modulus after yield strength is 1% of the Young's modulus). This tangent modulus, along with the ASME specified yield strength, is conservatively low, especially considering the low level of strains resulting from the analysis.

ASME Section II, Part C specifies a 30% elongation limit for the E316-XX electrode. This electrode is chosen as a conservative representative design, as the elongation limit is lower than that of a 304 SS matching electrode. Furthermore, Figure EE-1230-1 in Appendix EE [3.9.1-10] shows that the engineering uniform strain is approximately 75% of the elongation limit. Therefore, the value used for the uniform strain is equal to:

$$\epsilon_{uniform} = \ln(1 + 0.75 \cdot 0.3) = 0.2 \cdot \frac{in}{in}$$

The bounding 75g side drop load case on rails with 20 psig internal pressure is evaluated using the above material properties. Furthermore, per Section FF-1145, strain rate effects are considered with two additional analyses; the yield strength value was increased by 20%, successively, while the slope was unchanged.

To decrease the resources required in post processing, the maximum equivalent plastic strain (including consideration of the triaxiality factor) was conservatively compared against the uniform strain limit, ϵ_{limit}, equal to:

$$\epsilon_{limit} = 0.85 \cdot \epsilon_{uniform} = 0.17 \frac{in}{in}$$

The results are shown in Table 3.9.1-15. Figure 3.9.1-27 shows the confinement weld strain distribution along the entire circumference of the DSC.

3.9.1.2.7 Load Cases for DSC Shell Stress Analysis

This section discusses the different load cases considered to evaluate the stresses generated in the EOS-37PTH DSC and EOS-89BTH DSC shell assembly during transfer operations and in storage conditions under normal, off-normal and accident loading. During fuel transfer, the DSC is oriented horizontally inside the EOS-TC, which is mounted to the transfer skid and transferred from the reactor or fuel building to the independent spent fuel storage installation (ISFSI). During storage, the DSC is in the horizontal position within EOS-HSM.

Each load case analysis utilizes the FEM that is described in Section 3.9.1.2.3, along with pertinent loads and boundary conditions. Bounding storage load cases, transfer load cases and load combinations used to evaluate the DSC shell assembly are tabulated in Table 2-5. In general, major loads (ram push/pull loading with internal/external pressure) are combined within the ANSYS analyses, while stress intensities from minor loads (i.e. dead weight and pressure) are added algebraically.

3.9.1.2.7.1 Dead Weight

The dead weight is analyzed for the following three basic configurations:

- When the DSC is vertical in the EOS-TC135,
- When the DSC is horizontal in the EOS-TC135,
- When the DSC is horizontal in the EOS-HSM.

The model for the EOS-TC135 and EOS-HSM differ in boundary conditions representing support rails.

Vertical in EOS-TC

The DSC shell supports the entire weight of the top end components in addition to its self-weight. The weight of the fuel is assumed to be uniformly distributed over the area of the IBCP. The fuel load and the weight of the bottom end components are transferred directly to the ground through bearing between the IBCP, IBS, and OBCP.

The bottom end surface of the EOS-TC135 is constrained in the vertical direction. The contact elements are generated between DSC shell and OBCP outermost nodes (excluding the surface of OBCP, which is bounded by the grapple ring support) and the EOS-TC135 surface. The payload of 105 kips is applied as uniform pressure acting on the IBCP.

Horizontal in EOS-TC

When the DSC is in a horizontal position, the end components and basket assembly bear against the DSC shell.

The inertial loads for DSC internals are accounted for by applying an equivalent pressure on the inside surface of the DSC represented by the projection of first 6.5° support rail only. This pressure is determined based on the payload of 105 kips and the projected area of the DSC shell that is in interface with the EOS-TC135 support rail. Figure 3.9.1-7 and Figure 3.9.1-7a show the pressure load and boundary conditions applied to the FEM.

The interface between the DSC and the EOS-TC135 support rails is modeled through node-to-node contact elements (CONTA178). Nodes that interface with the rails are selected and copied, creating new nodes that are restrained in all DOF and connected to the original nodes belonging to the DSC shell through the CONTA178 contact elements.

Three sets of rails, at 6.5°,17.5° and 25.5°, are modeled in the FEM. The 6.5° rail is modeled as contacts with closed gaps between the DSC shell and the EOS-TC135 rail. For the second and third rail, at 17.5° and 25.5°, respectively, from the plane of symmetry, contact elements between the rail nodes and the DSC shell nodes are created through the same type of contact element, but the real constant of these elements is modified to the true geometric gap value between the DSC shell and the EOS-TC135 rail.

Horizontal Position in EOS-HSM

When stored in the EOS-HSM, the DSC shell is supported by two, 3-inch wide EOS-HSM slide rails at ±30° from the bottom centerline. The inertial loads for DSC internals are accounted for by applying equivalent pressure onto the inner surface of DSC shell representing the EOS-HSM support rail only. The magnitude of the pressure is determined based on the payload of 105 kips and projected area that are in interface with the EOS-HSM support rail.

The interface between the DSC and the EOS-HSM support rail is modeled through node-to-node contact elements (CONTA178). Nodes that interface with the EOS-HSM support rail are selected and copied, creating new nodes. Each row of nodes represents the width of the EOS-HSM support rail (there are three nodes across the width of the rail). Each node of the row is coupled with its neighboring node in all DOF using CERIG command, creating a rigid platform. Figure 3.9.1-7 and Figure 3.9.1-7a show the pressure load and boundary conditions applied to the FEM.

Each middle node of this platform is connected in the axial direction of the DSC through BEAM188 element. Finally, these new nodes representing the EOS-HSM are connected to the original nodes belonging to the DSC shell through the CONTA178 contact elements. Gaps are set to zero, placing the DSC shell and the EOS-HSM support rail in initial contact. Nodes representing the EOS-HSM support rail are constrained in all DOF along a length of 16.5 inches from bottom end and 20.5 inches from the top end. The BEAM188 elements have the properties of the wide-flange steel beam that supports the DSC when inside the EOS-HSM. Therefore, the flexibility of the support beam is considered in the analysis.

3.9.1.2.7.2 Fabrication Pressure and Leak Testing

Pressurization and leak testing is performed on the DSC shell and IBCP during fabrication. No other DSC components are in place during this test. A seal plate is placed on the open top of the DSC shell and preloaded through the application of torque on eight bolts that are connected with a flange at the bottom of the DSC shell. The resulting preload to be considered in the evaluation is 155 kips. The DSC is then evacuated to a partial vacuum (simplified to full vacuum) and then re-pressurized with helium. Therefore, two load conditions are evaluated for the DSC shell and IBCP:

1. Leak Test: 155 kip axial compression + 14.7 psi external pressure (full vacuum) on the DSC shell between the top edge and the IBCP + 14.7 psi external pressure on the IBCP. Note that the vacuum will add axial load to the 155 kips preload.

2. Pressure Test: 155 kip axial compression + 23.0 psig internal pressure on the DSC shell between the top edge and the IBCP + 23.0 psig internal pressure on the IBCP. Note that the internal pressure will not affect the reaction on the DSC shell due to the preload.

In order to simulate the leak testing conditions, the OTCP, ITCP and OBCP, TSP and IBS, grapple ring and its support are removed from the FEM, including all contact pair elements.

The bottom surface of the DSC shell surface is constrained in the vertical direction. The 155 kips load is represented by equivalent pressure that is applied at the top surface of the DSC shell.

External pressure is applied at all external nodes of the DSC shell-IBCP assembly with the exception of the top surface of the DSC shell that is loaded with the 155 kips preload. Internal pressure is applied at all nodes on the inside surface of the DSC shell-IBCP assembly. Two load steps are performed, one for the internal pressure and the second one for the external pressure as stated above.

3.9.1.2.7.3 Internal and External Pressure

The DSC pressure boundary is defined by the DSC shell, the IBCP, the ITCP and the associated welds. Since there are no gaps between the top end plate components, the ITCP bears against the OTCP. Since the ITCP meets the leaktight requirements of ANSI N14.5, no leakage is feasible and, therefore, the pressure load is shared by the two plates according to their relative stiffness. Similarly, the absence of gaps between the bottom end components allows the IBCP to bear against the IBS, which, in turn, bears against the OBCP.

Normal (Level A)	15 psig (Elastic)
Off-Normal (Level B)	20 psig (Elastic)
Accident (Level D)	130 psig (Elastic-plastic)

The design pressure of the DSC is 15 psig. A bounding pressure of 20 psig was used in structural evaluations for normal and off-normal conditions. Two load cases were analyzed: one with an internal pressure of 20 psig and the second with an internal pressure of 130 psig.

All of the nodes of the inner surface of DSC shell confined by ITCP and IBCP are selected for application of internal pressure. A node of the grapple is constrained in axial (z-direction) and vertical (x-direction) directions and a node of the OTCP is also constrained in the vertical direction to prevent rigid body motion. Figure 3.9.1-6 shows the internal pressure applied onto the inside of the DSC cavity.

In addition to the internal pressure loads listed above, the DSC will be subjected to hydrostatic, blowdown, vacuum, and test pressures during the fuel loading and draining/drying processes. Prior to loading fuel and without the top end components in place, the TC/DSC annulus is filled with water resulting in a hydrostatic external load on the DSC shell. The hydrostatic load is then balanced by filling the DSC with water.

After the fuel is loaded, the TSP and ITCP are installed and an internal blowdown pressure of 15 psig is applied to evacuate the DSC of water. The DSC internals are then dried under vacuum conditions. The DSC is backfilled with helium at 20 psig. The pressure is then reduced to 3.5 psig and the OTCP is welded in place.

External pressure is applied at all external nodes of the DSC at a level below 12 inches from the top of the DSC. Internal pressure is applied at all surface nodes inside the DSC from the inside of the IBCP up to the ITCP-DSC shell weld. Nodes in contact between the lifting lugs and the DSC shell are not subject to pressure load. Contact elements are modeled on the lateral surface of the shell and the bottom of the OBCP.

Two load steps are performed for the blowdown/pressure test and the vacuum drying with combinations of internal and external pressures without the OTCP installed. Figure 3.9.1-14 and Figure 3.9.1-15 show the stress results for normal and accident internal pressure load cases.

3.9.1.2.7.4 EOS-HSM Loading/Unloading

To load the DSC into the EOS-HSM, the DSC is pushed out of the EOS-TC using a hydraulic ram. The load is applied at the center of the OBCP within the diameter of the grapple ring support. Based on the relative stiffnesses of the cover plates and the IBS, a portion of the insertion load will be transferred through the IBS to the IBCP and associated welds.

Loading is defined as:

Level A/B/C/D: 135 kips (Ram Push)

Unloading (grapple) loads are defined as:

Level A/B: 80 kips (Grapple Pull)

Level C/D: 135 kips (Grapple Pull)

To unload the EOS-HSM, the DSC is pulled using grapple hooks, which engage the grapple ring. The loads applied by the hydraulic ram are balanced by friction between the DSC shell and the EOS-TC135 and/or EOS-HSM rails.

For the grapple push simulation, the cask is modeled by copying the outer surface nodes of the DSC, creating a new pattern of nodes representing the cask inner surface. These new nodes are restrained in all DOF and connected to the original nodes belonging to the DSC shell through the CONTA178 contact elements. Furthermore, gaps are set to zero at the first rail placing the DSC and the first rail in initial contact. Real constants of contact elements at the second and third rail are set to the gap calculated based on the nodal coordinates of the contact element nodes on both the DSC side and the rail side.

The outer top nodes of the DSC shell are constrained in the axial direction and a node of the ITCP is constrained in the vertical direction to aid in convergence. The insertion force is modeled through a uniform pressure applied within the inner diameter of the grapple support. Two load cases were analyzed: one with a push load of 135 kips, and the second with an internal pressure of 20 psig and a push load of 135 kips. Table 3.9.1-12 lists the load conditions. Figure 3.9.1-10 and Figure 3.9.1-10a show the load and boundary conditions applied to the FEM.

For the grapple pull simulation, the outer top nodes of the DSC shell are constrained in the axial direction and a node of ITCP is constrained in the vertical direction to aid in convergence. The extraction force is modeled through nodal forces applied on selected nodes within the footprint of the grapple hook. Five load cases were analyzed combining pressure loads and are described in the table below. Refer to Table 3.9.1-12 for load combinations. Figure 3.9.1-9 and Figure 3.9.1-9a show the load and boundary conditions applied to the FEM.

Internal Pressure	Pull Force (kips)	Analysis Type
0	80	Elastic
20	80	Elastic
0	135	Elastic-plastic
20	135	Elastic-plastic
20	80	Limit Load Elastic-perfectly plastic

For the normal condition pull load cases, a limit load analysis is performed to show that the stresses at the junction between the grapple ring support and the outer bottom cover plate are secondary stresses. The limit load analysis is described in NB-3228.1 [3.9.1-2]. The grapple ring assembly is acceptable for the normal pull load if the lower bound limit load (LL) is equal to or greater than 1.5 times the normal pull load (2/3 * LL) without any excessive deformation and plastic strain. The lower bound limit load is determined using elastic-perfect plastic material properties with a yield strength defined as $1.5S_m$. The last converged load step for the limit load analysis corresponds to a 200 kip axial pull load, which is greater than 1.5*80 kip = 120 kip.

3.9.1.2.7.5 Transfer/Handling Load

The same model described above for HSM loading and unloading is used and updated to reflect the effect of the vertical 1g load, transverse 1g load, axial 1g load and internal pressure of 20 psig.

Two runs were performed for this load:

1. Deadweight +1g vertical + 1g transverse + 1g axial with the weight of DSC internals modeled by equivalent pressure application on TSP with addition of internal pressure of 20 psig.

2. Deadweight +1g vertical + 1g transverse + 1g axial with the weight of DSC internals modeled by equivalent pressure application on IBCP with addition of internal pressure of 20 psig.

3.9.1.2.7.6 Seismic Load during Storage

The same model described in Section 3.9.1.2.7.1 for dead weight in EOS-HSM is used and updated to reflect the effect of the vertical 1g load, transverse 2g load, axial (longitudinal) 1.25g load, and the internal pressure load of 20 psig.

Two elastic-plastic runs are performed for this load:

1. 1g vertical + 2g transverse + 1.25g axial with the weight of DSC internals modeled by equivalent pressure application on TSP with addition of internal pressure of 20 psig.

2. 1g vertical + 2g transverse + 1.25g axial with the weight of DSC internals modeled by equivalent pressure application on IBS with addition of internal pressure of 20 psig.

The dead weight and 1g vertical and 2g transverse effect is modeled by multiplying the pressure projected at the EOS-HSM support rail through the DSC shell by a conservative factor of 5.

DSC support within an EOS-HSM is provided by two, 3.00-inch wide rails at ± 30° from the bottom centerline. Seismic axial forces toward the EOS-HSM door are resisted by the axial retainer. The retainer is a 4-inch x 2-inch steel bar located on the vertical centerline, at the edge of the DSC shell below the center of the DSC. The retainer bears against the edge of the DSC shell and OBCP. The nodes of DSC shell and OBCP, which bears against the area of the retainer bar, are restrained in the axial direction. Figure 3.9.1-13 shows the pressure load and boundary conditions applied to the FEM.

The DSC shell and the OBCP experience compressive bearing stress in the vicinity of the axial retainer. The bearing stresses experienced by the DSC shell and OBCP need not be evaluated for Service Level D loads.

Seismic axial forces away from the EOS-HSM door are resisted by the canister stop plates located at the ends of the support rails. The stop plates are 11 inches wide. Because the top cover plate is recessed from the edge of the DSC shell, the stop plates bear against the bottom edge of the DSC shell only. The nodes of the top end of DSC shell, which come into contact with the DSC stop plate, are restrained in the axial direction. Figure 3.9.1-18 shows the stress results for seismic load acting towards the stop plates of the EOS-HSM support rails.

3.9.1.2.7.7 Cask Drop

Side and end drop accelerations of 75g are applied. Drops are only postulated for the DSC when positioned inside of the EOS-TC135. The following accident drops are analyzed:

- 65-inch side drop of the TC onto a concrete pad above a generic soil profile.
- A corner drop from a height of 65 inches at an angle of 30° to the horizontal, onto the top or bottom corner of the TC (two cases) using the bounding deceleration based on a 65-inch drop.

The top end drop and bottom end drop are not credible events under 10 CFR Part 72; therefore, these drop analyses are not required. However, consideration of end drops (for 10 CFR Part 71 conditions) and the 65-inch side drop is performed to conservatively envelope the effects of a corner drop.

In summary, three drop conditions are considered in the analyses:

- 75g bottom end drop
- 75g top end drop
- 75g side drop

End Drop

For the bottom end drop, the interface between the bottom surface of DSC shell and OBCP (excluding the OBCP surface, which falls inside the grapple ring support) with the EOS-TC135 is modeled through CONTA178 node-to-node contact elements. The nodes of the EOS-TC135 are constrained in the vertical direction representing TC as a rigid surface. The payload is applied as a load of 105 kips multiplied by 75. The inertial load of the basket assembly and fuel is applied as uniform pressure acting on the IBCP. An elastic-plastic material model is used in the analysis. In addition to pressure representing the payload inertia load, conservative internal pressure of 20 psig is added.

For the bottom end drop, the couplings (CP) representing the welds between the lug plate and the DSC shell are deleted from the model and these welds are modeled by spring elements (COMBIN14). Figure 3.9.1-12 and Figure 3.9.1-12a show the pressure load and boundary conditions applied to the FEM.

Two load cases are performed for bottom end drop:

- Bottom end drop without internal pressure
- Bottom end drop with internal pressure

For the top end drop, the interface between the top surface of the DSC and the EOS-TC135 is modeled through CONTA178 node-to-node contact elements. The nodes of the EOS-TC135 (node position 2 of CONTA178 elements) are constrained in all directions representing TC as a rigid surface. The payload is applied as a total load of 105 kips multiplied by 75g. The inertial load of the basket assembly and fuel is applied as uniform pressure acting on the bottom side of the TSP. An elastic-plastic material model is used in the analysis. In addition to pressure representing the payload inertial load, this load case includes a 20 psig internal pressure in the model, as opposed to adding the internal pressure load case later.

Two load cases are performed for top end drop:

- Top end drop without internal pressure
- Top end drop with internal pressure

Side Drop

The side drop analysis of the DSC shell assembly is simplified by considering the distribution of the basket load to the DSC as uniform. The basket is flexible enough to deform under the action of 75g deceleration of its contents and, therefore, during an accident side drop, the basket will tend to bend under the action of the higher g-loads on its contents. This results in a uniform radial pressure load applied to the inner surface of the DSC to represent the basket load.

An elastic-plastic analysis was performed for side drop analysis. For elastic-plastic analyses, the steel components (except shield plugs) are modeled by a bilinear kinematic hardening method. At the specified yield stress, the curve continues along the second slope defined by the plastic modulus. It is assumed that the plastic modulus is 5% of the elastic modulus, except for shield plugs, which are modeled with elastic material properties.

Side Drop on Cask Rails

A uniform pressure load is applied to the DSC inner surface. The inner nodes of the DSC are selected from 0° to 45° and a uniform pressure is applied. The interface between the DSC and the EOS-TC135 is modeled through node-to-node contact elements CONTA178. Nodes that interface with the DSC are selected and copied, creating new pattern of nodes. These new nodes are restrained in all DOF and connected to the original nodes belonging to the DSC shell through the CONTA178 contact elements. Gaps are set to zero at the 6.5° and 17.5° rail, placing the DSC and the 6.5° and 17.5° rail in initial contact. Real constants of contact elements at the 25.5° rail are set to a gap calculated based on the nodal coordinates of the contact element node at the DSC side and the rail side. The small radial gaps between the shield plugs and the DSC shell are set to zero, since during a side drop event these gaps will close.

In addition to pressure representing the payload inertial load, this load case includes a 20 psig internal pressure in the model, as opposed to adding the internal pressure load case later.

Two load cases are analyzed for the side drop onto the cask rail:

- Side drop onto the cask rail without internal pressure
- Side drop onto the cask rail with internal pressure

Side Drop Away From Cask Rails

The interface between the DSC and the EOS-TC135 is modeled through node-to-node contact elements CONTA178. Nodes that interface with the DSC are selected and copied, creating new pattern of nodes. These new nodes are restrained in all DOF and connected to the original nodes belonging to the DSC shell through the CONTA178 contact elements. Gaps between the DSC shell and the cask inner surface are set to the gap calculated based on nodal coordinates of the contact element node at the DSC side and the cask side. At the point where the DSC contacts the rigid cask, the initial contact gap is zero. Circumferentially away from this initial contact point, the initial contact gap increases. The small radial gap between the shield plugs and the DSC shell is set to zero since during a side drop event, this gap will close.

In addition to pressure representing the payload inertial load, this load case includes a 20 psig internal pressure in the model, as opposed to adding the internal pressure load case later. Figure 3.9.1-11 and Figure 3.9.1-11a show the load and boundary conditions applied to the FEM.

Two load cases are analyzed for side drop away from the cask rail:

- Side drop away from the cask rail without internal pressure
- Side drop away from the cask rail with internal pressure

Figure 3.9.1-16 shows the stress results for side drop away from cask rails without internal pressure.

3.9.1.2.7.8 Thermal Loads

Per Chapter 4, the thermal storage load cases have lower temperature gradients in the DSC shell compared to thermal transfer load cases. Therefore, only bounding off-normal thermal transfer load cases have been selected for thermal stress analysis of the EOS-37PTH DSC.

For thermal stress analysis, temperature profiles and maximum component temperatures are based on the thermal analyses of the EOS-37PTH DSC in TC125 for transfer conditions, which is discussed in Chapter 4. Only the off-normal load cases with higher temperature gradients in the DSC shell are taken for thermal stress analysis.

Since the TC125 is shorter than TC135, there is a higher temperature distribution in TC125. Therefore, the thermal analysis of the EOS-37PTH in TC125 bounds the thermal analysis of EOS-37PTH in TC135. The thermal conditions have been evaluated separately to minimize the number of analyses to be performed. For all DSC components, the thermal stresses have been combined by adding the maximum stress intensities of components from thermal load runs to the primary membrane plus bending stresses of components from mechanical load runs.

Thermal stresses are classified as secondary stresses per the ASME Code, [3.9.1-3]. These secondary stresses are a result of dissimilar material properties, primarily differential thermal growth of a structure due to material thermal expansion coefficient differences between different materials used for construction of the structure, or differential temperature distribution throughout the structure, or a combination of both.

Nodal temperature from thermal analyses is transferred to the structural model described in Section 3.9.1.2.3. The structural model is solved and stresses of thermal load of each load step are post-processed and the largest stresses for all the transfer cases are selected. Only the largest selected stresses are used for further stress evaluation and stress combination.

3.9.1.2.8 Load Combinations

The bounding load combinations, along with the applicable ASME service level, are listed in Chapter 2, Table 2-5 for the shell assembly. Stresses generated by applied loads described in Section 3.9.1.2.7.1 are combined in a manner that bounds all load conditions under consideration. The methodologies for combining the load cases into their corresponding load combinations are described in the following sections.

Load Combination 1

Load Combination 1 (LC1) addresses the DSC when it is in a vertical position. LC1 is developed by adding the linearized stress intensities of a vertical dead weight load case, an internal pressure of 20 psig within the DSC and the maximum stress intensities due to thermal loading.

Load Combinations 2 and 3

Load Combinations 2 and 3 (LC23) addresses the DSC when it is in a horizontal position. LC23 is developed by adding linearized stress intensities from a model comprised of the dead weight, an internal pressure of 20 psig within the DSC and handling loads with thermal loads.

Load Combination 4

Load Combination 4 (LC4) addresses the DSC when it is in a horizontal position. LC4 describes a hydraulic ram push case. The stress intensities from the dead weight load case, the 135-kip insertion load cases and thermal load cases are determined independently and subsequently added together to develop the maximum stress intensity on the DSC components and welds. The 135-kip insertion model evaluates the system with and without a 20-psig internal pressure load.

Load Combination 5

Load Combination 5 (LC5) addresses the DSC when it is in a horizontal position. LC5 describes a hydraulic ram pull case. The stress intensities from the dead weight load case, the 80-kip retrieval load cases and thermal load cases are determined independently and subsequently added to develop the maximum stress intensity on the DSC component and weld. The 80-kip retrieval model evaluates the system with and without a 20-psig internal pressure load.

Load Combination 6

Load Combination 6 (LC6) addresses the DSC when it is in a horizontal position. LC6 describes a hydraulic ram pull case. The stress intensities from the dead weight load case and the 135-kip retrieval load cases are determined independently and subsequently added to develop the maximum stress intensity on the DSC component and weld. The 135-kip retrieval model evaluates the system with and without a 20-psig internal pressure load.

Load Combination 7A

Load Combination 7A (LC7A) addresses the DSC when it is in a horizontal position. LC7A describes the 65-inch accident drop condition. LC7A is developed by post-processing the stresses from a FEM that includes the 20-psig off-normal internal pressure load and the 75g side drop load.

Load Combination 7B

Load Combination 7B (LC7B) addresses the DSC when it is in a vertical position. LC7B describes the 65-inch accident drop condition. LC7B is developed by post-processing the stresses from a FEM that includes the 20-psig off-normal internal pressure load and the 75g end drop load.

Load Combination 8

Load Combination 8 (LC8) addresses the DSC when it is in the horizontal position. LC8 describes the accident internal pressure load case. The stress intensities from the dead weight load case and the 130-psig internal pressure load case are determined independently and subsequently added to develop the maximum stress intensity on the DSC component and weld.

Load Combination 9

Load Combination 9 (LC9) addresses the DSC when it is in the horizontal position. LC9 describes the off-normal internal pressure load case. The stress intensities from the dead weight load case, 20-psig internal pressure load case and thermal load cases are determined independently and subsequently added to develop the maximum stress intensity on the DSC component and weld.

Load Combination 10

Load Combination 10 (LC10) addresses the DSC when it is in the horizontal position. LC10 describes the seismic load case. LC10 is developed by post-processing the stresses from an FEM that includes the internal off-normal pressure loads and the seismic loads.

Load Combination 11

Load Combination 11 (LC11) addresses the DSC when it is in the vertical position. LC11 describes the fabrication pressure and leak testing loads. LC11 is developed by post-processing the stresses from stresses from the fabrication pressure/leak test load case.

3.9.1.3 DSC Shell Buckling Evaluation

An FE plastic analysis with large displacement option is performed to monitor occurrence of canister shell buckling under the specified loads.

The bottom end drop envelopes the top end drop because the top end structure is heavier than the bottom end structure, which will impose a larger load on the DSC shell. A drop on the bottom end is therefore chosen for buckling analysis.

The buckling analysis uses the same model as the end drop simulation.

The inertia load of the basket assembly and fuel is applied as uniform pressure acting on the IBCP. Elastic-plastic bilinear kinematic hardening material model is used at a uniform temperature of 500 °F with a plastic tangent modulus conservatively taken at 1% of the elastic modulus for buckling. Conservatively, no internal pressure that could have a stabilizing effect is applied. Large deformation effect NLGEOM is enabled in the ANSYS model.

The uniform pressure at the IBCP that represents the payload is multiplied by acceleration as a g-factor that is computed at two values, 75g and 130g. The 130g simulation represents the stability load qualification.

The 130g load is conservatively used as the buckling load. Two thirds of the maximum compressive load of 130g is equal to the 87g limit load per F-1331.5 of Appendix F, [3.9.1-3], which is higher than required load of 75g. It is, therefore, concluded that buckling of the DSC will not occur during a hypothetical accident end drop.

3.9.1.4 DSC Fatigue Analysis

Fatigue effects on the EOS-37PTH DSC is addressed using NB-3222.4 criteria of [3.9.1-3]. Fatigue effects need not be specifically evaluated, provided the criteria contained in NB-3222.4(d) are met. A summary of the six criteria and their application to the DSC is presented below:

A. The first criterion states that the DSC is adequate for fatigue effects, provided that the total number of atmospheric-to-operating pressure cycles during normal operation (including startup and shutdown) does not exceed the number of cycles on the applicable fatigue curve corresponding to a S_a value of three times the S_m value of the material at operating temperatures. This condition is satisfied for the DSC since the pressure is not cycled during its design life. The pressure established at the time that the DSC is sealed following fuel loading and DSC closure operations is maintained during normal storage in the EOS-HSM.

B. The second criterion states that DSC is adequate for fatigue effects, provided that the specified full range of pressure fluctuations during normal operation does not exceed the quantity (1/3) x design pressure x (S_a/S_m), where S_a is the value obtained from the applicable fatigue curve for the total specified number of significant pressure fluctuations, and S_m is the allowable stress intensity for the material at operating temperatures.

   Significant pressure fluctuations are those for which the total excursion exceeds (1/3) x design pressure x (S/S_m), where S equals the value of S_a for 10^6 cycles. Using a design pressure of 20.0 psig, an S_m value of 17,500 psi, and an S value of 28,200 psi, the total range for a significant pressure fluctuation is 10.7 psig. This pressure fluctuation is not expected to occur during normal storage as a result of seasonal ambient temperature changes.

Ambient temperature cycles significant enough to cause a measurable pressure fluctuation are assumed to occur five times per year for 80 years. The number of fluctuations with this pressure range is expected to be 400 for the DSC. The value of S_a associated with this number of cycles is 170 ksi. Therefore, the value of (1/3) x design pressure x (S_a/S_m) is equal to 64.76 psig. Clearly, this value will not be exceeded during the normal condition lifetime of the DSC. Therefore, the second criterion is satisfied for the DSC.

C. The third criterion states that the DSC is adequate for fatigue effects, provided that the temperature differences between any two adjacent points on the DSC during normal operation do not exceed $S_a/2E\alpha$, where S_a is the value obtained from the applicable fatigue curve for the specified number of startup-shutdown cycles, α is the instantaneous coefficient of thermal expansion at the mean value of the temperatures at the two points, and E is the modulus of elasticity at the mean value of the temperatures at the two points.

   For an operational cycle of the DSC, thermal gradients occur during fuel loading, DSC closure, transport to the EOS-HSM, and transfer of the DSC to the EOS-HSM. This half-cycle is approximately reversed for DSC unloading operations. However, this normal operational cycle occurs only once in the design service life of a DSC. Since there is only one startup-shutdown cycle associated with the DSC, the value of S_a is very large (>800 ksi). Therefore, the value of $S_m/2E\alpha$ is very large (>1500°F). This is far greater than the temperature difference between any two adjacent points on the dry shielded canister. Therefore, the third criterion is satisfied for the DSC.

D. The fourth criterion states that the DSC is adequate for fatigue effects, provided that the temperature difference between any two adjacent points on the DSC does not change during normal operation by more than the quantity $S_a/2E\alpha$, where S_a is the value obtained from the applicable fatigue curve for the total specified number of significant temperature difference fluctuations.

   A temperature difference fluctuation is considered to be significant if its total algebraic range exceeds the quantity $S/2E\alpha$ where S is value of S_a (28,200 psi) obtained from the applicable fatigue curve for 10^6 cycles if the number of cycles is 10^6 or less.

   Small fluctuations in the DSC thermal gradients during normal storage in the EOS-HSM occur as a result of seasonal ambient temperature changes. Ambient temperature cycles significant enough to cause a measurable thermal gradient fluctuation are assumed to occur five times per year for 80 years. The temperature gradient fluctuation is 250 cycles. Since this is less than 10^6 cycles, the value of $S/2E\alpha$ at 10^6 cycles is 112.7 °F.

The most significant fluctuation in normal operating temperature occurs during a change in ambient temperature from -20° F to 100 °F. A review of thermal evaluation of EOS-HSM loaded with EOS-37PTH DSC storage load cases in Chapter 4 concluded that the temperature difference between adjacent points in the DSC does not exceed the quantity 112.7 °F, therefore the fourth condition is satisfied for the DSC.

E. The fifth criterion states that for components fabricated from materials of differing moduli of elasticity or coefficients of thermal expansion, the total algebraic range of temperature fluctuation experienced by the component during normal operation must not exceed the magnitude $S_a/2(E_1\alpha_1 - E_2\alpha_2)$, where S_a is the value obtained from the applicable fatigue curve for the total specified number of significant temperature fluctuations, E_1 and E_2 are the moduli of elasticity, and α_1 and α_2 are the values of the instantaneous coefficients of thermal expansion at the mean temperature value involved for the two materials of construction.

A temperature fluctuation is considered to be significant if its total excursion exceeds the quantity $S/2(E_1\alpha_1 - E_2\alpha_2)$, where S is the value of S_a obtained from the applicable fatigue curve for 10^6 cycles. If the two materials have different applicable design fatigue curves, the lower value of S_a has to be used. Since the structural material used to construct the DSC shell is 240 Type 304 and shield plug is A-36, therefore taking the values of $E_1 = 25.9 \times 10^6$ psi, $E_2 = 27.3 \times 10^6$, $\alpha_1 = 10.5 \times 10^{-6}$ and $\alpha_2 = 8.0 \times 10^{-6}$ (Section II, Part D, [3.9.1-2]), the quantity $S/2(E_1\alpha_1 - E_2\alpha_2) = 268.6°F$.

Since the DSC experiences temperature fluctuation from -20 °F to 100 °F, the range of temperature fluctuation is 120°F which is less than 268.6 °F. Therefore, the fifth criterion is satisfied for the DSC.

F. The sixth criterion states that the DSC is adequate for fatigue effects, provided that the specified full range of mechanical loads does not result in a stress range that exceeds the S_a value obtained from the applicable fatigue curve for the total specified number of significant load fluctuations. If the total specified number of significant load fluctuations exceeds 10^6, the S_a value at $N = 10^6$ can be used.

A load fluctuation is considered to be significant if the total excursion of stresses exceed the value of S_a obtained from the applicable fatigue curve for 10^6 cycles. The only mechanical loads that affect the DSC are those associated with handling loads and a seismic event. One handling load cycle and a major seismic event are postulated during the design life of the DSC. The DSC stresses resulting from these mechanical load fluctuations are small since the structural capacity of the DSC is designed for extreme accident loads such as a postulated cask drop.

The number of significant cycles associated with mechanical load fluctuations is conservatively assumed to be 1,000. The value of S_a associated with this number of cycles is 120 ksi. Since the maximum stress range intensity permitted by the code is 3.0 S_m, or 52.5 ksi for SA-240, Type 304 stainless steel at 500 °F, this sixth condition is satisfied for the DSC.

The evaluation presented in the preceding paragraphs demonstrates that the six criteria contained in NB-3222.4(d) are satisfied for all components of the EOS-37PTH DSC.

3.9.1.5 DSC Weld Flaw Size Evaluation

EOS-37PTH DSC is considered as the bounding DSC for weld flaw evaluation because the weight of EOS-37PTH DSC (long) is greater than the weight of EOS-89BTH DSC.

3.9.1.5.1 Methodology

It is stipulated that the critical flaw configuration is a circumferential weld flaw exposed to the tensile component radial stress. The determination of the allowable surface and sub-surface flaw depth is accomplished by means of the methodology outlined below.

- Determine the tensile radial membrane stresses in the weld. Evaluate membrane radial stresses occurring at the weld between the OTCP and the DSC shell for all individual loads.
- Determine limiting membrane radial stresses in the OTCP weld for all load combinations, for Service levels A, B, C, and D.
- Limiting stresses are multiplied by safety factors SF_m for the corresponding service levels.
- Since OTCP weld is gas tungsten arc welding (GTAW) (non-flux weld), according to ASME Code Sec XI, Division 1, Figure C-4210-1 [3.9.1-4], maximum allowable flaw depth is estimated using limit load criteria.

The allowable membrane stress, S_t, in the flawed section for each service level is determined from Article C-5322, Appendix C [3.9.1-4] where the relation between the applied membrane stress and flaw depth at incipient stress is given.

3.9.1.5.2 Flaw Size Calculation

For 3D, half-symmetric model, as described in Section 3.9.1.2.3, the tensile radial membrane stresses in the weld are evaluated by the stress linearization method explained in Section 3.9.1.2.5.

Radial stresses for controlling load combination are calculated by adding individual load cases. Bounding radial tensile stresses in OTCP weld for all load combinations for Service Level A, B, and D are assessed. The allowable flaw depths, calculated by means of the methodology described in previous Section and are shown in Table 3.9.1-13.

Based on the evaluation, requirements for welding and weld inspections should be based on limiting the weld critical depth for surface and subsurface flaws to the following values:

- Surface Crack: 0.38 inch.
- Subsurface Crack: 0.38 inch.

3.9.1.6 Conclusions

The EOS DSC shell assembly has been analyzed for normal, off-normal, and accident load conditions using three dimensional finite element analyses. The load combinations provided in Section 3.9.1.2.8 are used in the analysis of the EOS DSC. Table 3.9.1-7 through Table 3.9.1-12 summarize the stress intensities in different components of DSC shell assembly, compared with ASME code stress intensity allowables *and the resulting stress ratios. The stress ratio is calculated by dividing the maximum stress intensity by the stress intensity allowable value, with the stress ratio required to be less than 1.* Figure 3.9.1-20 shows the linearized component stresses for the DSC shell for the internal pressure (normal) load case. *Figure 3.9.1-27* shows the strain criteria state of the DSC.

The maximum ratio of induced load to allowable load for a confinement boundary area is 0.76, in the weld between the ITCP and the DSC shell during a side drop event. The maximum overall ratio of 0.92 occurs in the grapple ring support, seconded by a ratio of 0.85 in the non-confinement area of the DSC shell during a grapple pull/accident scenario.

The above evaluations, specifically the closure welds, are supplemented with additional limit load and strain criteria analyses. These analyses are presented in Section 3.9.1.2.6. The results of the limit load analysis show that there is sufficient margin compared to the design loads. The results of the strain criteria analysis show a maximum equivalent plastic strain of 0.065 in/in during a side drop event, compared to the allowable uniform strain limit of 0.17 in/in, demonstrating a minimum factor of safety of 2.6 in the design. The factor of safety is calculated by dividing the maximum allowable strain by the maximum equivalent plastic strain, and must be greater than 1.

The structural integrity of the DSC shell, including closure welds, is maintained since the maximum stress ratio is less than 1 and the limit load and strain criteria analyses results were lower than their respective limits.

Convergence/Sensitivity Studies

The base model and mesh used to evaluate the EOS DSC is validated by three sensitivity studies focused on gap modeling methodology, radial and longitudinal element size in an axisymmetric internal pressure environment, and circumferential element sizes in a lateral load side drop environment. A model with midside nodes was added to the axisymmetric model and showed lower stresses than the other models, and thus these midside nodes were conservatively excluded from the analytical model. No significant difference in results were observed between the employed model and the refined models, therefore the employed model is producing accurate results.

It is on these bases that the EOS DSC assembly is determined to be, as designed, structurally adequate under all anticipated load conditions for service during storage and transfer.

3.9.1.7 References

3.9.1-1 Title 10, Code of Federal Regulations, Part 72, "Licensing Requirements for the Independent Storage of Spent Nuclear Fuel, High-Level Radioactive Waste, and Reactor-Related Greater than Class C Waste."

3.9.1-2 American Society of Mechanical Engineers, ASME Boiler and Pressure Vessel Code, Section II, Part D, 2010 Edition through 2011 Addenda.

3.9.1-3 American Society of Mechanical Engineers, ASME Boiler and Pressure Vessel Code, Section III, 2010 Edition through 2011 Addenda.

3.9.1-4 American Society of Mechanical Engineers, ASME Boiler and Pressure Vessel Code, Section XI, Division 1, Appendix C, 2010 Edition Addenda through 2011 Addenda.

3.9.1-5 ANSI N14.5, "Leakage Tests on Packages for Shipment of Radioactive Materials," 1997.

3.9.1-6 ANSI N14.6 – 1993, "American National Standard for Radioactive Materials – Special Lifting Devices for Shipping Containers Weighing 10000 pounds (4500 kg) or More," American National Standards Institute, Inc., New York.

3.9.1-7 NUREG-1536, "Standard Review Plan for Spent Fuel Dry Cask Storage Systems at a General License Facility," Revision 1, U.S. Nuclear Regulatory Commission, July 2010.

3.9.1-8 U.S. Nuclear Regulatory Commission, Regulatory Guide 1.60, "Design Response Spectra for Seismic Design of Nuclear Power Plants," Revision 1, 1973.

3.9.1-9 ANSYS Computer Code and User's Manual, Release 14.0.

3.9.1-10 American Society of Mechanical Engineers, ASME Boiler and Pressure Vessel Code, 2013, Section III Appendices.

Table 3.9.1-1
EOS37PTH DSC Major Dimensions

Component	Dimensions
Outer Diameter of DSC Shell	75.50 inches
DSC Shell Thickness	0.5 inch
DSC Length	219 inches(1)
OTCP Thickness	2 inches
ITCP Thickness	2 inches
TSP Thickness	6 inches
OBCP Thickness	2 inches
IBCP Thickness	2 inches
IBS	4 inches

(1) Indicated length is for longest EOS-37PTH DSC

Table 3.9.1-2
Material of EOS DSC Components (Analysis)

DSC Shell	ASME SA-240 Type 304
OTCP	ASME SA-240 Type 304
ITCP	ASME SA-240 Type 304
TSP	ASTM A36
OBCP	ASTM A240 Type 304
IBCP	ASME SA-240 Type 304
IBS	ASTM A36
Grapple Ring Support	ASTM A240 Type 304
Grapple Ring	ASTM A240 Type 304
Lifting Lug Plate	ASTM A240 Type 304
Lifting Lug	ASTM A240 Type 304

Table 3.9.1-3
Elastic-Plastic Material Properties

Material Property	SA-240 Type 304 at 500 °F	SA-36 at 500 °F
Elastic Modulus (psi)	25.9×10^6	27.3×10^6
Yield Strength (psi)	19,400	29,300
Tangent Modulus, E_t (psi)	5% of $E = 1.295 \times 10^6$	5% of $E = 1.365 \times 10^6$

Table 3.9.1-4
Allowable Weld Stresses for Pressure Boundary Partial Penetration Welds, Material Type 304

Service Level	Stress Region / Category	Stress Criteria	Allowable Stress Value at 350 °F [ksi]
Level A / Level B	Primary Local Membrane Stress, P_L	$P_L = 0.8\ [1.5\ S_m]$	23.2
	Primary Local Membrane + Bending Stress, $P_L + P_b$	$P_L + P_b = 0.8\ [1.5\ S_m]$	23.2
	Primary + Secondary Stress, P+Q	$P_L + P_b + Q = 0.8\ [3.0\ S_m]$	46.3
Level D (Elastic)	Primary Local Membrane Stress, P_L	$0.8\ [\text{Min}(3.6\ S_m, S_u)]$	52.08
	Primary Local Membrane + Bending Stress, $P_L + P_b$	$0.8\ [\text{Min}(3.6\ S_m, S_u)]$	52.08
Level D (Elastic Plastic)	Primary Local Membrane Stress, P_L	$0.8\ [0.9\ S_u]$	46.9
	Primary Local Membrane + Bending Stress, $P_L + P_b$	$0.8\ [0.9\ S_u]$	46.9

Table 3.9.1-5
SA-240/SA-479 304 & SA-182 F304 -Stress Allowables

Temp (°F)	S_m (ksi)	S_y (ksi)	S_u (ksi)	Level A/B			Level D (Elastic)		Level D (Plastic)	
				P_m	$P_m + P_b$	$P_m + P_b + Q$	P_m	$P_m + P_b$	P_m	$P_m + P_b$
70	20	30	75	20.0	30.0	60.0	48.0	72.0	52.5	67.5
200	20	25	71	20.0	30.0	60.0	48.0	71.0	49.7	63.9
300	20	22.4	66.2	20.0	30.0	60.0	46.3	66.2	46.3	59.6
400	18.6	20.7	64	18.6	27.9	55.8	44.6	64.0	44.8	57.6
500	17.5	19.4	63.4	17.5	26.3	52.5	42.0	63.0	44.4	57.1
600	16.6	18.4	63.4	16.6	24.9	49.8	39.8	59.8	44.4	57.1
700	15.8	17.6	63.4	15.8	23.7	47.4	37.9	56.9	44.4	57.1

Table 3.9.1-6
Allowable Base Metal Stresses for Non Pressure Boundary Partial Penetration & Fillet Welds Type 304 Base Metal

Temp. (°F)	S_y (ksi)	Level A $F_W = .40S_y$	Level B $F_W = .53S_y$	Level C $F_W = .60S_y$	Level D $F_W = .80S_y$
100	30	12	15.9	18	24
200	25	10	13.3	15	20
300	22.4	8.96	11.9	13.4	17.9
400	20.7	8.28	11	12.4	16.6
500	19.4	7.76	10.3	11.6	15.5
600	18.4	7.36	9.75	11	14.7
650	18	7.2	9.54	10.8	14.4
700	17.6	7.04	9.33	10.6	14.1

Table 3.9.1-7
DSC Shell Stress Results, Confinement Boundary – Load Combinations
3 Pages

Load Comb No.	Service Level	DSC Orientation	Stress Category	Loads	Stress intensity (ksi)	Allowable Stress (ksi)	Stress Ratio
1	A	Vertical(1)	P_m	DWv+ max($PI_{(20)}$,BD,VD)	2.51	17.50	0.14
			P_m+P_b	DWv+ max($PI_{(20)}$,BD,VD)	7.87	26.25	0.30
			P_L	DWv+ max($PI_{(20)}$,BD,VD)	6.80	26.25	0.26
			P_m (or P_L)+P_b+Q	DWv+ max($PI_{(20)}$,BD,VD)	12.28	52.50	0.23
			P_m (or P_L)+P_b+Q+P_e	DWv+ max($PI_{(20)}$,BD,VD)+TH	29.82	52.50	0.57
2/3	A	Horizontal(2)	P_m	DWh+ 1g axial + 1g transverse + 1g Vertical + $PI_{(20)}$	2.49	17.50	0.14
			P_m+P_b	DWh+ 1g axial + 1g transverse + 1g Vertical + $PI_{(20)}$	3.30	26.25	0.13
			P_L	DWh+ 1g axial + 1g transverse + 1g Vertical + $PI_{(20)}$	6.21	26.25	0.24
			P_m (or P_L)+P_b+Q	DWh+ 1g axial + 1g transverse + 1g Vertical + $PI_{(20)}$	10.98	52.50	0.21
			P_m (or P_L)+P_b+Q+P_e	DWh+ 1g axial + 1g transverse + 1g Vertical + $PI_{(20)}$ +TH	28.52	52.50	0.54
4	A/B	Horizontal(2)	P_m	DWh+ 135kips + $PI_{(20)}$	2.89	17.50	0.17
			P_m+P_b	DWh+ 135kips + $PI_{(20)}$	4.19	26.25	0.16
			P_L	DWh+ 135kips + $PI_{(20)}$	7.17	26.25	0.27
			P_m (or P_L)+P_b+Q	DWh+ 135kips + $PI_{(20)}$	16.09	52.50	0.31
			P_m (or P_L)+P_b+Q+P_e	DWh+ 135kips + TH	33.63	52.50	0.64
5	A/B	Horizontal(2)	P_m	DWh+ 80 kips + $PI_{(20)}$	2.20	17.50	0.13
			P_m+P_b	DWh+ 80 kips + $PI_{(20)}$	3.75	26.25	0.14
			P_L	DWh+ 80 kips + $PI_{(20)}$	6.31	26.25	0.24
			P_m (or P_L)+P_b+Q	DWh+ 80 kips + $PI_{(20)}$	13.50	52.50	0.26
			P_m (or P_L)+P_b+Q+P_e	DWh+ 80 kips + TH	31.04	52.50	0.59

Table 3.9.1-7
DSC Shell Stress Results, Confinement Boundary – Load Combinations
3 Pages

Load Comb No.	Service Level	DSC Orientation	Stress Category	Loads	Stress intensity (ksi)	Allowable Stress (ksi)	Stress Ratio
6	D	Horizontal(2)	P_m	DWh+ 135 kips + $PI_{(20)}$	2.81	44.38	0.06
			P_m+P_b	DWh+ 135 kips + $PI_{(20)}$	4.62	57.06	0.08
			P_L	DWh+ 135 kips + $PI_{(20)}$	6.67	57.06	0.12
			P_m (or P_L)+P_b+Q	DWh+ 135 kips + $PI_{(20)}$	NA		
7A	D	Horizontal(2)	P_m	DWh+ max.(SD_AWAY, SD_RAIL_EP,SD_TOP_RAIL_EP)+ $PI_{(20)}$	24.36	44.38	0.55
			P_m+P_b	DWh+ max.(SD_AWAY_EP, SD_RAIL_EP)+ $PI_{(20)}$	41.08	57.06	0.72
			P_L	DWh+ max.(SD_AWAY, SD_RAIL_EP,SD_TOP_RAIL_EP)+ $PI_{(20)}$	34.25	57.06	0.60
			P_m (or P_L)+P_b+Q	DWh+ max.(SD_AWAY_EP, SD_RAIL_EP)+ $PI_{(20)}$	NA		
7B	D	Vertical	P_m	DWv+ max.(ED_TOP, ED_BOT)+ $PI_{(20)}$	21.48	44.38	0.48
			P_m+P_b	DWv+ max.(ED_TOP, ED_BOT)+ $PI_{(20)}$	33.49	57.06	0.59
			P_L	DWv+ max.(ED_TOP, ED_BOT)+ $PI_{(20)}$	15.84	57.06	0.28
			P_m (or P_L)+P_b+Q	DWv+ max.(ED_TOP, ED_BOT)+ $PI_{(20)}$	NA		
8	D	Horizontal(2)	P_m	DWh+ $PI_{(130)}$	12.26	44.38	0.28
			P_m+P_b	DWh+ $PI_{(130)}$	19.19	57.06	0.34
			P_L	DWh+ $PI_{(130)}$	16.91	57.06	0.30
			P_m (or P_L)+P_b+Q	DWh+ $PI_{(130)}$	NA		
9	A	Horizontal(3)	P_m	DWh+ $PI_{(20)}$	3.65	17.50	0.21
			P_m+P_b	DWh+ $PI_{(20)}$	7.78	26.25	0.30
			P_L	DWh+ $PI_{(20)}$	9.23	26.25	0.35
			P_m (or P_L)+P_b+Q	DWh+ $PI_{(20)}$	16.56	52.50	0.32
			P_m (or P_L)+P_b+Q+P_e	DWh+ $PI_{(20)}$ +TH	34.10	52.50	0.65

Table 3.9.1-7
DSC Shell Stress Results, Confinement Boundary – Load Combinations
3 Pages

Load Comb No.	Service Level	DSC Orientation	Stress Category	Loads	Stress intensity (ksi)	Allowable Stress (ksi)	Stress Ratio
10	D	Horizontal(3)	P_m	DWh+ max.(HS_TOP, HS_BOT)+$PI_{(20)}$	9.25	44.38	0.21
			P_m+P_b	DWh+ max.(HS_TOP, HS_BOT)+$PI_{(20)}$	28.98	57.06	0.51
			P_L	DWh+ max.(HS_TOP, HS_BOT)+$PI_{(20)}$	21.50	57.06	0.38
			P_m (or P_L)+P_b+Q	DWh+ max.(HS_TOP, HS_BOT)+$PI_{(20)}$	NA		
11	Test	Vertical	P_m	max. (PI(23)+155 kips ,$PE_{(14.7)}$+155 kips)	3.97	17.50	0.23
			P_m+P_b	max. (PI(23)+155 kips,$PE_{(14.7)}$+155 kips)	9.00	26.25	0.34
			P_L	max. (PI(23)+155 kips ,$PE_{(14.7)}$+155 kips)	3.21	26.25	0.12
			P_m (or P_L)+P_b+Q	max. (PI(23)+155 kips,$PE_{(14.7)}$+155 kips)	NA		
12	D	Horizontal	External Pressure		21.70	45.10	0.48

Notes:

(1) DSC in transfer cask in vertical orientation. Only Inner top cover is installed

(2) DSC in TC with TC in a horizontal orientation.

(3) DSC in EOS-HSM supported on the steel rails

Table 3.9.1-7a
DSC Shell Stress Results, Non-Confinement Boundary – Load Combinations
3 Pages

Load Comb No.	Service Level	DSC Orientation	Stress Category	Loads	Stress intensity (ksi)	Allowable Stress (ksi)	Stress Ratio
1	A	Vertical(1)	P_m	DWv+ max($PI_{(20)}$,BD,VD)	0.82	17.50	0.05
			P_m+P_b	DWv+ max($PI_{(20)}$,BD,VD)	2.25	26.25	0.09
			P_L	DWv+ max($PI_{(20)}$,BD,VD)	1.28	26.25	0.05
			P_m (or P_L)+P_b+Q	DWv+ max($PI_{(20)}$,BD,VD)	3.88	52.50	0.07
			P_m (or P_L)+P_b+Q+P_e	DWv+ max($PI_{(20)}$,BD,VD)+TH	23.27	52.50	0.44
2/3	A	Horizontal(2)	P_m	DWh+ 1g axial + 1g transverse + 1g Vertical + $PI_{(20)}$	3.46	17.50	0.20
			P_m+P_b	DWh+ 1g axial + 1g transverse + 1g Vertical + $PI_{(20)}$	4.49	26.25	0.17
			P_L	DWh+ 1g axial + 1g transverse + 1g Vertical + $PI_{(20)}$	4.80	26.25	0.18
			P_m (or P_L)+P_b+Q	DWh+ 1g axial + 1g transverse + 1g Vertical + $PI_{(20)}$	5.30	52.50	0.10
			P_m (or P_L)+P_b+Q+P_e	DWh+ 1g axial + 1g transverse + 1g Vertical + $PI_{(20)}$ + TH	24.69	52.50	0.47
4	A/B	Horizontal(2)	P_m	DWh+ 135kips + $PI_{(20)}$	1.69	17.50	0.10
			P_m+P_b	DWh+ 135kips + $PI_{(20)}$	5.78	26.25	0.22
			P_L	DWh+ 135kips + $PI_{(20)}$	7.92	26.25	0.30
			P_m (or P_L)+P_b+Q	DWh+ 135kips + $PI_{(20)}$	18.95	52.50	0.36
			P_m (or P_L)+P_b+Q+P_e	DWh+ 135kips + TH	38.34	52.50	0.73
5	A/B	Horizontal(2)	P_m	DWh+ 80 kips + $PI_{(20)}$	2.98	17.50	0.17
			P_m+P_b	DWh+ 80 kips + $PI_{(20)}$	13.40	26.25	0.51
			P_L	DWh+ 80 kips + $PI_{(20)}$	8.36	26.25	0.32
			P_m (or P_L)+P_b+Q	DWh+ 80 kips + $PI_{(20)}$	25.22	52.50	0.48
			P_m (or P_L)+P_b+Q+P_e	DWh+ 80 kips + TH	44.61	52.50	0.85

Table 3.9.1-7a
DSC Shell Stress Results, Non-Confinement Boundary – Load Combinations
3 Pages

Load Comb No.	Service Level	DSC Orientation	Stress Category	Loads	Stress intensity (ksi)	Allowable Stress (ksi)	Stress Ratio
6	D	Horizontal(2)	P_m	DWh+ 135 kips + $PI_{(20)}$	4.47	44.38	0.10
			P_m+P_b	DWh+ 135 kips + $PI_{(20)}$	20.49	57.06	0.36
			P_L	DWh+ 135 kips + $PI_{(20)}$	11.76	57.06	0.21
			P_m (or P_L)+P_b+Q	DWh+ 135 kips + $PI_{(20)}$	NA		
7A	D	Horizontal(2)	P_m	DWh+ max.(SD_AWAY, SD_RAIL_EP,SD_TOP_RAIL_EP)+ $PI_{(20)}$	21.44	44.38	0.48
			P_m+P_b	DWh+ max.(SD_AWAY_EP, SD_RAIL_EP)+ $PI_{(20)}$	24.63	57.06	0.43
			P_L	DWh+ max.(SD_AWAY, SD_RAIL_EP,SD_TOP_RAIL_EP)+ $PI_{(20)}$	29.17	57.06	0.51
			P_m (or P_L)+P_b+Q	DWh+ max.(SD_AWAY_EP, SD_RAIL_EP)+ $PI_{(20)}$	NA		
7B	D	Vertical	P_m	DWv+ max.(ED_TOP, ED_BOT)+ $PI_{(20)}$	15.14	44.38	0.34
			P_m+P_b	DWv+ max.(ED_TOP, ED_BOT)+ $PI_{(20)}$	24.68	57.06	0.43
			P_L	DWv+ max.(ED_TOP, ED_BOT)+ $PI_{(20)}$	16.10	57.06	0.28
			P_m (or P_L)+P_b+Q	DWv+ max.(ED_TOP, ED_BOT)+ $PI_{(20)}$	NA		
8	D	Horizontal(2)	P_m	DWh+ $PI_{(130)}$	3.43	44.38	0.08
			P_m+P_b	DWh+ $PI_{(130)}$	11.77	57.06	0.21
			P_L	DWh+ $PI_{(130)}$	7.95	57.06	0.14
			P_m (or P_L)+P_b+Q	DWh+ $PI_{(130)}$	NA		
9	A	Horizontal(3)	P_m	DWh+ $PI_{(20)}$	2.06	17.50	0.12
			P_m+P_b	DWh+ $PI_{(20)}$	3.78	26.25	0.14
			P_L	DWh+ $PI_{(20)}$	2.97	26.25	0.11
			P_m (or P_L)+P_b+Q	DWh+ $PI_{(20)}$	5.03	52.50	0.10
			P_m (or P_L)+P_b+Q+P_e	DWh+ $PI_{(20)}$ + TH	24.42	52.50	0.47

Table 3.9.1-7a
DSC Shell Stress Results, Non-Confinement Boundary – Load Combinations
3 Pages

Load Comb No.	Service Level	DSC Orientation	Stress Category	Loads	Stress intensity (ksi)	Allowable Stress (ksi)	Stress Ratio
10	D	Horizontal(3)	P_m	DWh+ max.(HS_TOP, HS_BOT)+$PI_{(20)}$	15.53	44.38	0.35
			P_m+P_b	DWh+ max.(HS_TOP, HS_BOT)+$PI_{(20)}$	20.26	57.06	0.36
			P_L	DWh+ max.(HS_TOP, HS_BOT)+$PI_{(20)}$	21.19	57.06	0.37
			P_m (or P_L)+P_b+Q	DWh+ max.(HS_TOP, HS_BOT)+$PI_{(20)}$	NA		
11	Test	Vertical	P_m	max. (PI(23)+155 kips ,$PE_{(14.7)}$+155 kips)	4.98	17.50	0.28
			P_m+P_b	max. (PI(23)+155 kips,$PE_{(14.7)}$+155 kips)	10.70	26.25	0.41
			P_L	max. (PI(23)+155 kips ,$PE_{(14.7)}$+155 kips)	4.72	26.25	0.18
			P_m (or P_L)+P_b+Q	max. (PI(23)+155 kips,$PE_{(14.7)}$+155 kips)	NA		
12	D	Horizontal	External Pressure		21.7	45.1	0.481

Notes:

(1) DSC in transfer cask in vertical orientation. Only Inner top cover is installed

(2) DSC in TC with TC in a horizontal orientation.

(3) DSC in EOS-HSM supported on the steel rails

Table 3.9.1-8
OTCP Stress Results – Load Combinations
3 Pages

Load Comb No.	Service Level	DSC Orientation	Stress Category	Loads	Stress intensity (ksi)	Allowable Stress (ksi)	Stress Ratio
1	A	Vertical(1)	P_m	DWv+ max($PI_{(20)}$,BD,VD)	0.42	17.50	0.02
			P_m+P_b	DWv+ max($PI_{(20)}$,BD,VD)	3.95	26.25	0.15
			P_L	DWv+ max($PI_{(20)}$,BD,VD)	0.50	26.25	0.02
			P_m (or P_L)+P_b+Q	DWv+ max($PI_{(20)}$,BD,VD)	2.47	52.50	0.05
			P_m (or P_L)+P_b+Q+P_e	DWv+ max($PI_{(20)}$,BD,VD)+TH	10.57	52.50	0.20
2/3	A	Horizontal(2)	P_m	DWh+ 1g axial + 1g transverse + 1g Vertical + $PI_{(20)}$	0.49	17.50	0.03
			P_m+P_b	DWh+ 1g axial + 1g transverse + 1g Vertical + $PI_{(20)}$	3.60	26.25	0.14
			P_L	DWh+ 1g axial + 1g transverse + 1g Vertical + $PI_{(20)}$	1.39	26.25	0.05
			P_m (or P_L)+P_b+Q	DWh+ 1g axial + 1g transverse + 1g Vertical + $PI_{(20)}$	4.53	52.50	0.09
			P_m (or P_L)+P_b+Q+P_e	DWh+ 1g axial + 1g transverse + 1g Vertical + $PI_{(20)}$ + TH	11.15	52.50	0.21
4	A/B	Horizontal(2)	P_m	DWh+ 135kips + $PI_{(20)}$	0.58	17.50	0.03
			P_m+P_b	DWh+ 135kips + $PI_{(20)}$	4.30	26.25	0.16
			P_L	DWh+ 135kips + $PI_{(20)}$	0.76	26.25	0.03
			P_m (or P_L)+P_b+Q	DWh+ 135kips + $PI_{(20)}$	3.07	52.50	0.06
			P_m (or P_L)+P_b+Q+P_e	DWh+ 135kips + TH	10.92	52.50	0.21
5	A/B	Horizontal(2)	P_m	DWh+ 80 kips + $PI_{(20)}$	0.56	17.50	0.03
			P_m+P_b	DWh+ 80 kips + $PI_{(20)}$	4.18	26.25	0.16
			P_L	DWh+ 80 kips + $PI_{(20)}$	0.80	26.25	0.03
			P_m (or P_L)+P_b+Q	DWh+ 80 kips + $PI_{(20)}$	3.13	52.50	0.06
			P_m (or P_L)+P_b+Q+P_e	DWh+ 80 kips + TH	10.80	52.50	0.21

Table 3.9.1-8
OTCP Stress Results – Load Combinations
3 Pages

Load Comb No.	Service Level	DSC Orientation	Stress Category	Loads	Stress intensity (ksi)	Allowable Stress (ksi)	Stress Ratio
6	D	Horizontal(2)	P_m	DWh+ 135 kips + $PI_{(20)}$	0.55	44.38	0.01
			P_m+P_b	DWh+ 135 kips + $PI_{(20)}$	4.15	57.06	0.07
			P_L	DWh+ 135 kips + $PI_{(20)}$	0.85	57.06	0.01
			P_m (or P_L)+P_b+Q	DWh+ 135 kips + $PI_{(20)}$	NA		
7A	D	Horizontal(2)	P_m	DWh+ max.(SD_AWAY, SD_RAIL_EP,SD_TOP_RAIL_EP)+ $PI_{(20)}$	9.82	44.38	0.22
			P_m+P_b	DWh+ max.(SD_AWAY_EP, SD_RAIL_EP)+ $PI_{(20)}$	25.08	57.06	0.44
			P_L	DWh+ max.(SD_AWAY, SD_RAIL_EP,SD_TOP_RAIL_EP)+ $PI_{(20)}$	16.07	57.06	0.28
			P_m (or P_L)+P_b+Q	DWh+ max.(SD_AWAY_EP, SD_RAIL_EP)+ $PI_{(20)}$	NA		
7B	D	Vertical	P_m	DWv+ max.(ED_TOP, ED_BOT)+ $PI_{(20)}$	2.90	44.38	0.07
			P_m+P_b	DWv+ max.(ED_TOP, ED_BOT)+ $PI_{(20)}$	16.06	57.06	0.28
			P_L	DWv+ max.(ED_TOP, ED_BOT)+ $PI_{(20)}$	3.21	57.06	0.06
			P_m (or P_L)+P_b+Q	DWv+ max.(ED_TOP, ED_BOT)+ $PI_{(20)}$	NA		
8	D	Horizontal(2)	P_m	DWh+ $PI_{(130)}$	2.39	44.38	0.05
			P_m+P_b	DWh+ $PI_{(130)}$	25.74	57.06	0.45
			P_L	DWh+ $PI_{(130)}$	2.38	57.06	0.04
			P_m (or P_L)+P_b+Q	DWh+ $PI_{(130)}$	NA		
9	A	Horizontal(3)	P_m	DWh+ $PI_{(20)}$	0.69	17.50	0.04
			P_m+P_b	DWh+ $PI_{(20)}$	4.48	26.25	0.17
			P_L	DWh+ $PI_{(20)}$	1.08	26.25	0.04
			P_m (or P_L)+P_b+Q	DWh+ $PI_{(20)}$	4.04	52.50	0.08
			P_m (or P_L)+P_b+Q+P_e	DWh+ $PI_{(20)}$ + TH	11.10	52.50	0.21

Table 3.9.1-8
OTCP Stress Results – Load Combinations
3 Pages

Load Comb No.	Service Level	DSC Orientation	Stress Category	Loads	Stress intensity (ksi)	Allowable Stress (ksi)	Stress Ratio
10	D	Horizontal(3)	P_m	DWh+ max.(HS_TOP, HS_BOT)+$PI_{(20)}$	1.61	44.38	0.04
			P_m+P_b	DWh+ max.(HS_TOP, HS_BOT)+$PI_{(20)}$	4.58	57.06	0.08
			P_L	DWh+ max.(HS_TOP, HS_BOT)+$PI_{(20)}$	5.01	57.06	0.09
			P_m (or P_L)+P_b+Q	DWh+ max.(HS_TOP, HS_BOT)+$PI_{(20)}$	NA		
11	Test	Vertical	P_m	max. (PI(23)+155 kips ,$PE_{(14.7)}$+155 kips)	NA		
			P_m+P_b	max. (PI(23)+155 kips,$PE_{(14.7)}$+155 kips)	NA		
			P_L	max. (PI(23)+155 kips ,$PE_{(14.7)}$+155 kips)	NA		
			P_m (or P_L)+P_b+Q	max. (PI(23)+155 kips,$PE_{(14.7)}$+155 kips)	NA		

Notes:

(1) DSC in transfer cask in vertical orientation. Only Inner top cover is installed

(2) DSC in TC with TC in a horizontal orientation.

(3) DSC in EOS-HSM supported on the steel rails

Table 3.9.1-9
ITCP Stress Results – Load Combinations
3 Pages

Load Comb No.	Service Level	DSC Orientation	Stress Category	Loads	Stress intensity (ksi)	Allowable Stress (ksi)	Stress Ratio
1	A	Vertical(1)	P_m	DWv+ max($PI_{(20)}$,BD,VD)	0.80	17.50	0.05
			P_m+P_b	DWv+ max($PI_{(20)}$,BD,VD)	9.02	26.25	0.34
			P_L	DWv+ max($PI_{(20)}$,BD,VD)	0.67	26.25	0.03
			P_m (or P_L)+P_b+Q	DWv+ max($PI_{(20)}$,BD,VD)	5.20	52.50	0.10
			P_m (or P_L)+P_b+Q+P_e	DWv+ max($PI_{(20)}$,BD,VD)+TH	19.20	52.50	0.37
2/3	A	Horizontal(2)	P_m	DWh+ 1g axial + 1g transverse + 1g Vertical + $PI_{(20)}$	0.56	17.50	0.03
			P_m+P_b	DWh+ 1g axial + 1g transverse + 1g Vertical + $PI_{(20)}$	3.66	26.25	0.14
			P_L	DWh+ 1g axial + 1g transverse + 1g Vertical + $PI_{(20)}$	1.18	26.25	0.04
			P_m (or P_L)+P_b+Q	DWh+ 1g axial + 1g transverse + 1g Vertical + $PI_{(20)}$	3.66	52.50	0.07
			P_m (or P_L)+P_b+Q+P_e	DWh+ 1g axial + 1g transverse + 1g Vertical + $PI_{(20)}$ + TH	13.84	52.50	0.26
4	A/B	Horizontal(2)	P_m	DWh+ 135kips + $PI_{(20)}$	0.56	17.50	0.03
			P_m+P_b	DWh+ 135kips + $PI_{(20)}$	4.31	26.25	0.16
			P_L	DWh+ 135kips + $PI_{(20)}$	0.98	26.25	0.04
			P_m (or P_L)+P_b+Q	DWh+ 135kips + $PI_{(20)}$	3.47	52.50	0.07
			P_m (or P_L)+P_b+Q+P_e	DWh+ 135kips + TH	14.49	52.50	0.28
5	A/B	Horizontal(2)	P_m	DWh+ 80 kips + $PI_{(20)}$	0.54	17.50	0.03
			P_m+P_b	DWh+ 80 kips + $PI_{(20)}$	4.21	26.25	0.16
			P_L	DWh+ 80 kips + $PI_{(20)}$	0.93	26.25	0.04
			P_m (or P_L)+P_b+Q	DWh+ 80 kips + $PI_{(20)}$	3.33	52.50	0.06
			P_m (or P_L)+P_b+Q+P_e	DWh+ 80 kips + TH	14.39	52.50	0.27

Table 3.9.1-9
ITCP Stress Results – Load Combinations
3 Pages

Load Comb No.	Service Level	DSC Orientation	Stress Category	Loads	Stress intensity (ksi)	Allowable Stress (ksi)	Stress Ratio
6	D	Horizontal(2)	P_m	DWh+ 135 kips + $PI_{(20)}$	0.54	44.38	0.01
			P_m+P_b	DWh+ 135 kips + $PI_{(20)}$	4.18	57.06	0.07
			P_L	DWh+ 135 kips + $PI_{(20)}$	0.89	57.06	0.02
			P_m (or P_L)+P_b+Q	DWh+ 135 kips + $PI_{(20)}$	NA		
7A	D	Horizontal(2)	P_m	DWh+ max.(SD_AWAY, SD_RAIL_EP,SD_TOP_RAIL_EP)+ $PI_{(20)}$	7.33	44.38	0.17
			P_m+P_b	DWh+ max.(SD_AWAY_EP, SD_RAIL_EP)+ $PI_{(20)}$	20.14	57.06	0.35
			P_L	DWh+ max.(SD_AWAY, SD_RAIL_EP,SD_TOP_RAIL_EP)+ $PI_{(20)}$	13.28	57.06	0.23
			P_m (or P_L)+P_b+Q	DWh+ max.(SD_AWAY_EP, SD_RAIL_EP)+ $PI_{(20)}$	NA		
7B	D	Vertical	P_m	DWv+ max.(ED_TOP, ED_BOT)+ $PI_{(20)}$	3.40	44.38	0.08
			P_m+P_b	DWv+ max.(ED_TOP, ED_BOT)+ $PI_{(20)}$	18.01	57.06	0.32
			P_L	DWv+ max.(ED_TOP, ED_BOT)+ $PI_{(20)}$	4.09	57.06	0.07
			P_m (or P_L)+P_b+Q	DWv+ max.(ED_TOP, ED_BOT)+ $PI_{(20)}$	NA		
8	D	Horizontal(2)	P_m	DWh+ $PI_{(130)}$	2.46	44.38	0.06
			P_m+P_b	DWh+ $PI_{(130)}$	25.82	57.06	0.45
			P_L	DWh+ $PI_{(130)}$	3.07	57.06	0.05
			P_m (or P_L)+P_b+Q	DWh+ $PI_{(130)}$	NA		
9	A	Horizontal(3)	P_m	DWh+ $PI_{(20)}$	0.74	17.50	0.04
			P_m+P_b	DWh+ $PI_{(20)}$	4.55	26.25	0.17
			P_L	DWh+ $PI_{(20)}$	1.31	26.25	0.05
			P_m (or P_L)+P_b+Q	DWh+ $PI_{(20)}$	4.51	52.50	0.09
			P_m (or P_L)+P_b+Q+P_e	DWh+ $PI_{(20)}$ + TH	14.73	52.50	0.28

Table 3.9.1-9
ITCP Stress Results – Load Combinations
3 Pages

Load Comb No.	Service Level	DSC Orientation	Stress Category	Loads	Stress intensity (ksi)	Allowable Stress (ksi)	Stress Ratio
10	D	Horizontal(3)	P_m	DWh+ max.(HS_TOP, HS_BOT)+$PI_{(20)}$	2.05	44.38	0.05
			P_m+P_b	DWh+ max.(HS_TOP, HS_BOT)+$PI_{(20)}$	4.60	57.06	0.08
			P_L	DWh+ max.(HS_TOP, HS_BOT)+$PI_{(20)}$	3.73	57.06	0.07
			P_m (or P_L)+P_b+Q	DWh+ max.(HS_TOP, HS_BOT)+$PI_{(20)}$	NA		
11	Test	Vertical	P_m	max. (PI(23)+155 kips ,$PE_{(14.7)}$+155 kips)	NA		
			P_m+P_b	max. (PI(23)+155 kips,$PE_{(14.7)}$+155 kips)	NA		
			P_L	max. (PI(23)+155 kips ,$PE_{(14.7)}$+155 kips)	NA		
			P_m (or P_L)+P_b+Q	max. (PI(23)+155 kips,$PE_{(14.7)}$+155 kips)	NA		

Notes:

(1) DSC in transfer cask in vertical orientation. Only Inner top cover is installed

(2) DSC in TC with TC in a horizontal orientation.

(3) DSC in EOS-HSM supported on the steel rails

Table 3.9.1-10
IBCP Stress Results – Load Combinations
3 Pages

Load Comb No.	Service Level	DSC Orientation	Stress Category	Loads	Stress intensity (ksi)	Allowable Stress (ksi)	Stress Ratio
1	A	Vertical(1)	P_m	DWv+ max($PI_{(20)}$,BD,VD)	0.43	17.50	0.02
			P_m+P_b	DWv+ max($PI_{(20)}$,BD,VD)	1.00	26.25	0.04
			P_L	DWv+ max($PI_{(20)}$,BD,VD)	0.44	26.25	0.02
			P_m (or P_L)+P_b+Q	DWv+ max($PI_{(20)}$,BD,VD)	1.18	52.50	0.02
			P_m (or P_L)+P_b+Q+P_e	DWv+ max($PI_{(20)}$,BD,VD)+TH	17.40	52.50	0.33
2/3	A	Horizontal(2)	P_m	DWh+ 1g axial + 1g transverse + 1g Vertical + $PI_{(20)}$	0.40	17.50	0.02
			P_m+P_b	DWh+ 1g axial + 1g transverse + 1g Vertical + $PI_{(20)}$	0.67	26.25	0.03
			P_L	DWh+ 1g axial + 1g transverse + 1g Vertical + $PI_{(20)}$	0.80	26.25	0.03
			P_m (or P_L)+P_b+Q	DWh+ 1g axial + 1g transverse + 1g Vertical + $PI_{(20)}$	2.77	52.50	0.05
			P_m (or P_L)+P_b+Q+P_e	DWh+ 1g axial + 1g transverse + 1g Vertical + $PI_{(20)}$ + TH	18.99	52.50	0.36
4	A/B	Horizontal(2)	P_m	DWh+ 135kips + $PI_{(20)}$	1.46	17.50	0.08
			P_m+P_b	DWh+ 135kips + $PI_{(20)}$	5.56	26.25	0.21
			P_L	DWh+ 135kips + $PI_{(20)}$	1.60	26.25	0.06
			P_m (or P_L)+P_b+Q	DWh+ 135kips + $PI_{(20)}$	6.71	52.50	0.13
			P_m (or P_L)+P_b+Q+P_e	DWh+ 135kips + TH	22.93	52.50	0.44
5	A/B	Horizontal(2)	P_m	DWh+ 80 kips + $PI_{(20)}$	0.47	17.50	0.03
			P_m+P_b	DWh+ 80 kips + $PI_{(20)}$	2.08	26.25	0.08
			P_L	DWh+ 80 kips + $PI_{(20)}$	0.79	26.25	0.03
			P_m (or P_L)+P_b+Q	DWh+ 80 kips + $PI_{(20)}$	3.05	52.50	0.06
			P_m (or P_L)+P_b+Q+P_e	DWh+ 80 kips + TH	19.27	52.50	0.37

Table 3.9.1-10
IBCP Stress Results – Load Combinations
3 Pages

Load Comb No.	Service Level	DSC Orientation	Stress Category	Loads	Stress intensity (ksi)	Allowable Stress (ksi)	Stress Ratio
6	D	Horizontal(2)	P_m	DWh+ 135 kips + $PI_{(20)}$	0.56	44.38	0.01
			P_m+P_b	DWh+ 135 kips + $PI_{(20)}$	2.71	57.06	0.05
			P_L	DWh+ 135 kips + $PI_{(20)}$	0.89	57.06	0.02
			P_m (or P_L)+P_b+Q	DWh+ 135 kips + $PI_{(20)}$	NA		
7A	D	Horizontal(2)	P_m	DWh+ max.(SD_AWAY, SD_RAIL_EP,SD_TOP_RAIL_EP)+ $PI_{(20)}$	18.03	44.38	0.41
			P_m+P_b	DWh+ max.(SD_AWAY_EP, SD_RAIL_EP)+ $PI_{(20)}$	23.81	57.06	0.42
			P_L	DWh+ max.(SD_AWAY, SD_RAIL_EP,SD_TOP_RAIL_EP)+ $PI_{(20)}$	23.67	57.06	0.41
			P_m (or P_L)+P_b+Q	DWh+ max.(SD_AWAY_EP, SD_RAIL_EP)+ $PI_{(20)}$	NA		
7B	D	Vertical	P_m	DWv+ max.(ED_TOP, ED_BOT)+ $PI_{(20)}$	6.56	44.38	0.15
			P_m+P_b	DWv+ max.(ED_TOP, ED_BOT)+ $PI_{(20)}$	21.21	57.06	0.37
			P_L	DWv+ max.(ED_TOP, ED_BOT)+ $PI_{(20)}$	5.05	57.06	0.09
			P_m (or P_L)+P_b+Q	DWv+ max.(ED_TOP, ED_BOT)+ $PI_{(20)}$	NA		
8	D	Horizontal(2)	P_m	DWh+ $PI_{(130)}$	1.10	44.38	0.02
			P_m+P_b	DWh+ $PI_{(130)}$	5.44	57.06	0.10
			P_L	DWh+ $PI_{(130)}$	1.80	57.06	0.03
			P_m (or P_L)+P_b+Q	DWh+ $PI_{(130)}$	NA		
9	A	Horizontal(3)	P_m	DWh+ $PI_{(20)}$	0.58	17.50	0.03
			P_m+P_b	DWh+ $PI_{(20)}$	1.30	26.25	0.05
			P_L	DWh+ $PI_{(20)}$	1.12	26.25	0.04
			P_m (or P_L)+P_b+Q	DWh+ $PI_{(20)}$	2.46	52.50	0.05
			P_m (or P_L)+P_b+Q+P_e	DWh+ $PI_{(20)}$ + TH	18.68	52.50	0.36

Table 3.9.1-10
IBCP Stress Results – Load Combinations
3 Pages

Load Comb No.	Service Level	DSC Orientation	Stress Category	Loads	Stress intensity (ksi)	Allowable Stress (ksi)	Stress Ratio
10	D	Horizontal(3)	P_m	DWh+ max.(HS_TOP, HS_BOT)+$PI_{(20)}$	4.00	44.38	0.09
			P_m+P_b	DWh+ max.(HS_TOP, HS_BOT)+$PI_{(20)}$	12.66	57.06	0.22
			P_L	DWh+ max.(HS_TOP, HS_BOT)+$PI_{(20)}$	3.80	57.06	0.07
			P_m (or P_L)+P_b+Q	DWh+ max.(HS_TOP, HS_BOT)+$PI_{(20)}$	NA		
11	Test	Vertical	P_m	max. (PI(23)+155 kips ,$PE_{(14.7)}$+155 kips)	0.67	17.50	0.04
			P_m+P_b	max. (PI(23)+155 kips,$PE_{(14.7)}$+155 kips)	7.69	26.25	0.29
			P_L	max. (PI(23)+155 kips ,$PE_{(14.7)}$+155 kips)	1.13	26.25	0.04
			P_m (or P_L)+P_b+Q	max. (PI(23)+155 kips,$PE_{(14.7)}$+155 kips)	NA		

Notes:

(1) DSC in transfer cask in vertical orientation. Only Inner top cover is installed

(2) DSC in TC with TC in a horizontal orientation.

(3) DSC in EOS-HSM supported on the steel rails

Table 3.9.1-11
ITCP-DSC Shell Weld Stress Results – Load Combinations
2 Pages

Load Comb No.	Service Level	DSC Orientation	Stress Category	Loads	Stress intensity (ksi)	Allowable Stress	Stress Ratio
1	A	Vertical(1)	P_L	DWv+ max($PI_{(20)}$,BD,VD)	8.60	23.20	0.37
			$P_L+P_b+Q+P_e$	DWv+ max($PI_{(20)}$,BD,VD) + TH	34.48	46.30	0.74
2	A	Horizontal(2)	P_L	DWh+ 1g axial + 1g transverse + 1g Vertical + $PI_{(20)}$	5.95	23.20	0.26
			$P_L+P_b+Q+P_e$	DWh+ 1g axial + 1g transverse + 1g Vertical + $PI_{(20)}$ + TH	27.93	46.30	0.60
3	A	Horizontal(2)	P_L	DWh+ 1g axial + 1g transverse + 1g Vertical + $PI_{(20)}$	5.95	23.20	0.26
			$P_L+P_b+Q+P_e$	DWh+ 1g axial + 1g transverse + 1g Vertical + $PI_{(20)}$ + TH	27.93	46.30	0.60
4	A/B	Horizontal(2)	P_L	DWh+ 135kips + $PI_{(20)}$	6.02	23.20	0.26
			$P_L+P_b+Q+P_e$	DWh+ 135kips + $PI_{(20)}$ + TH	29.44	46.30	0.64
5	A/B	Horizontal(2)	P_L	DWh+ 80 kips + $PI_{(20)}$	6.50	23.20	0.28
			$P_L+P_b+Q+P_e$	DWh+ 80 kips + $PI_{(20)}$ + TH	29.11	46.30	0.63
6	D	Horizontal(2)	P_L	DWh+ 135 kips + $PI_{(20)}$	6.74	46.90	0.14
			$P_L+P_b+Q+P_e$	DWh+ 135 kips + $PI_{(20)}$ + TH	NA		
7A	D	Horizontal(2)	P_L	DWh+ max.(SD_AWAY, SD_RAIL_EP,SD_TOP_RAIL_EP)+ $PI_{(20)}$	35.77	46.90	0.76
			$P_L+P_b+Q+P_e$	DWh+ max.(SD_AWAY_EP, SD_RAIL_EP)+ $PI_{(20)}$ + TH	NA		
7B	D	Vertical	P_L	DWv+ max.(ED_TOP, ED_BOT)+ $PI_{(20)}$	13.22	52.08	0.25
			$P_L+P_b+Q+P_e$	DWv+ max.(ED_TOP, ED_BOT)+ $PI_{(20)}$ + TH	NA		
8	D	Horizontal(2)	P_L	DWh+ $PI_{(130)}$	16.41	46.90	0.35
			$P_L+P_b+Q+P_e$	DWh+ $PI_{(130)}$ + TH	NA		
9	A	Horizontal(3)	P_L	DWh+ $PI_{(20)}$	8.27	23.20	0.36
			$P_L+P_b+Q+P_e$	DWh+ $PI_{(20)}$ + TH	31.18	46.30	0.67

Table 3.9.1-11
ITCP-DSC Shell Weld Stress Results – Load Combinations
2 Pages

Load Comb No.	Service Level	DSC Orientation	Stress Category	Loads	Stress intensity (ksi)	Allowable Stress	Stress Ratio
10	D	Horizontal(3)	P_L	DWh+ max.(HS_TOP, HS_BOT)+$PI_{(20)}$	18.93	46.90	0.40
			$P_L+P_b+Q+P_e$	DWh+ max.(HS_TOP, HS_BOT)+$PI_{(20)}$ + TH	NA		
11	Test	Vertical	P_L	max. (PI(23)+155 kips ,$PE_{(14.7)}$+155 kips)	NA		
			$P_L+P_b+Q+P_e$	max. (PI(23)+155 kips,$PE_{(14.7)}$+155 kips) + TH	NA		

Notes:

(1) DSC in transfer cask in vertical orientation. Only Inner top cover is installed

(2) DSC in TC with TC in a horizontal orientation.

(3) DSC in EOS-HSM supported on the steel rails

Table 3.9.1-12
OTCP-DSC Shell Weld Stress Results – Load Combinations
2 Pages

Load Comb No.	Service Level	DSC Orientation	Stress Category	Loads	Stress intensity (ksi)	Allowable Stress	Stress Ratio
1	A	Vertical(1)	P_L	DWv+ max($PI_{(20)}$,BD,VD)	4.96	23.20	0.21
			$P_L+P_b+Q+P_e$	DWv+ max($PI_{(20)}$,BD,VD) + TH	21.15	46.30	0.46
2	A	Horizontal(2)	P_L	DWh+ 1g axial + 1g transverse + 1g Vertical + $PI_{(20)}$	7.45	23.20	0.32
			$P_L+P_b+Q+P_e$	DWh+ 1g axial + 1g transverse + 1g Vertical + $PI_{(20)}$ + TH	26.42	46.30	0.57
3	A	Horizontal(2)	P_L	DWh+ 1g axial + 1g transverse + 1g Vertical + $PI_{(20)}$	7.45	23.20	0.32
			$P_L+P_b+Q+P_e$	DWh+ 1g axial + 1g transverse + 1g Vertical + $PI_{(20)}$ + TH	26.42	46.30	0.57
4	A/B	Horizontal(2)	P_L	DWh+ 135kips + $PI_{(20)}$	5.45	23.20	0.23
			$P_L+P_b+Q+P_e$	DWh+ 135kips + $PI_{(20)}$ + TH	20.82	46.30	0.45
5	A/B	Horizontal(2)	P_L	DWh+ 80 kips + $PI_{(20)}$	5.78	23.20	0.25
			$P_L+P_b+Q+P_e$	DWh+ 80 kips + $PI_{(20)}$ + TH	22.80	46.30	0.49
6	D	Horizontal(2)	P_L	DWh+ 135 kips + $PI_{(20)}$	5.87	46.90	0.13
			$P_L+P_b+Q+P_e$	DWh+ 135 kips + $PI_{(20)}$ + TH	NA		
7A	D	Horizontal(2)	P_L	DWh+ max.(SD_AWAY, SD_RAIL_EP,SD_TOP_RAIL_EP)+ $PI_{(20)}$	31.73	46.90	0.68
			$P_L+P_b+Q+P_e$	DWh+ max.(SD_AWAY_EP, SD_RAIL_EP)+ $PI_{(20)}$ + TH	NA		
7B	D	Vertical	P_L	DWv+ max.(ED_TOP, ED_BOT)+ $PI_{(20)}$	12.97	46.90	0.28
			$P_L+P_b+Q+P_e$	DWv+ max.(ED_TOP, ED_BOT)+ $PI_{(20)}$ + TH	NA		
8	D	Horizontal(2)	P_L	DWh+ $PI_{(130)}$	14.77	46.90	0.31
			$P_L+P_b+Q+P_e$	DWh+ $PI_{(130)}$ + TH	NA		
9	A	Horizontal(3)	P_L	DWh+ $PI_{(20)}$	6.93	23.20	0.30
			$P_L+P_b+Q+P_e$	DWh+ $PI_{(20)}$ + TH	23.75	46.30	0.51

Table 3.9.1-12
OTCP-DSC Shell Weld Stress Results – Load Combinations
2 Pages

Load Comb No.	Service Level	DSC Orientation	Stress Category	Loads	Stress intensity (ksi)	Allowable Stress	Stress Ratio
10	D	Horizontal(3)	P_L	DWh+ max.(HS_TOP, HS_BOT)+$PI_{(20)}$	17.07	46.90	0.36
			$P_L+P_b+Q+P_e$	DWh+ max.(HS_TOP, HS_BOT)+$PI_{(20)}$ + TH	NA		
11	Test	Vertical	P_L	max. (PI(23)+155 kips ,$PE_{(14.7)}$+155 kips)	NA		
			$P_L+P_b+Q+P_e$	max. (PI(23)+155 kips,$PE_{(14.7)}$+155 kips) + TH	NA		

Notes:

(1) Maximum value of load case with and without internal pressure.

(2) DSC in TC with TC in a horizontal orientation.

(3) DSC in HSM supported on the steel rails.

Table 3.9.1-13
Weld Flaw Size for Controlling Load Combination

						Subsurface Flaws		Surface Flaws	
Service Level	**Controlling Load Combination**	**Tensile Radial Stress SX (ksi)**	**Safety Factor SFm**	**Radial Stress including Safety Factor (Sx)x (SFm)**	**Allowable a/t**	**Weld Thickness 2t (inch)**	**Flaw Depth, 2a (inch)**	**Weld Thickness t (inch)**	**Flaw Depth, a (inch)**
A	4	0.21	2.7	0.56	(0.99) 0.75	0.50	0.38	0.50	0.38
B	4	0.21	2.4	0.49	(0.99) 0.75	0.50	0.38	0.50	0.38
D	7A	3.65	1.3	4.75	(0.89) 0.75	0.50	0.38	0.50	0.38

Table 3.9.1-14
Not Used

Table 3.9.1-15
Summary of Maximum Strain for Side Drop (Strain Criteria)(1)

Load Case	Maximum Equivalent Plastic Strain (in/in)	Triaxiality Factor	Uniform Strain Limit (in/in)	*Factor of Safety*
Baseline 75g	0.065	-1.6 (1.0)	0.17	*2.6*
75g with 20% increase in yield strength	0.054	-1.6 (1.0)	0.17	*3.1*
75g with 40% increase in yield strength	0.045	-1.6 (1.0)	0.17	*3.8*

Notes:

(1) The maximum equivalent plastic strains are conservatively compared with the uniform strain limits.

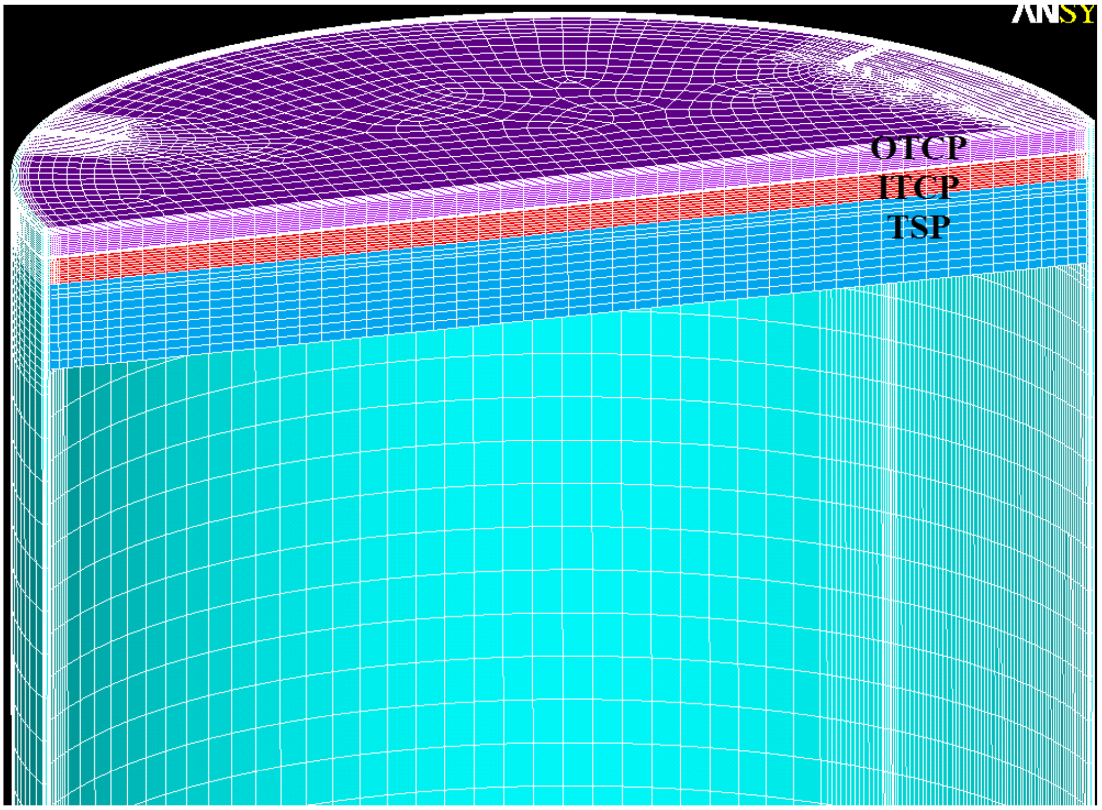

Length through the middle of the DSC not shown

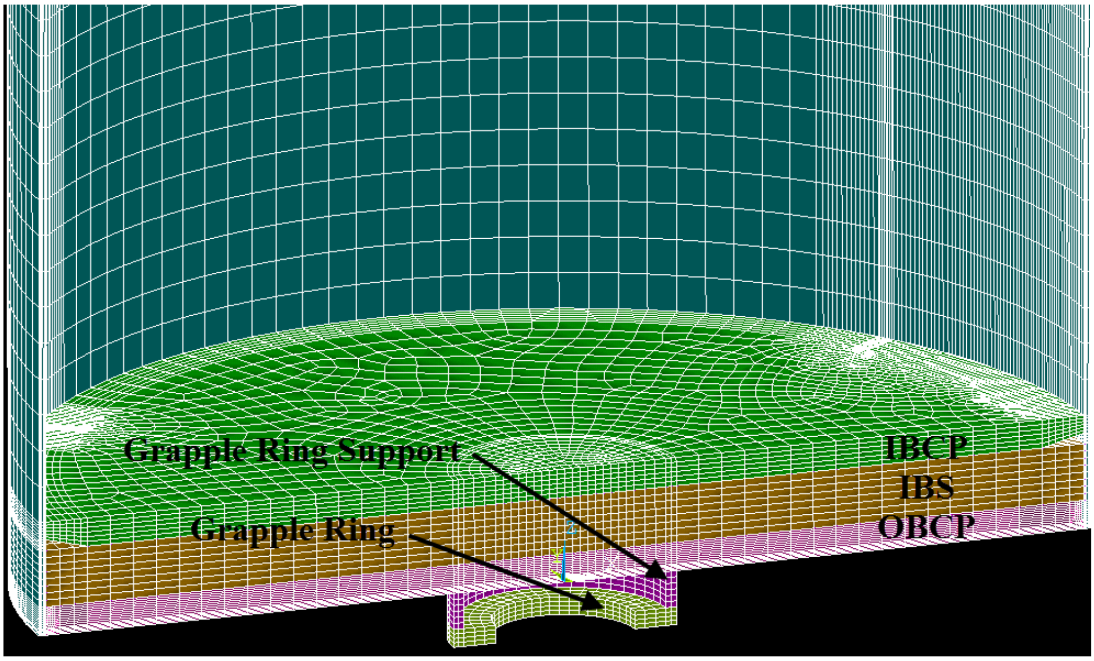

Figure 3.9.1-1
DSC FEM

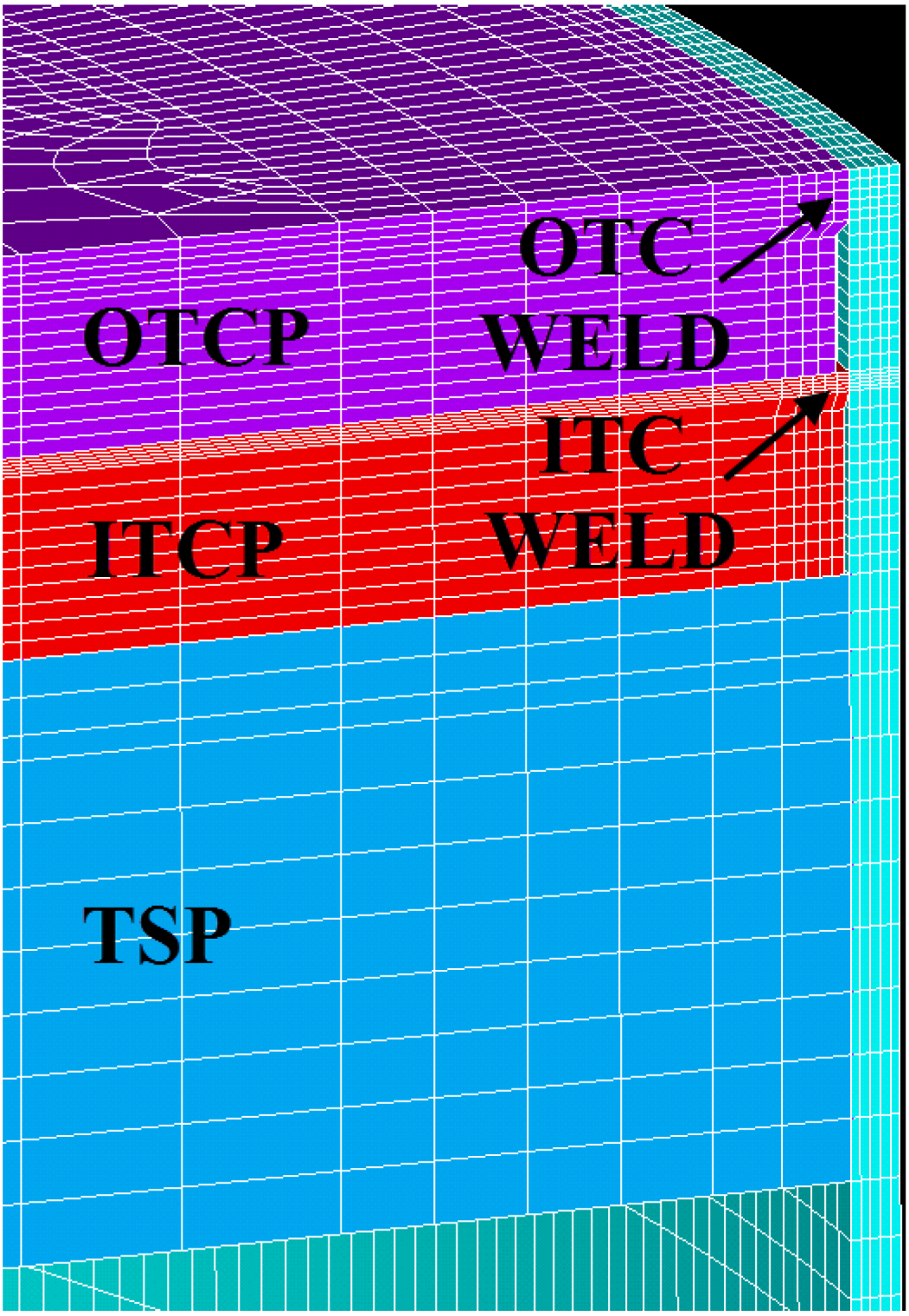

Figure 3.9.1-2
DSC FEM-Top End

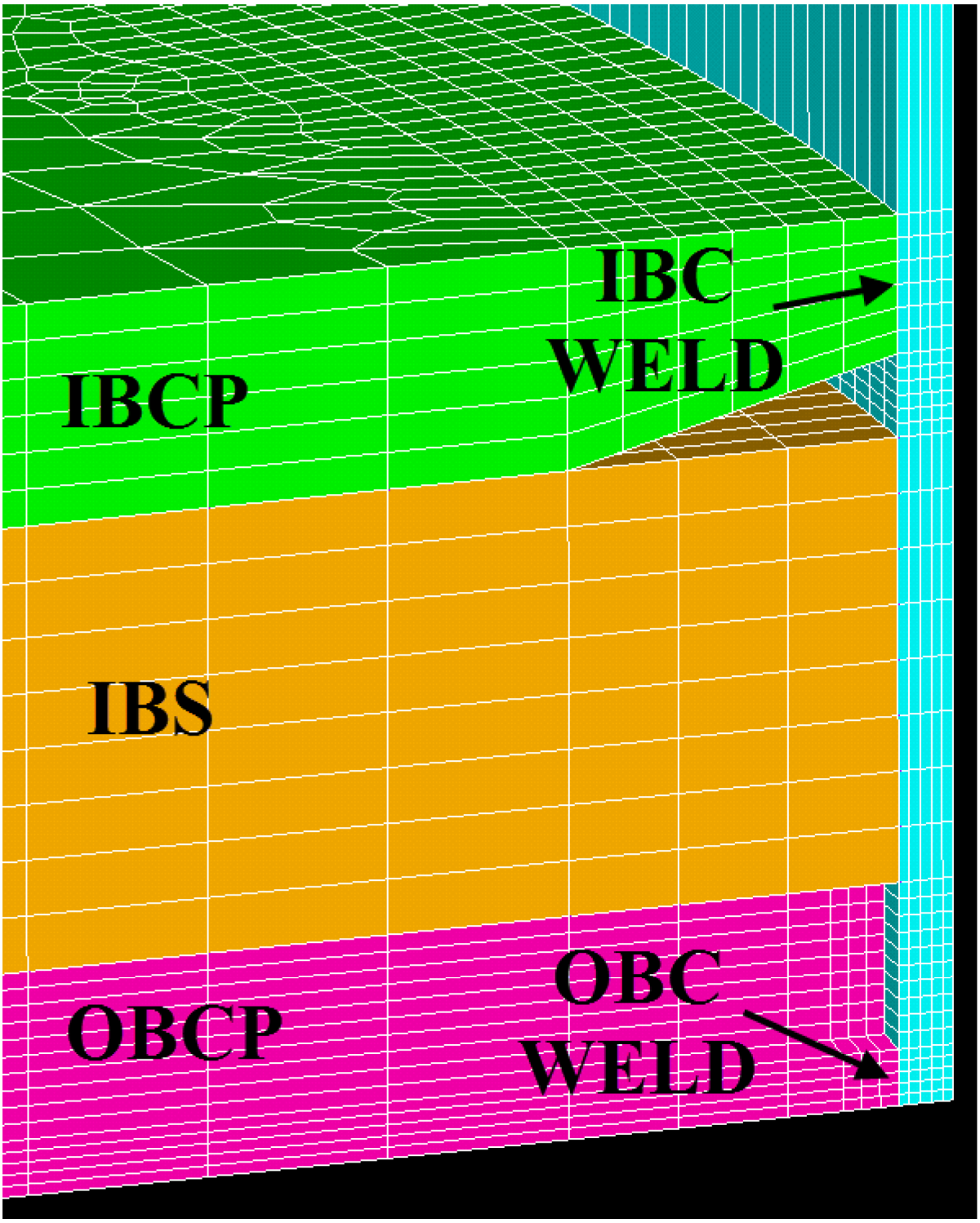

Figure 3.9.1-3
DSC FEM-Bottom End

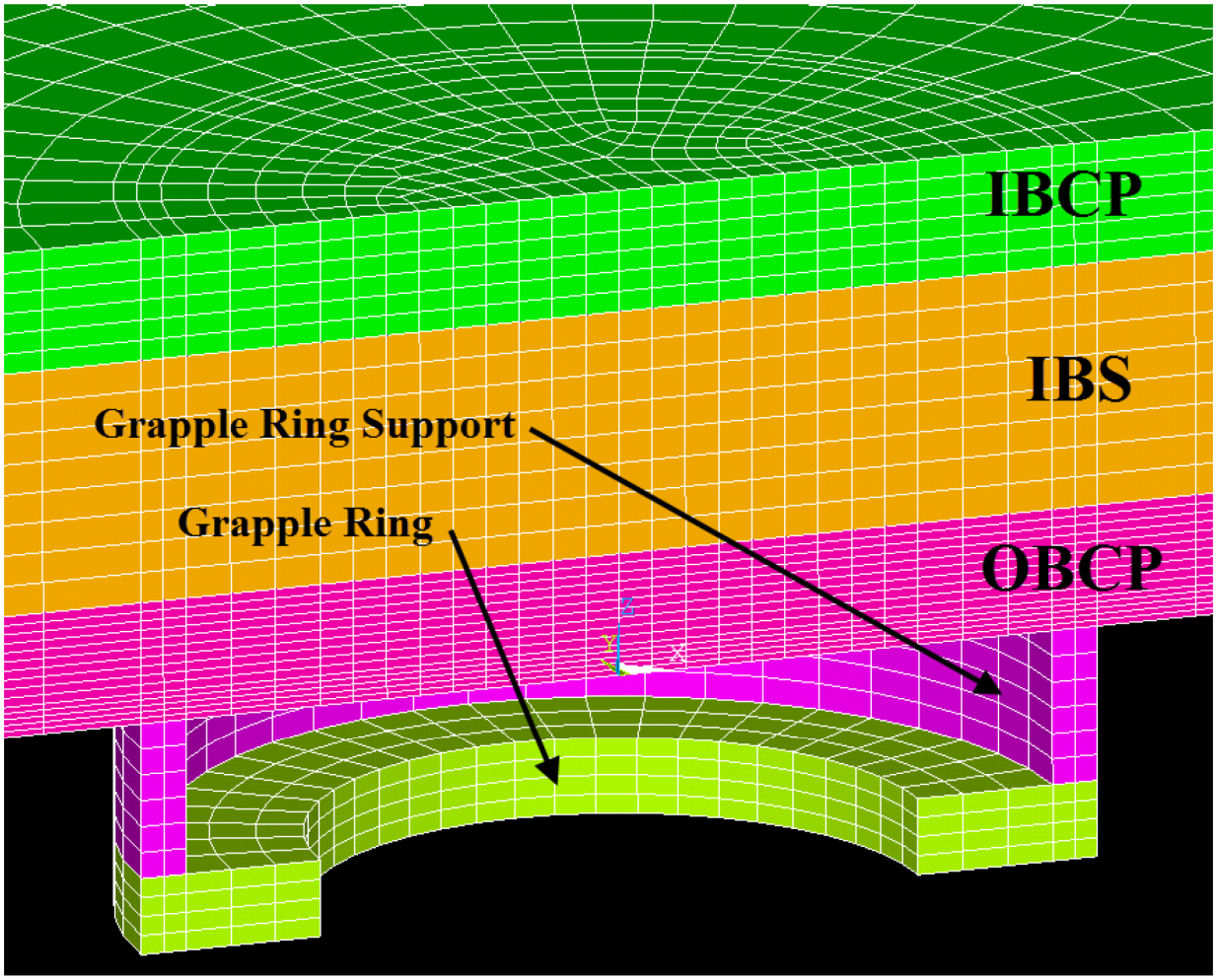

Figure 3.9.1-4
Mesh detail – Grapple Assembly

Figure 3.9.1-5
Not Used

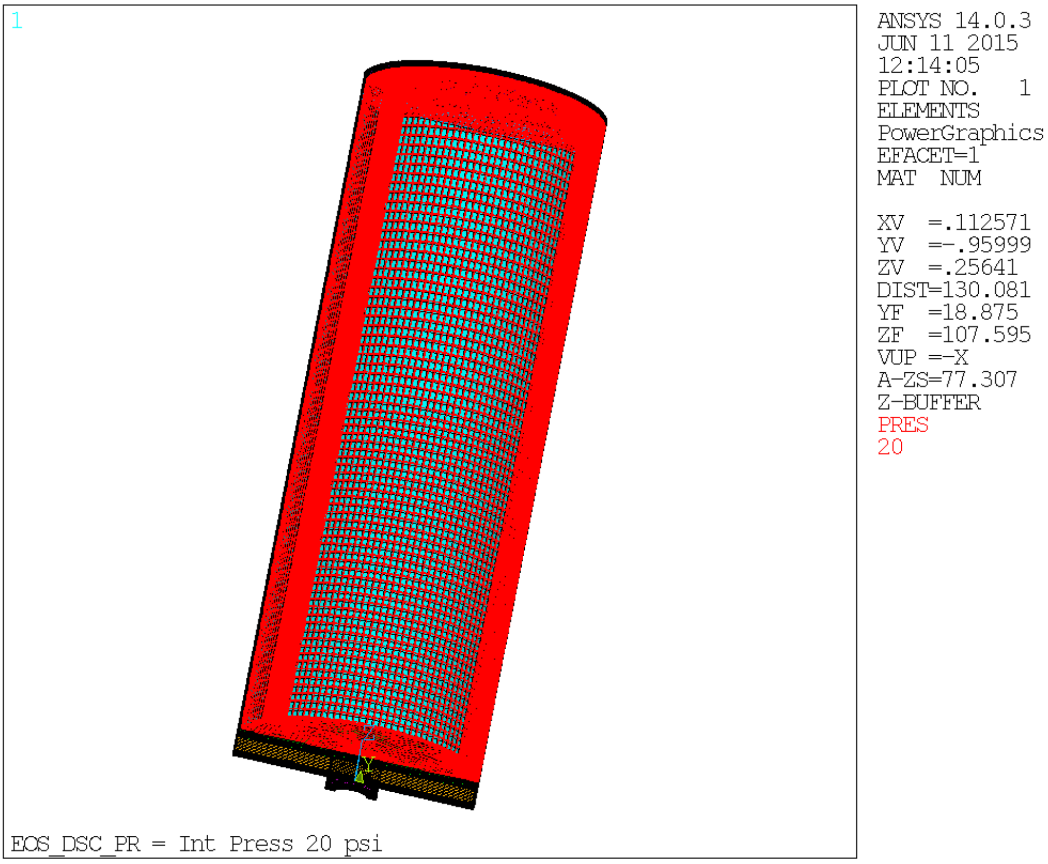

Figure 3.9.1-6
Internal Pressure – Load Application

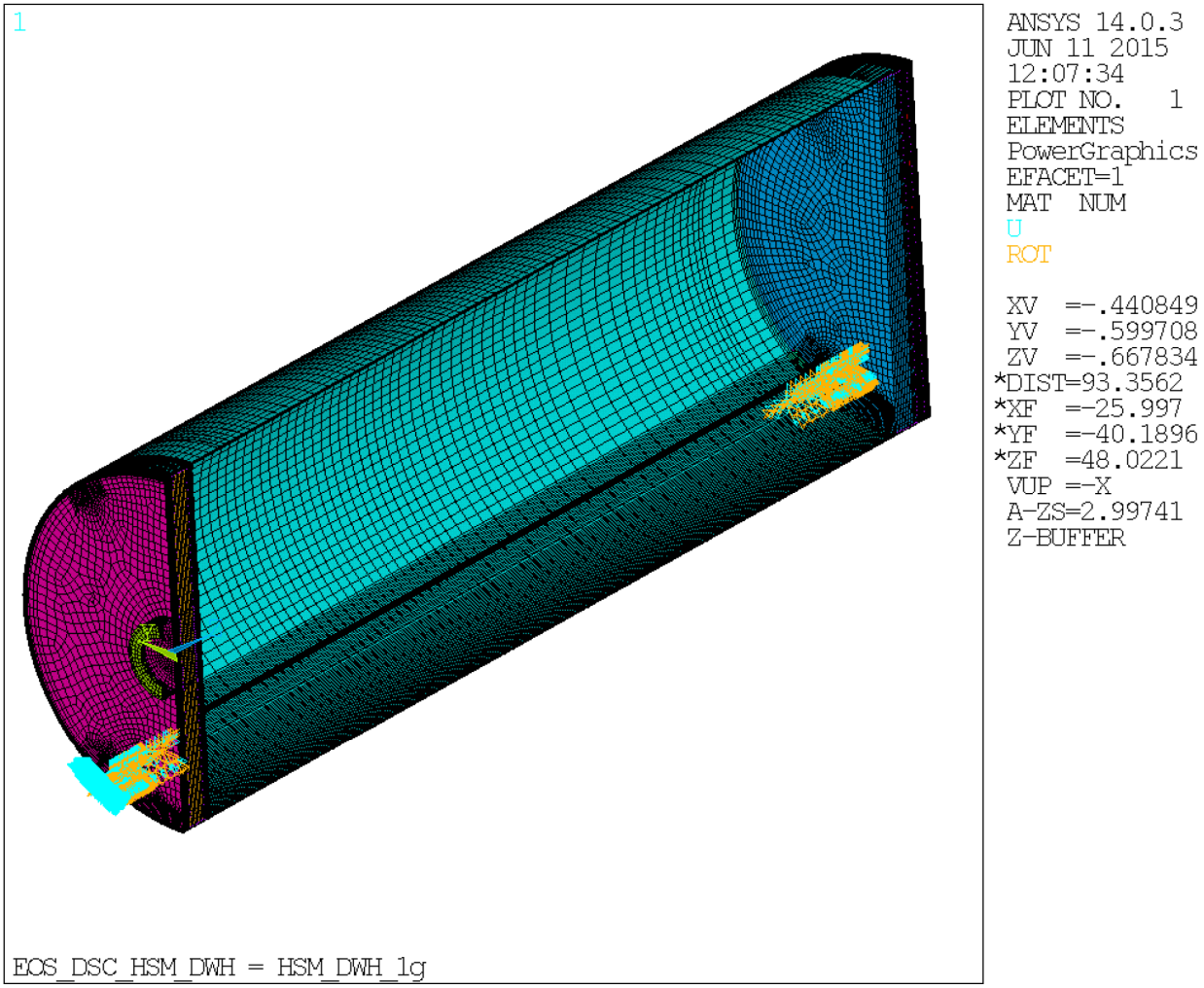

Figure 3.9.1-7
Dead Weight Simulation in EOS-HSM – Boundary Conditions

Note: Symmetry boundary conditions not shown for clarity.

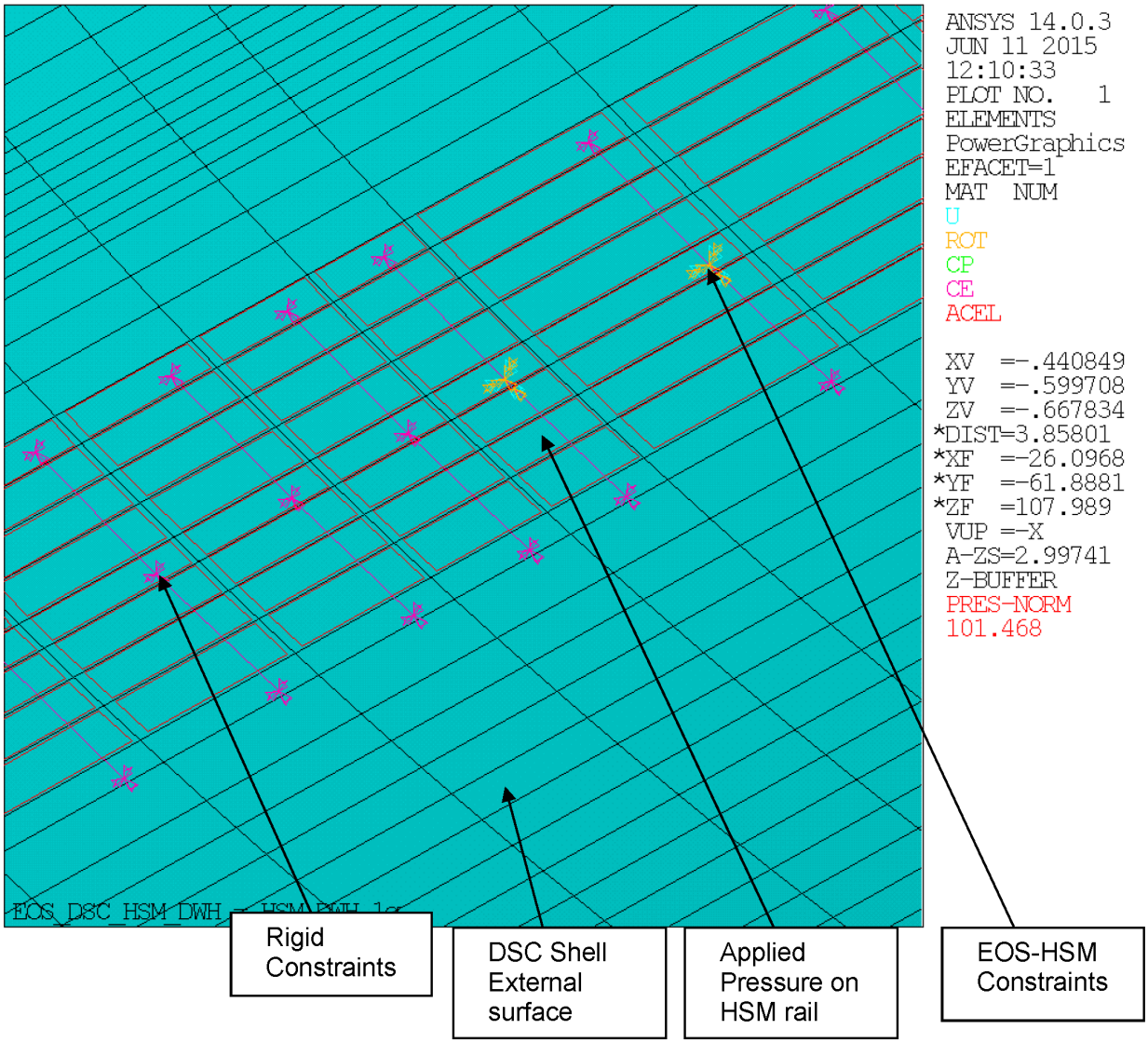

Figure 3.9.1-7a
Dead Weight Simulation in EOS-HSM Detail

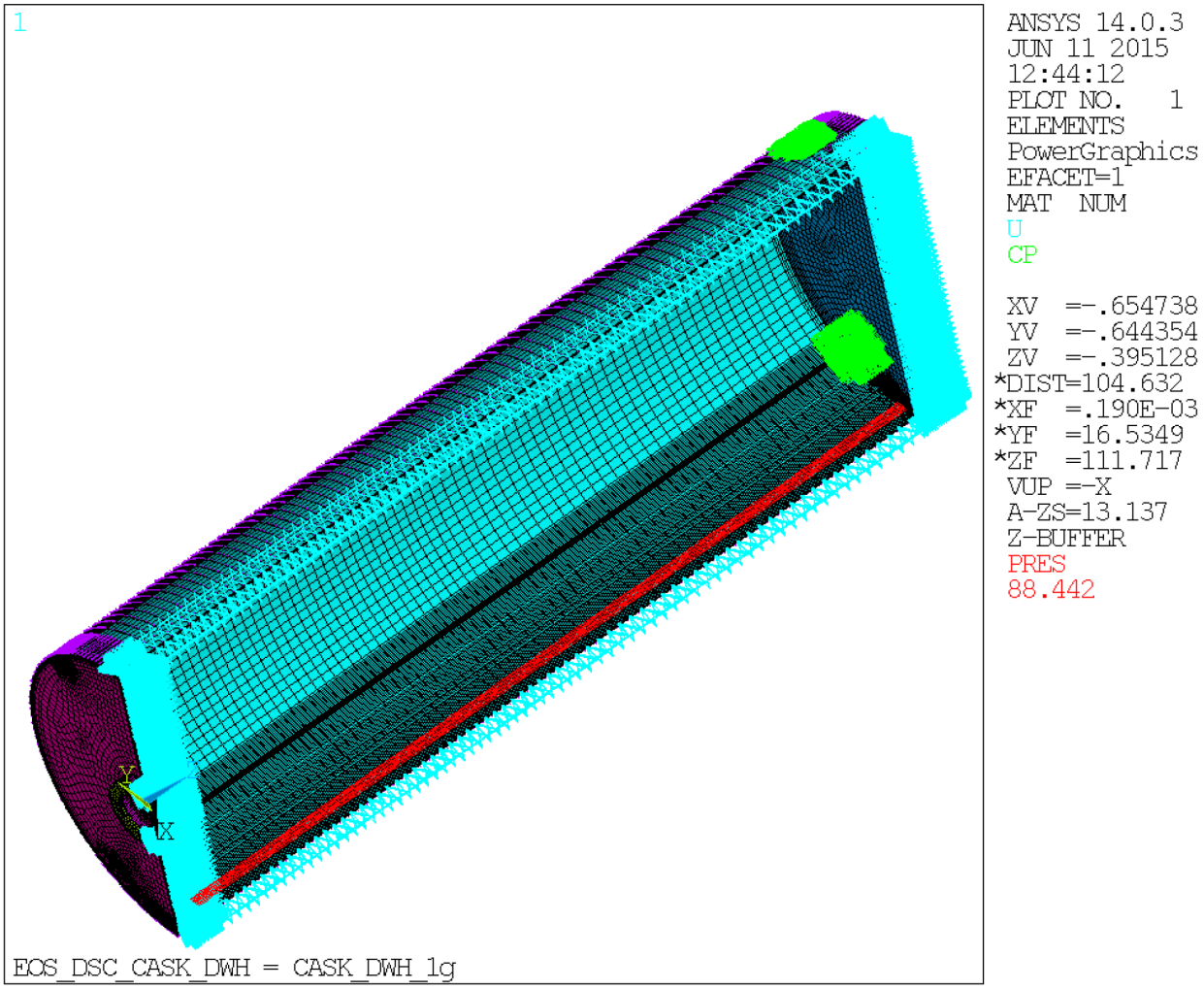

Figure 3.9.1-8
Dead Weight Simulation in EOS-TC

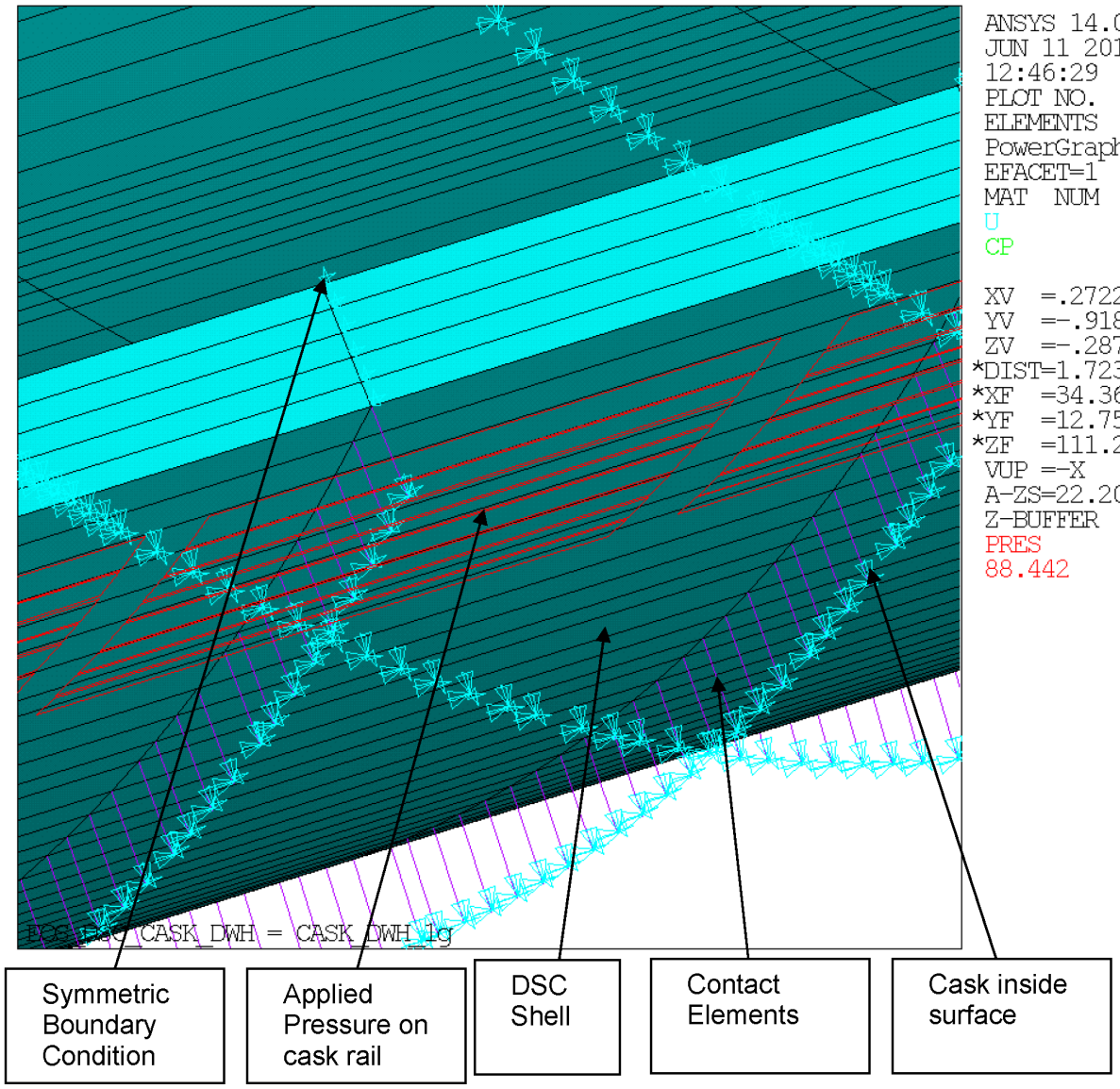

Figure 3.9.1-8a
Dead Weight Simulation in Cask Detail

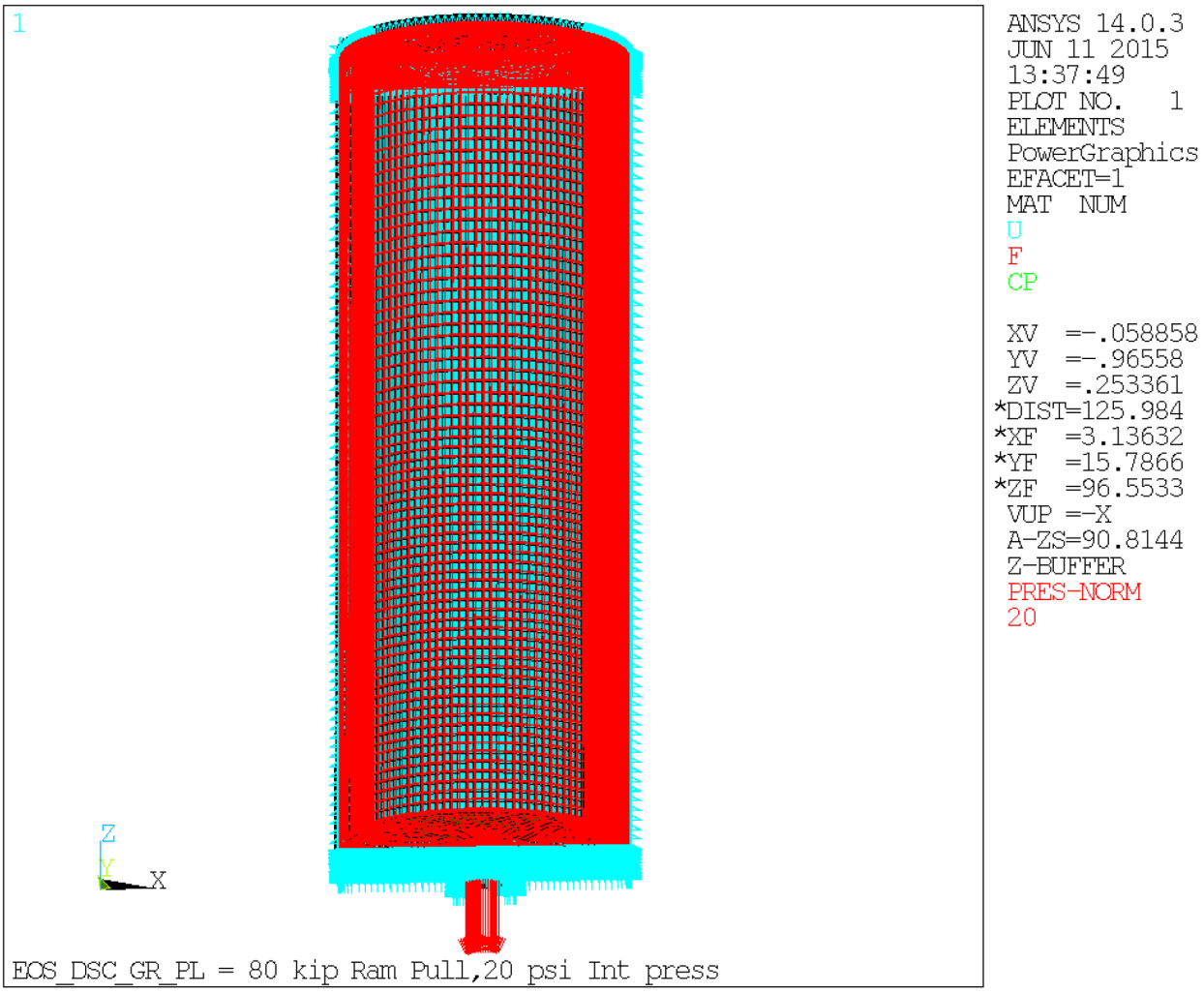

Figure 3.9.1-9
Pull Load with Internal Pressure

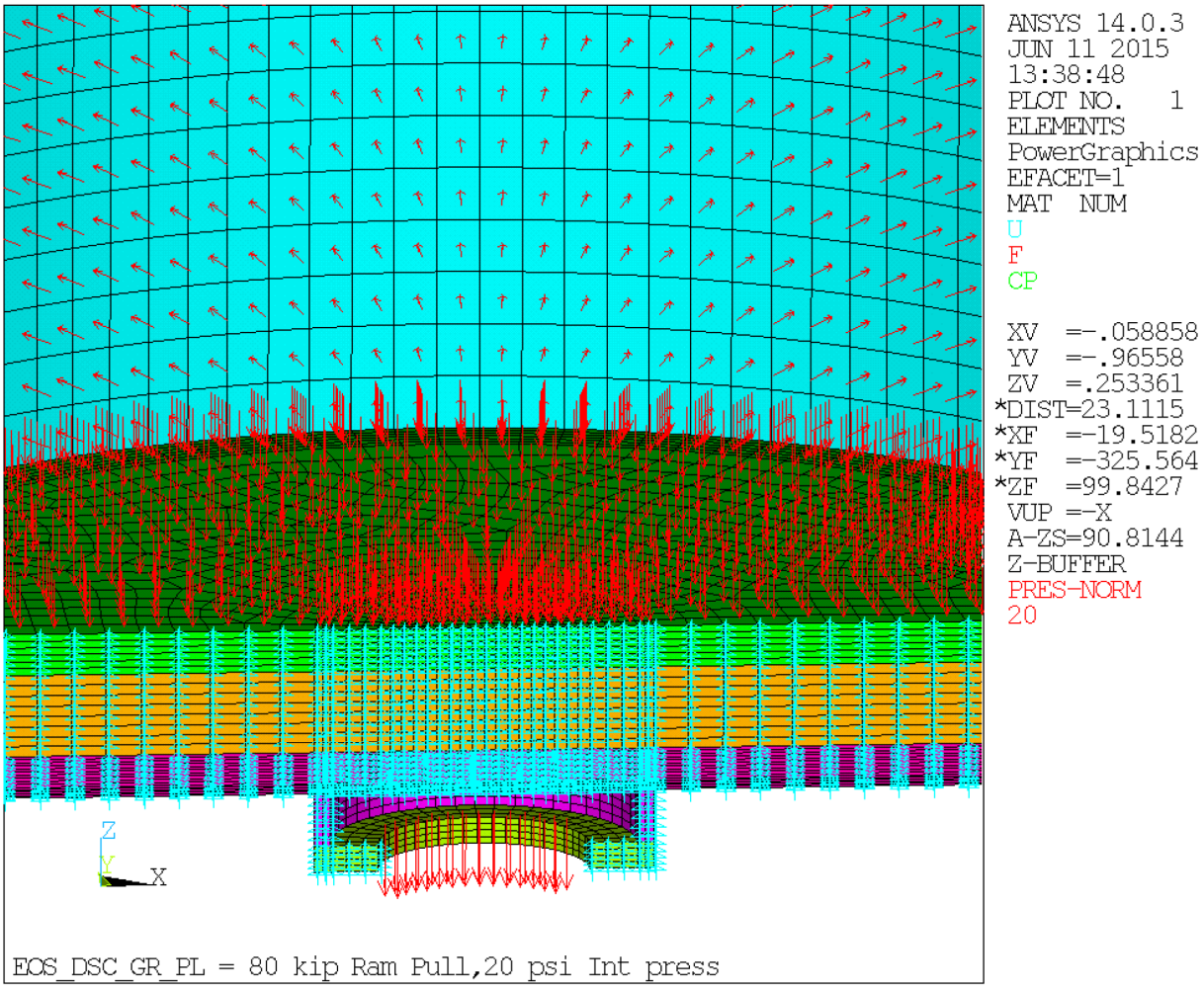

Figure 3.9.1-9a
Pull Load with Internal Pressure Detail

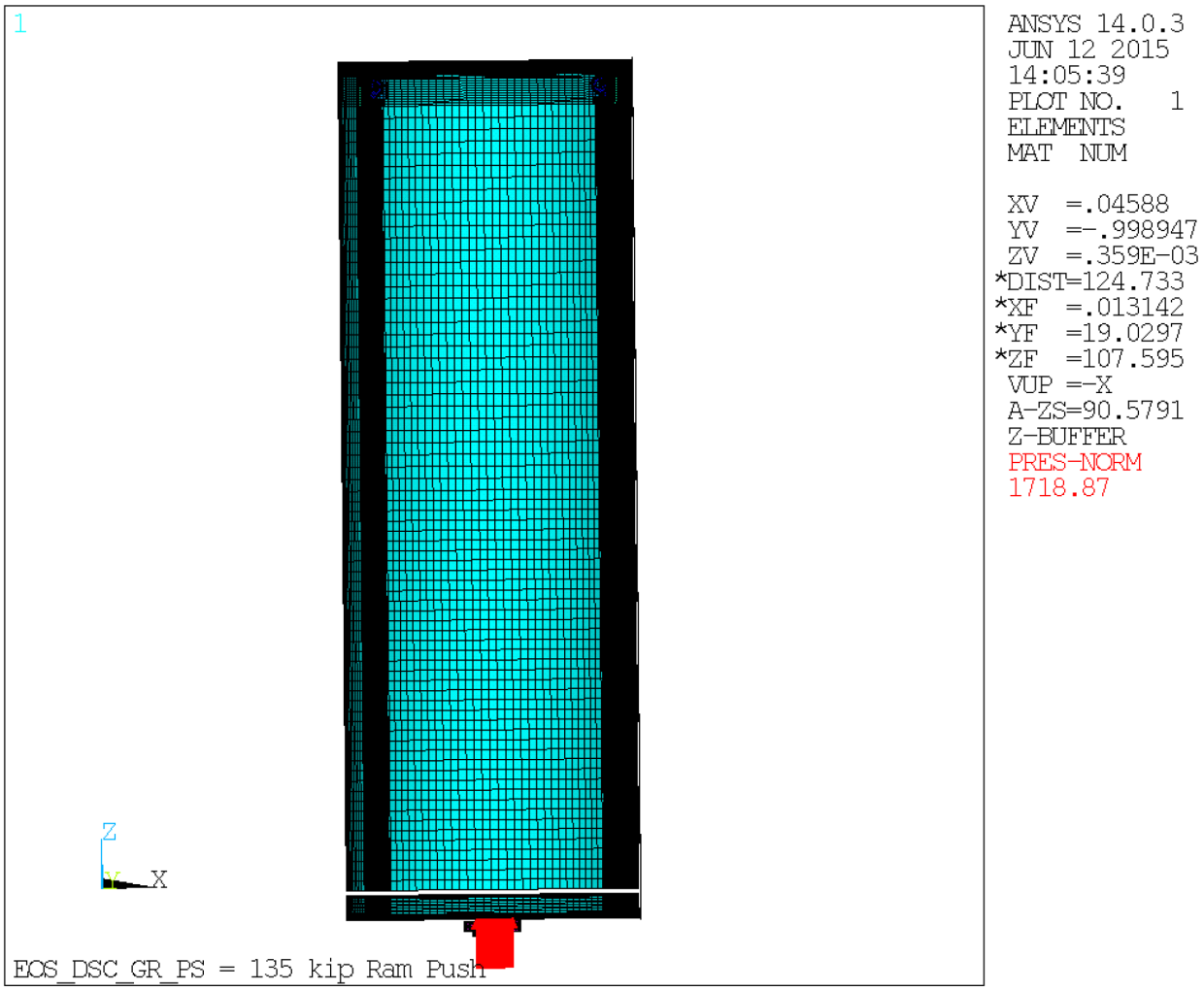

Figure 3.9.1-10
Push Load with Internal Pressure

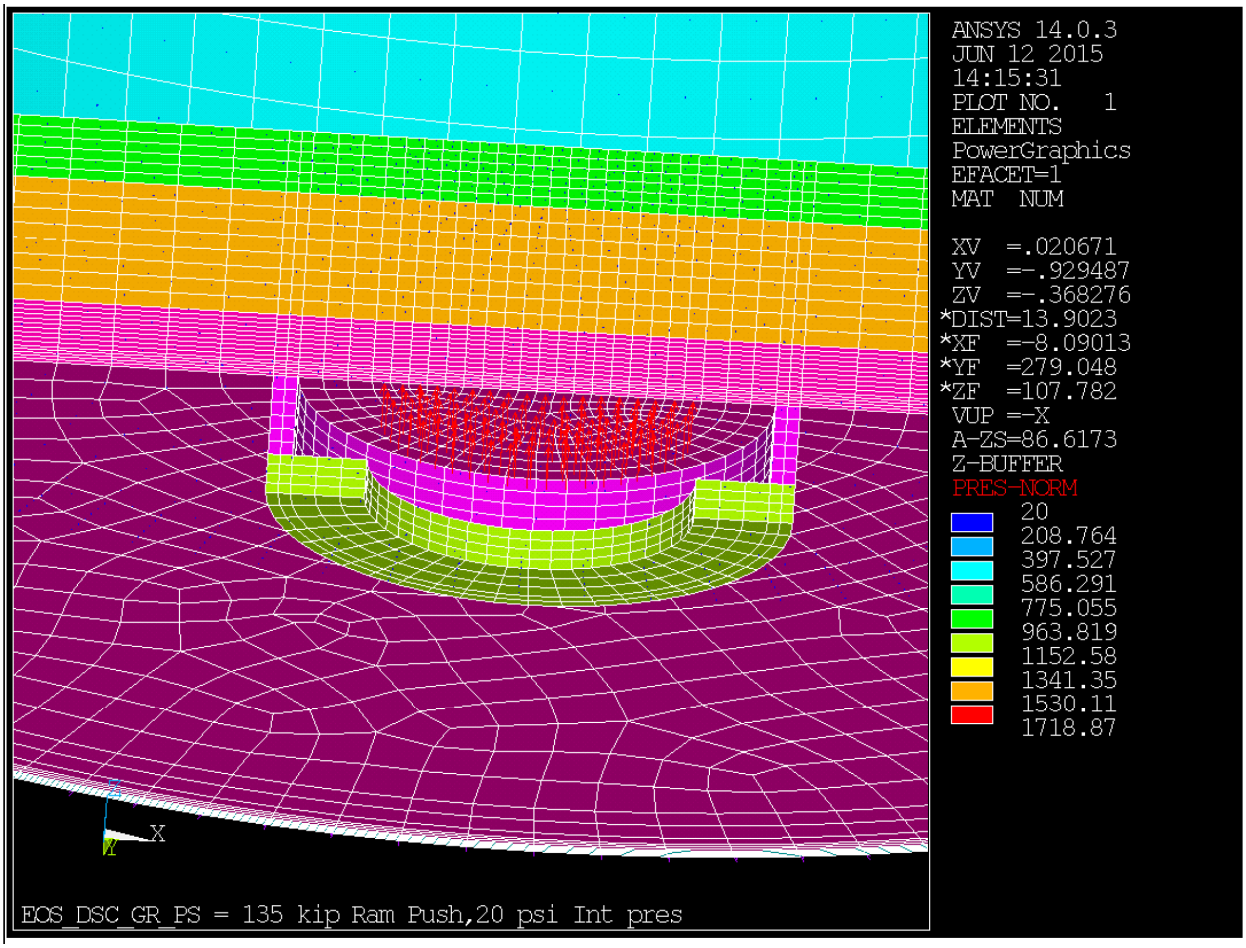

Figure 3.9.1-10a
Push Load with Internal Pressure Detail

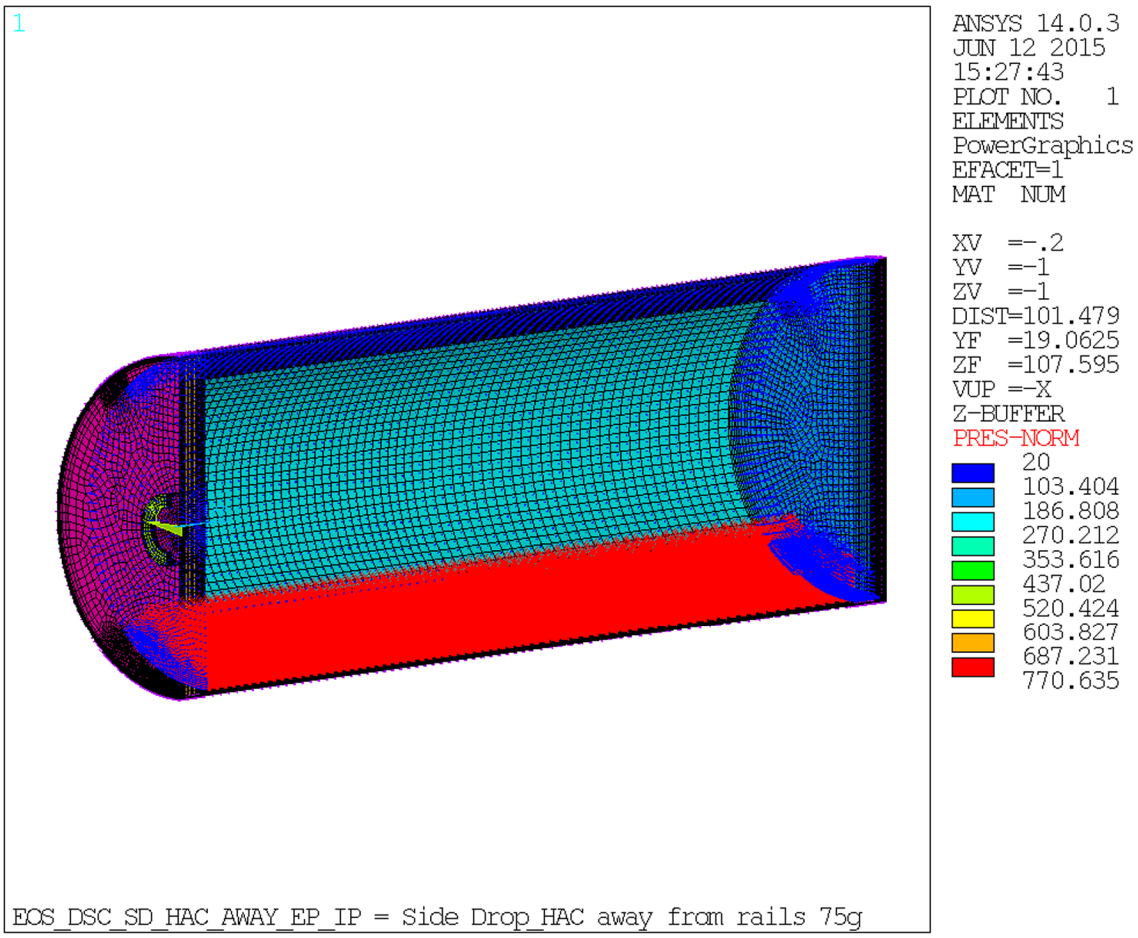

Figure 3.9.1-11
Side Drop Away from Cask Rail

Note: Internal pressure of 20 psi is applied within the pressure boundary. The magnitude of internal pressure is very small compared to canister internals' uniform pressure load and therefore is not noticeable.

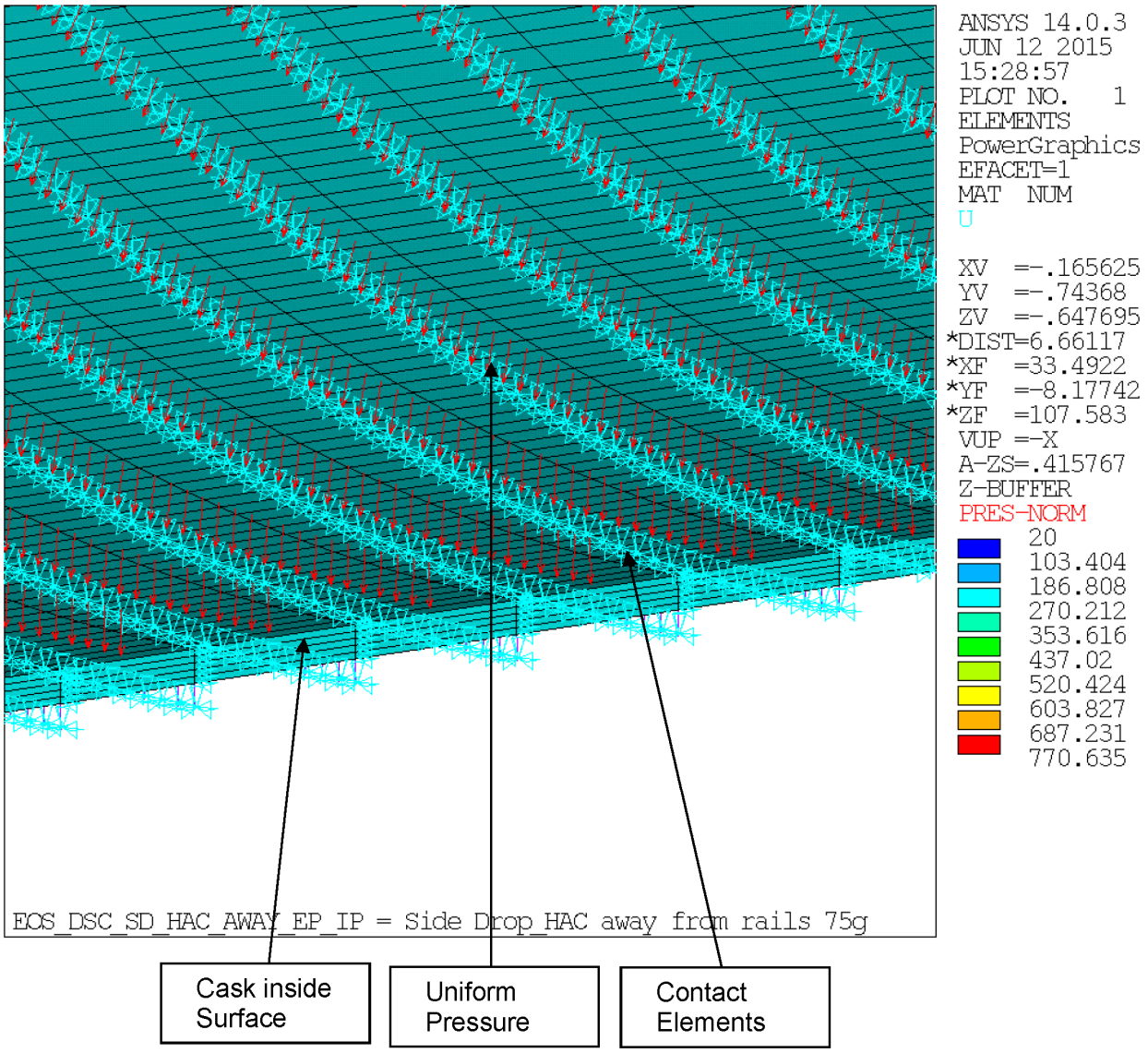

Figure 3.9.1-11a
Side Drop Away from Cask Rail– Boundary Condition Details

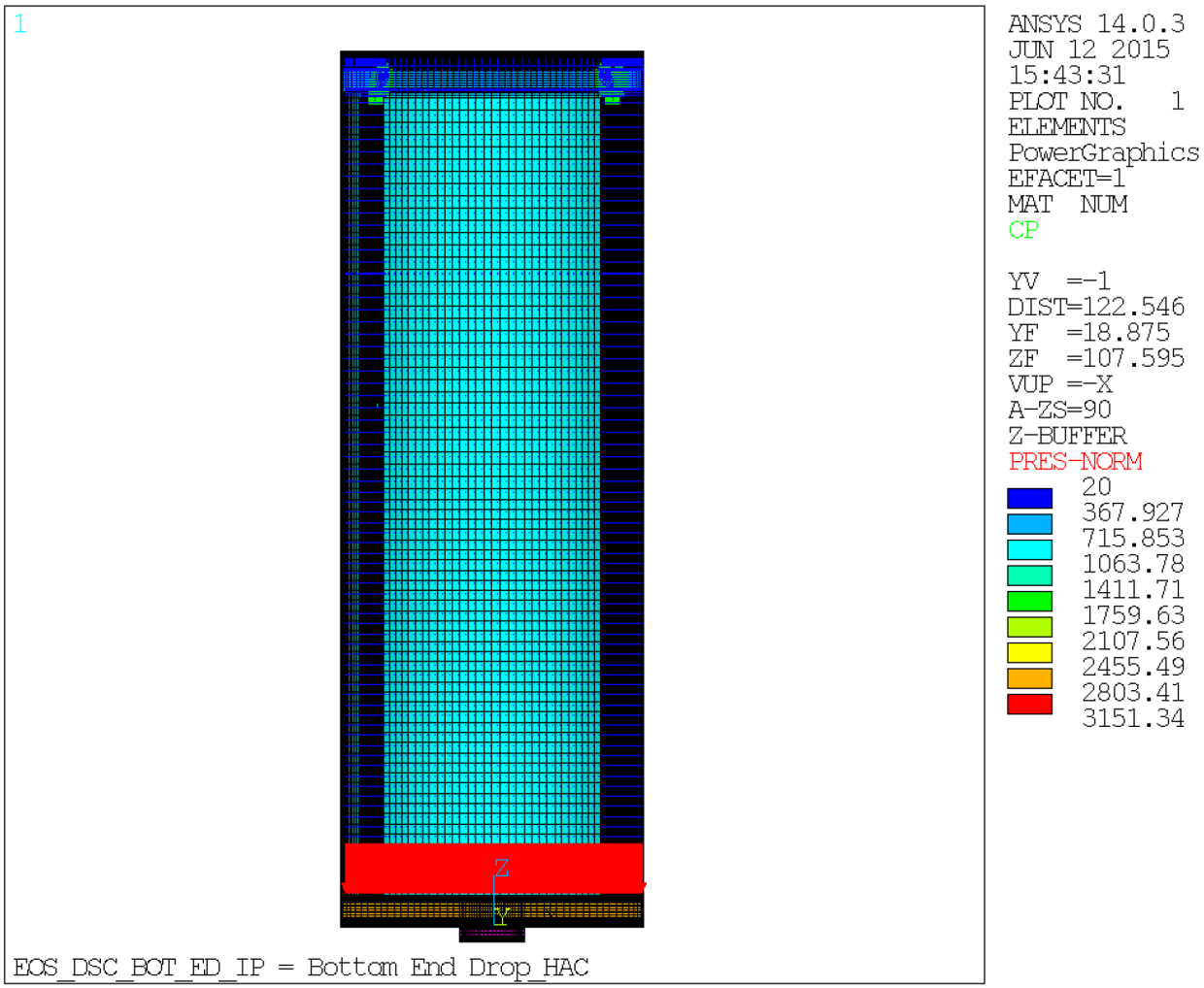

Figure 3.9.1-12
Bottom End Drop Simulation

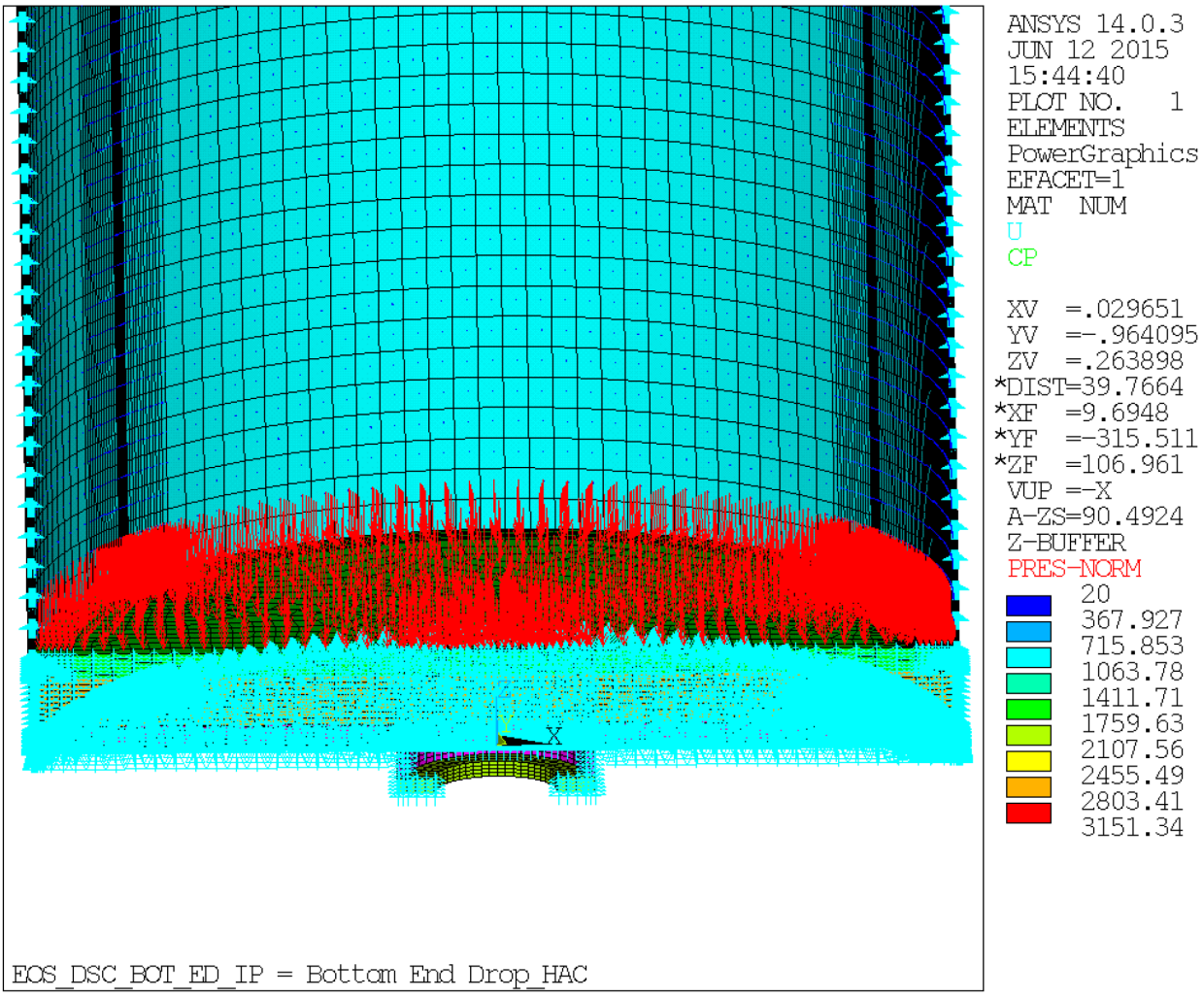

Figure 3.9.1-12a
Bottom End Drop Simulation Detail

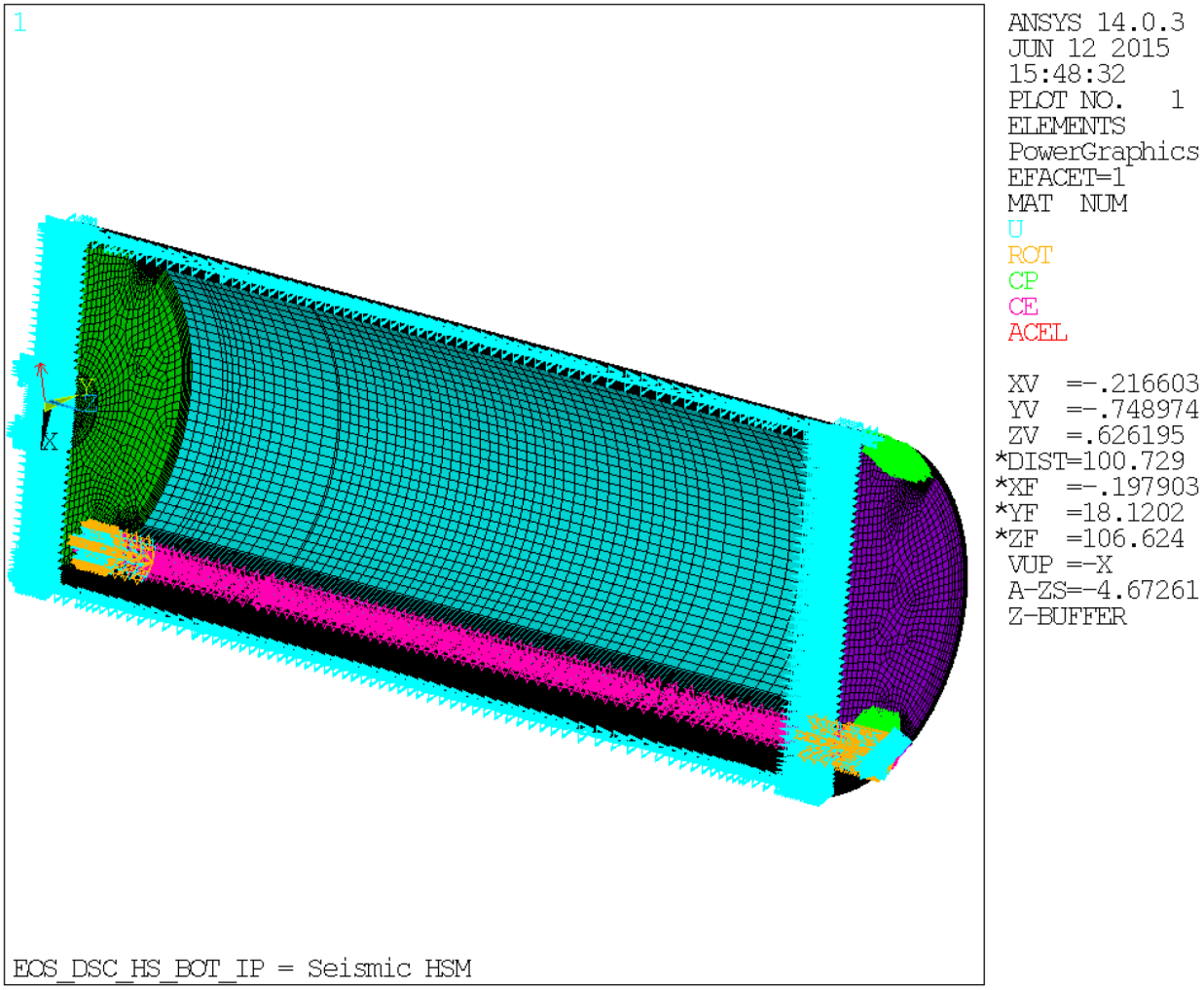

Figure 3.9.1-13
Seismic in EOS-HSM Simulation

Proprietary Information on Pages 3.9.1- 76 through 3.9.1- 78
Withheld Pursuant to 10 CFR 2.390

Figure 3.9.1-17
Not Used

Proprietary Information on Pages 3.9.1- 80 and 3.9.1- 81
Withheld Pursuant to 10 CFR 2.390

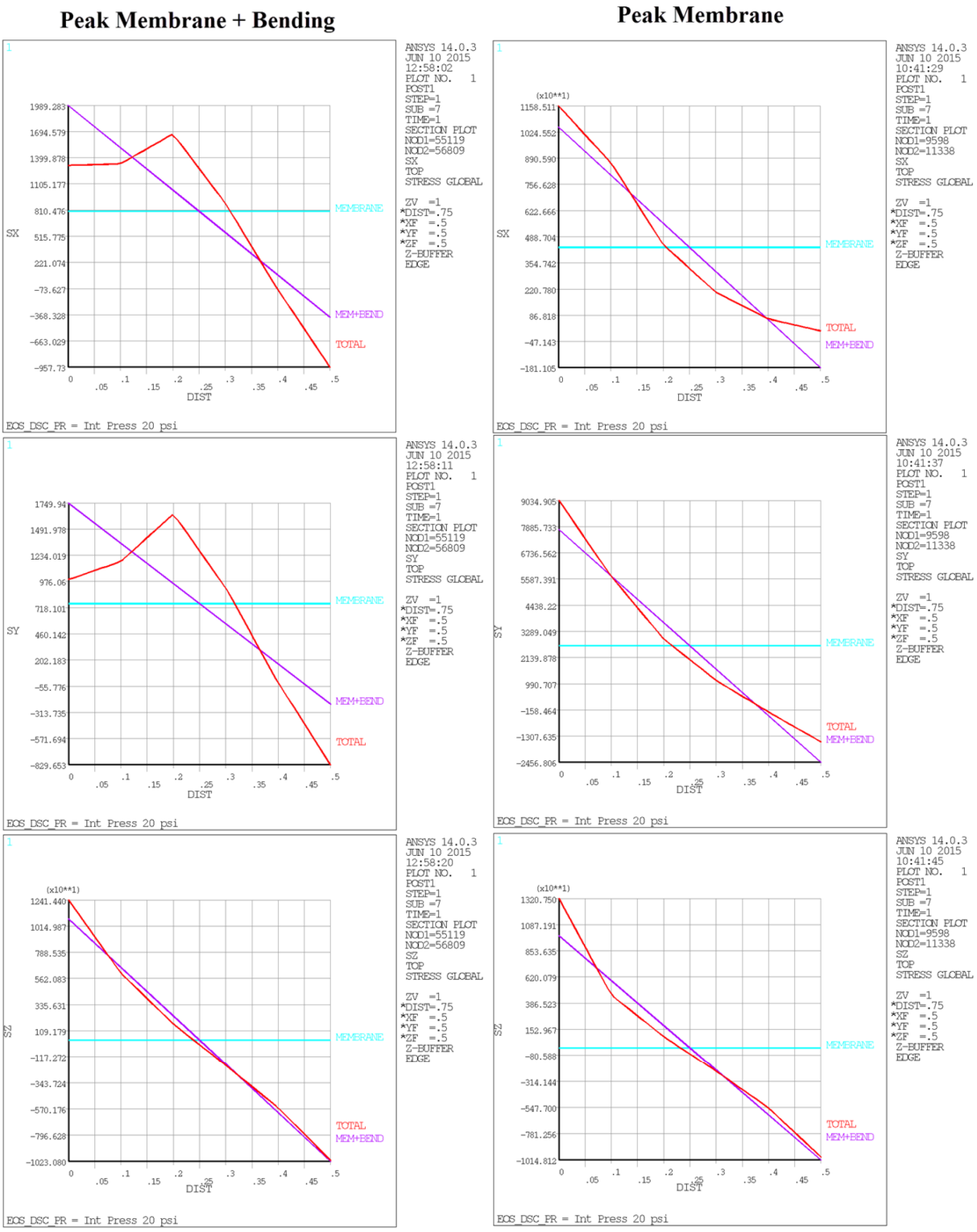

Figure 3.9.1-20
Maximum Linearized Component stresses for Internal Pressure (Normal) Load Case

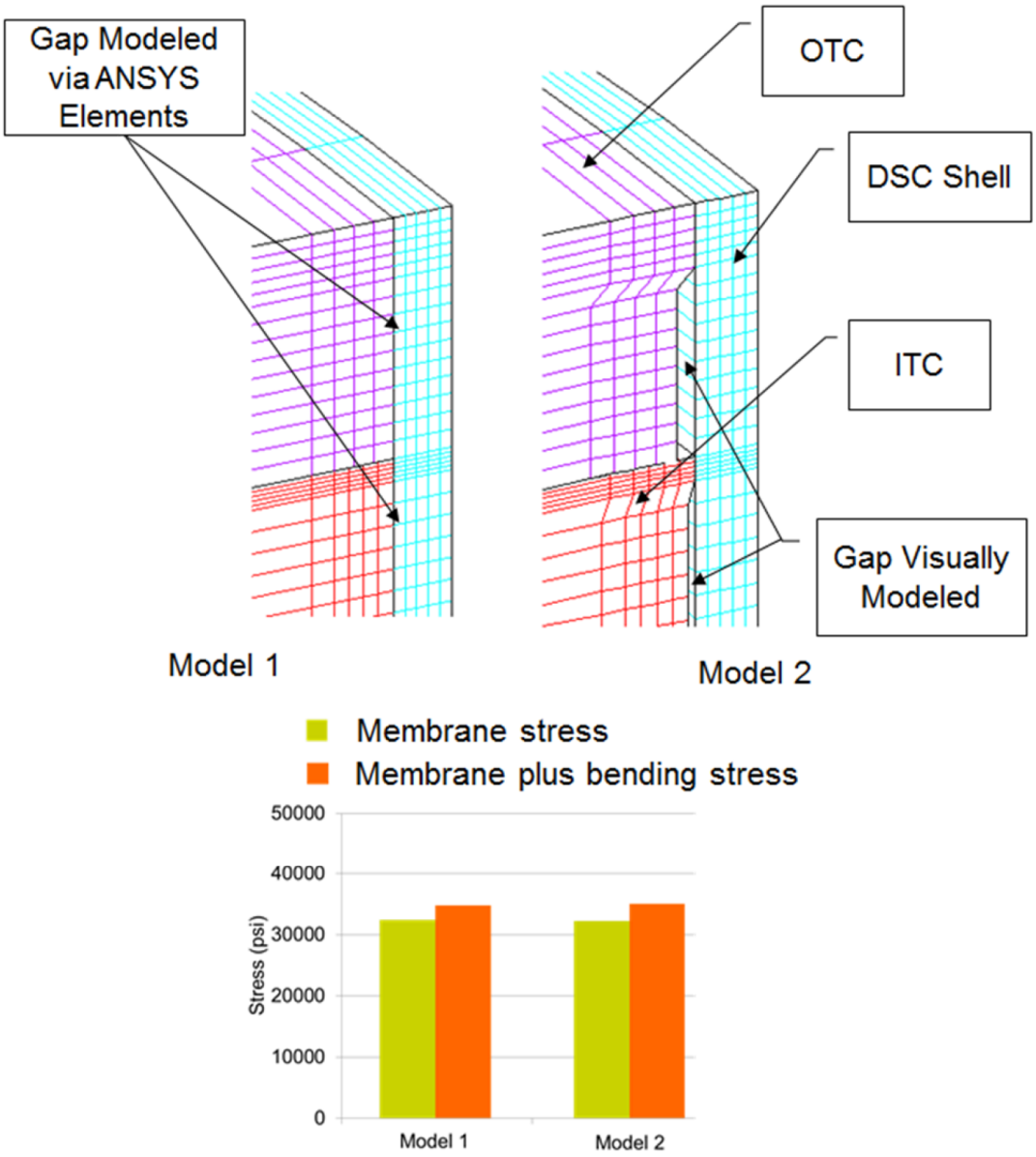

Figure 3.9.1-21
Mesh Sensitivity Study 01 – Models and ITCP Weld Stresses

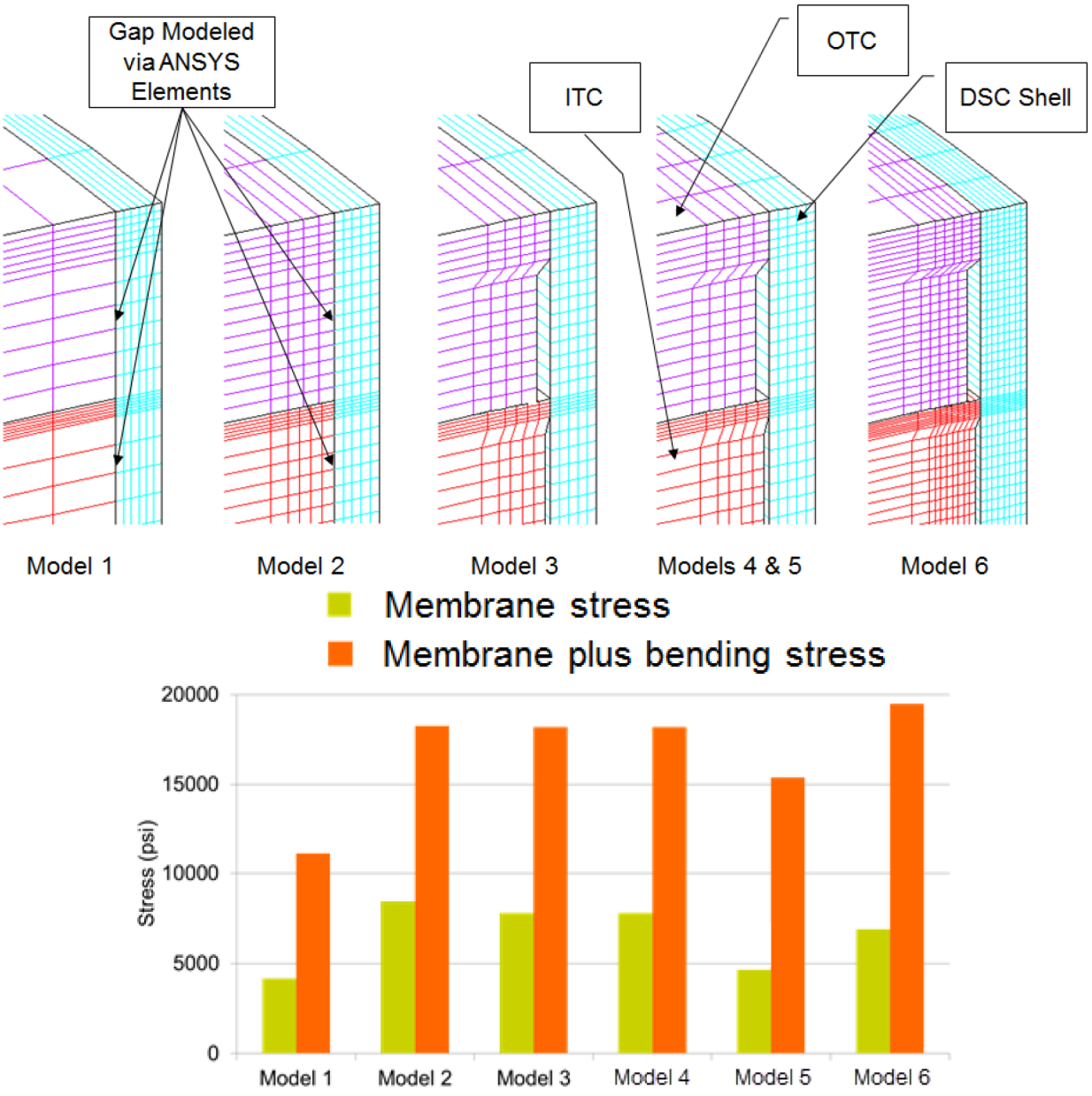

Figure 3.9.1-22
Mesh Sensitivity Study 02 – Models and ITCP Weld Stresses

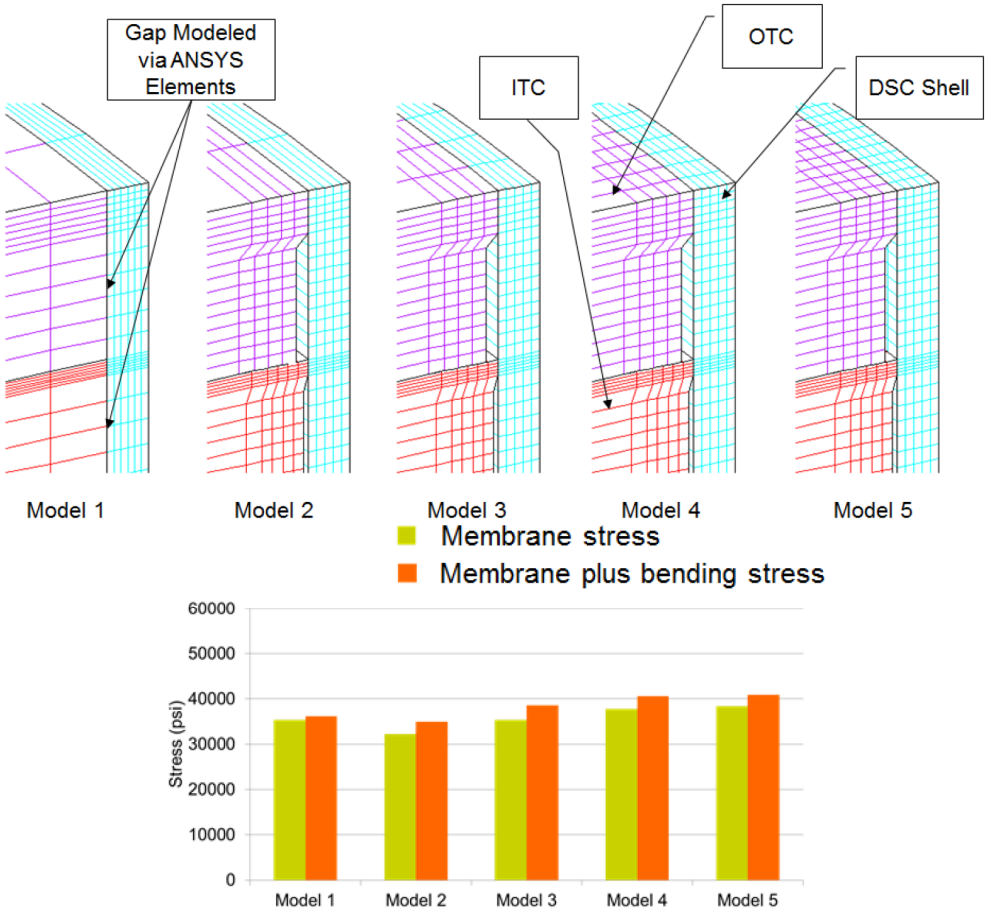

Figure 3.9.1-23
Mesh Sensitivity Study 03 – Models and ITCP Weld Stresses

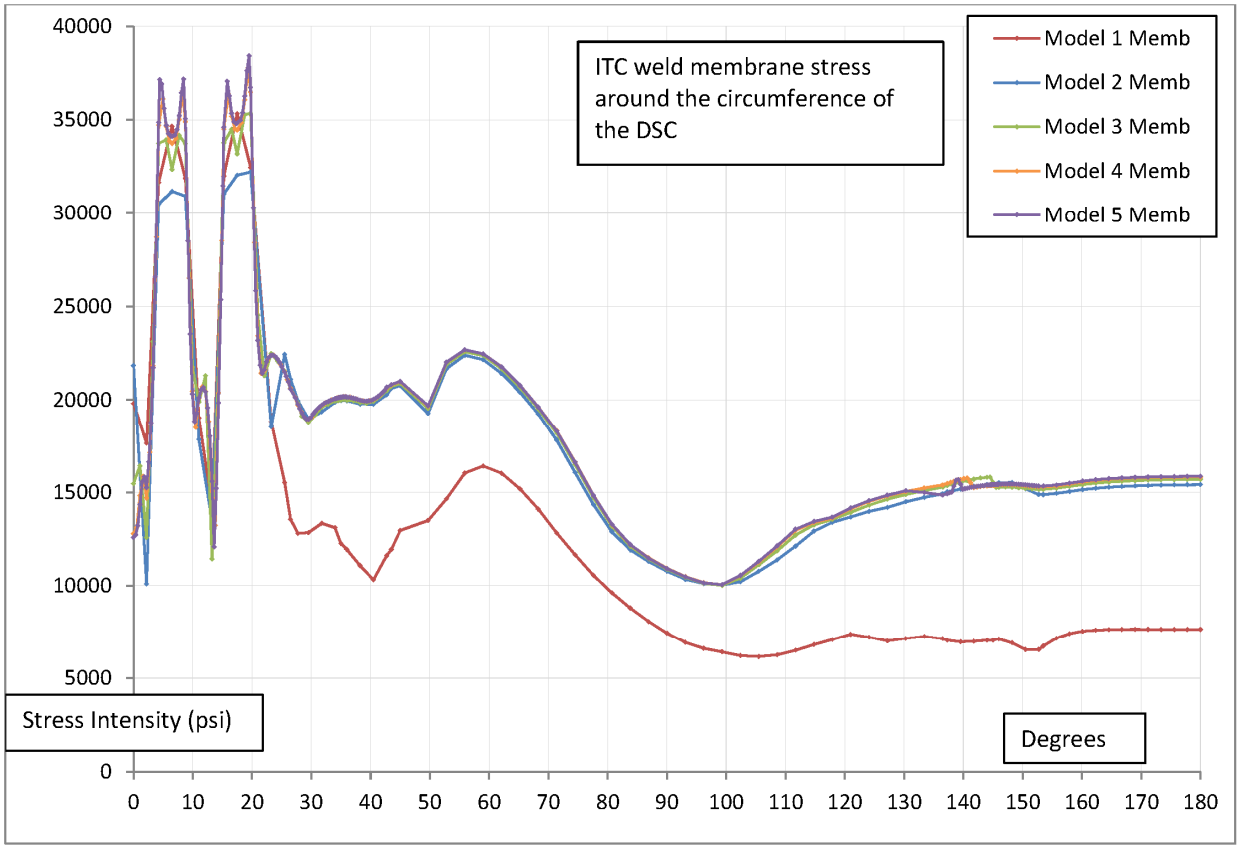

Figure 3.9.1-23a
Membrane Stresses around the Circumference within the ITCP Weld

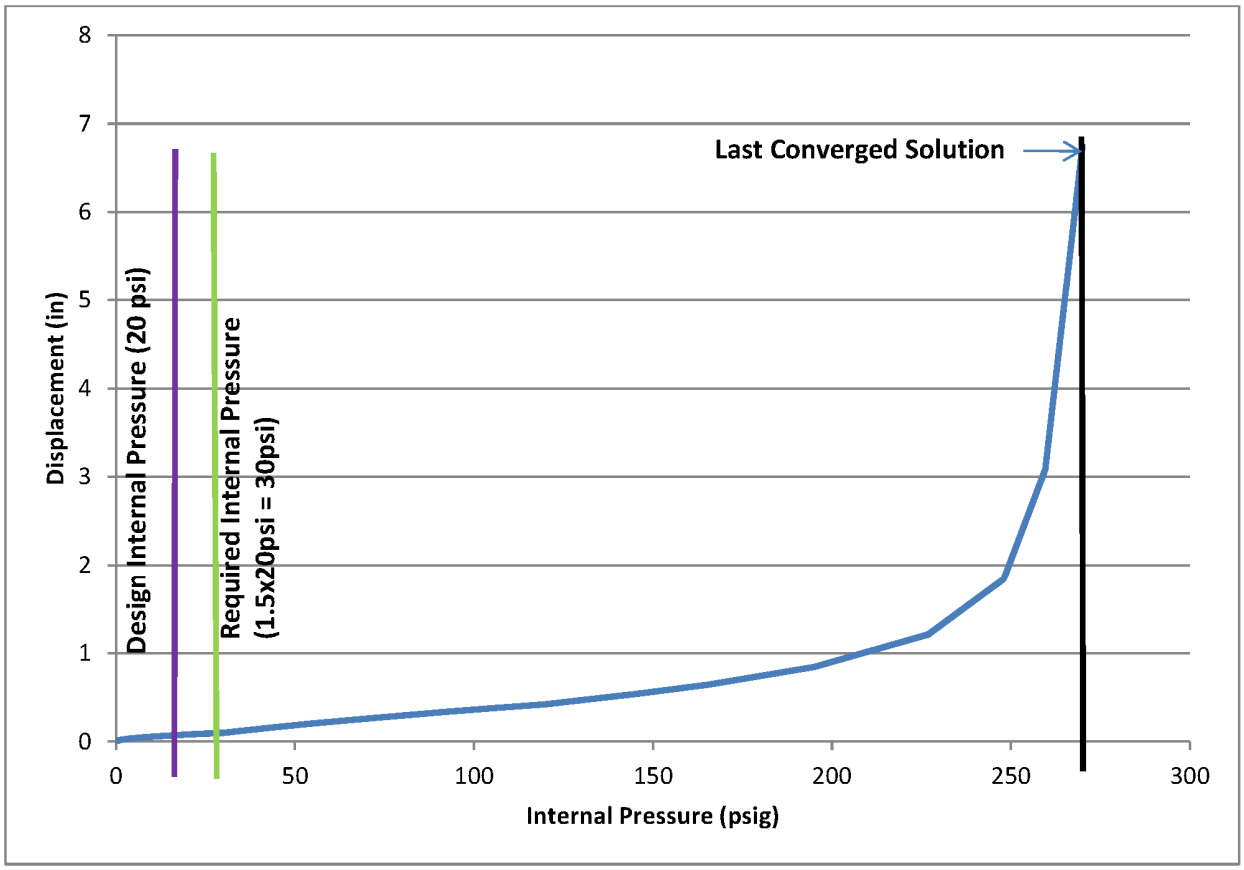

Figure 3.9.1-24
Limit Load – Load vs. Deflection – Internal Pressure

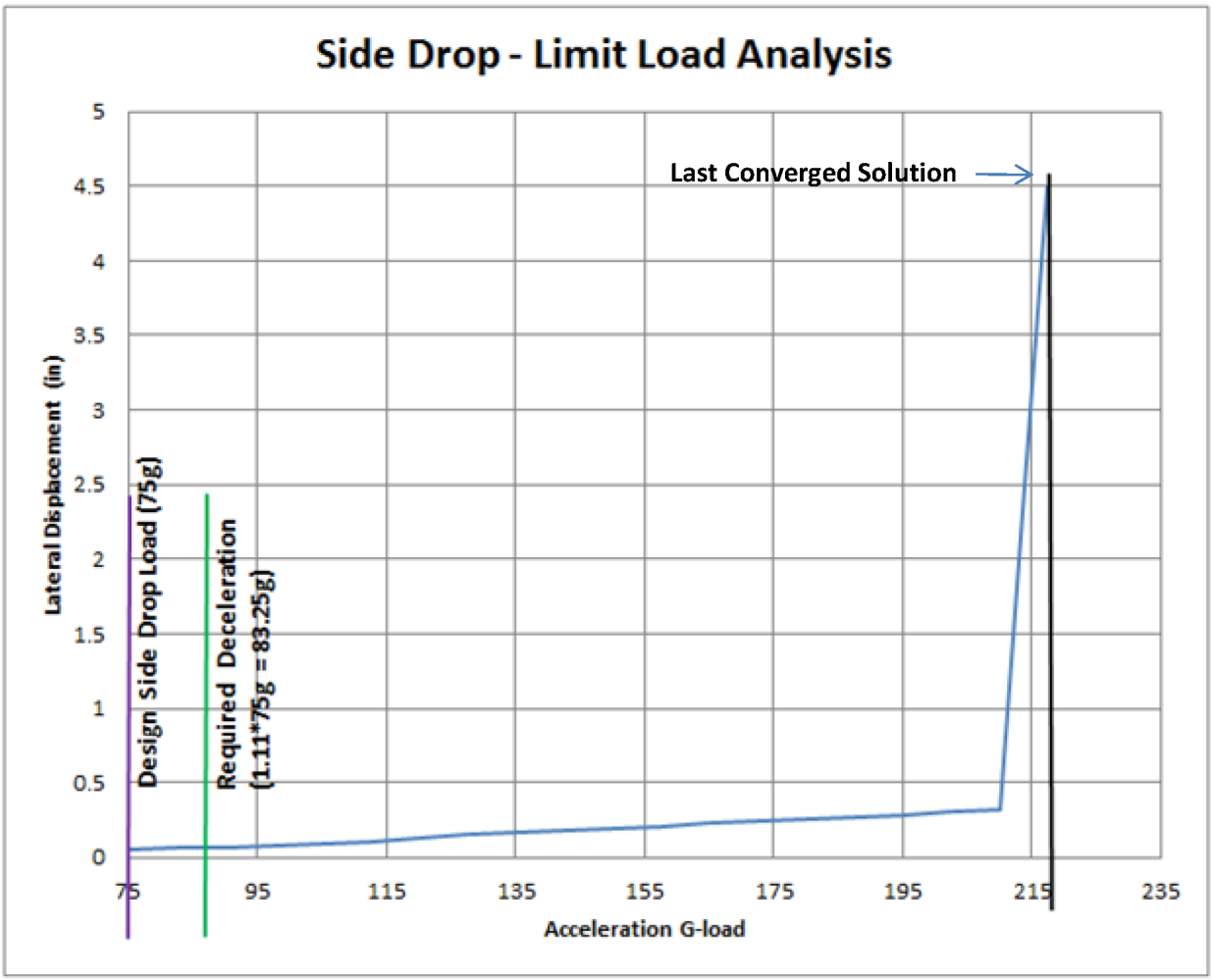

Figure 3.9.1-25
Limit Load – Load vs. Deflection – Side Drop Acceleration

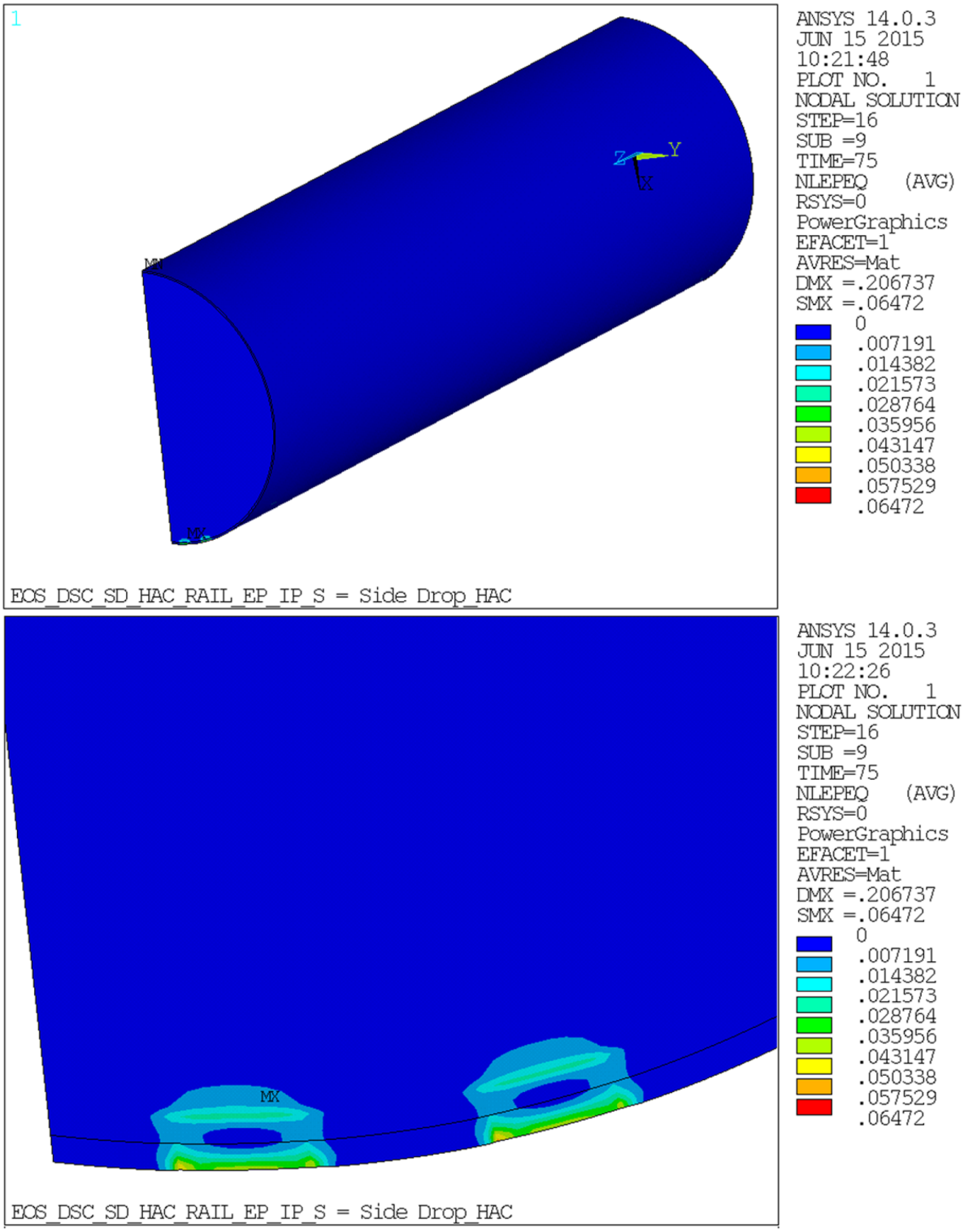

Figure 3.9.1-26
Equivalent Plastic Strain at 75g Side Drop Load for Strain Criteria Analysis

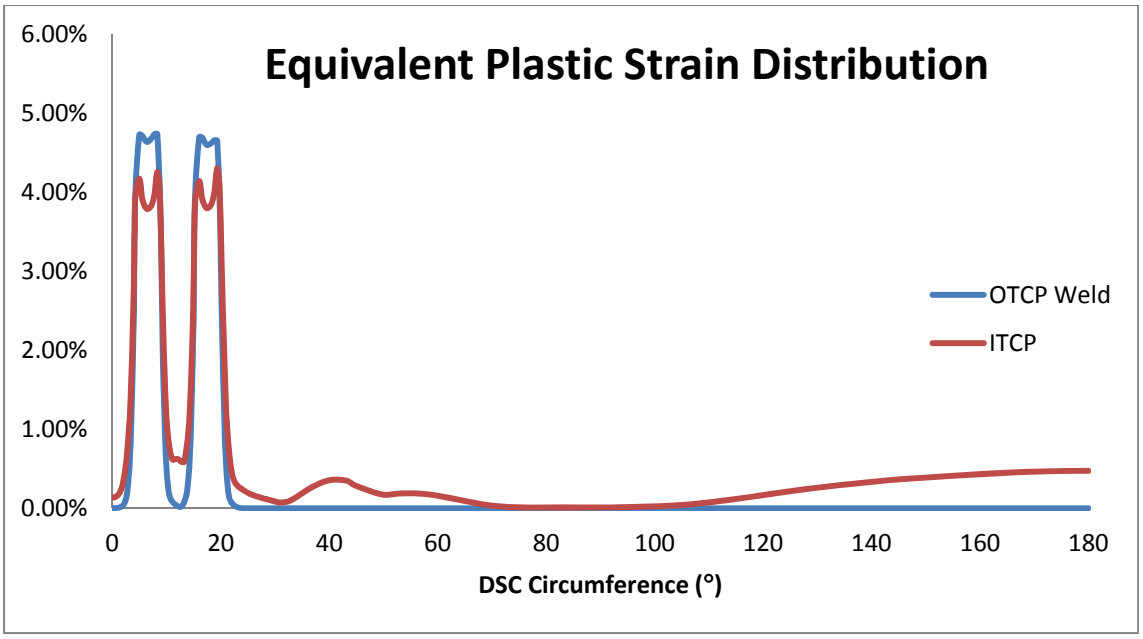

Figure 3.9.1-27
OTCP and ITCP Confinement Weld Equivalent Plastic Strain Distribution for Strain Criteria Analysis

CHAPTER 6
SHIELDING EVALUATION

Table of Contents

List of Tables

List of Figures

6. SHIELDING EVALUATION

The EOS system is designed to store intact pressurized water reactor (PWR) and boiling water reactor (BWR) fuel assemblies (FAs) within the EOS-37PTH dry shielded canister (DSC) and EOS-89BTH DSC, respectively. The transfer casks (TCs) EOS-TC108 and EOS-TC125/135 are used to transfer the EOS-DSC to the EOS horizontal storage module (EOS-HSM). Normal and off-normal condition, near-field dose rates are presented in this chapter for the EOS-TC and EOS-HSM. Detailed three-dimensional dose rate calculations are performed to determine the dose rate fields around the EOS-TCs during loading, decontamination, welding, drying, and transfer operations. Detailed three-dimensional dose rate calculations are also performed to determine the dose rate fields around an EOS-HSM. These near-field dose rates are used as input to the dose assessment documented in Chapter 11, Radiation Protection.

The methodology, source terms, and dose rates presented in this chapter are developed to be reasonably bounding for general licensee implementation of the EOS System. These results may be used in lieu of near-field calculations by the general licensee, although the inputs utilized in this chapter should be evaluated for applicability by each site. Site-specific EOS-TC and EOS-HSM near-field calculations may be performed by the general licensee to modify key input parameters.

Compliance with 10 CFR 72.106 is demonstrated in this chapter for a loss of neutron shield accident for a single EOS-TC. Further, site dose calculations for an array of EOS-HSMs under normal, off-normal, and accident conditions are documented in Chapter 11, based on the near-field EOS-HSM results presented in this chapter. Because the number and arrangement of EOS-HSMs and the distance to the site boundary is site-specific, compliance with 10 CFR 72.104 and 10 CFR 72.106 for an array of EOS-HSMs can only be demonstrated using a site-specific calculation. Inputs for the site dose calculations developed in the current chapter may be directly used as input to a site-specific dose calculation by the general licensee.

6.1 Discussions and Results

The following is a summary of the methodology and results of the shielding analysis of the EOS system. More detailed information is presented in the body of the chapter.

The EOS-37PTH DSC stores up to 37 PWR FAs, while the EOS-89BTH stores up to 89 BWR FAs. Each EOS-DSC is configured into three heat load zones in order to optimize the system performance for both thermal and shielding considerations. The bounding heat load zoning configurations for fuel qualification are provided in Figure 6-1 and Figure 6-2 for PWR and BWR fuel, respectively. Fuel to be stored is limited by the decay heat and minimum cooling times provided with these figures.

Source Terms

The ORIGEN-ARP module of the Oak Ridge National Laboratory (ORNL) SCALE6.0 code package [6-1] is used to develop reasonably bounding gamma and neutron source terms. [

]

Control components (CCs) are allowed to be stored within a PWR FA. Examples of CCs include burnable poison rod assemblies (BPRAs) and thimble plug assemblies. Control components typically have a Co-60 source because of its light element activation, which contributes substantially to the dose rates. The CC source term is provided in Table 6-37. CCs should be limited as follows:

- Zones 1, 2, and 3: 308 Ci Co-60 per CC in the active fuel region
- Zones 1 and 2: 63.0 Ci Co-60 per CC in the combined plenum/top region
- Zone 3: 24.3 Ci Co-60 per CC in the combined plenum/top region

BWR fuel does not include CCs other than the fuel channel, which is conservatively included in the source term. The BWR fuel channel is fabricated from zirconium alloy and does not require a Co-60 limit because the contribution to the source term from the fuel channel is negligible.

Dose Rates

The Monte Carlo transport code, MCNP5 [6-5], is used to compute dose fields around the EOS-TCs and EOS-HSM using detailed three-dimensional models for the following normal configurations:

- EOS-37PTH DSC inside the EOS-TC108
- EOS-37PTH DSC inside the EOS-TC125/135
- EOS-37PTH DSC inside the EOS-HSM-Short
- EOS-89BTH DSC inside the EOS-TC108
- EOS-89BTH DSC inside the EOS-TC125/135
- EOS-89BTH DSC inside the EOS-HSM-Medium

The EOS-TC125 and EOS-TC135 provide equivalent shielding, but accommodate different DSC lengths. The EOS-TC135 is used only with the EOS-37PTH DSC. The EOS-TC125 and EOS-TC135 designs are bounded by the same Monte Carlo N-particle (MCNP) model and are referred to in this chapter as EOS-TC125/135. The EOS-TC108 offers less shielding than the EOS-TC125/135 and features a removable neutron shield. The neutron shield is removed for fuel loading and attached subsequent to fuel loading. The neutron shield for the EOS-TC125/135 is integral to the cask and cannot be removed.

The EOS-37PTH and EOS-89BTH DSCs are custom-built for the fuel to be stored and, therefore, do not have a standard length. BWR fuel is typically longer than PWR fuel, so the EOS-89BTH DSC is longer than the EOS-37PTH DSC in the MCNP models. To accommodate the various DSC lengths, three versions of the EOS-HSM are available: short, medium, and long. In the EOS-HSM models, the EOS-37PTH DSC is paired with the EOS-HSM-Short, while the EOS-89BTH DSC is paired with the EOS-HSM-Medium, as these are the smallest EOS-HSMs that can accommodate the modeled EOS-DSCs.

All EOS-37PTH DSC calculations conservatively include both the FA and CC sources. BWR fuel does not include CC, other than the fuel channel, which is conservatively included in the source term.

[

]

Based on the near-field dose rates calculated for the EOS-TCs, a dose assessment is performed for the EOS-TC loading operation. This dose assessment is documented in Chapter 11.

[

]

The shielding effectiveness of the EOS-TC and EOS-HSM is not impacted by any off-normal events. Two accident events have been identified:

- Loss of neutron shielding for the EOS-TCs
- Loss of EOS-HSM outlet vent covers due to a tornado or missile event

[ ]

MCNP cases are developed for the EOS-HSM in which the vent covers are absent. The EOS-HSM accident increases the average dose rate on the roof of the module to 7400 mrem/hr. The fluxes and dose rates on the surface of the EOS-HSM in an accident condition are used as input to an accident site dose calculation documented in Chapter 11.

6.2 Source Specification

Design basis source terms for PWR and BWR fuels are developed in this section. The source terms are developed to be reasonably bounding consistent with the limits on fuel qualification. A site-specific analysis must evaluate the site-specific used fuel to be stored and determine if the parameters utilized in the FSAR analysis are bounding and appropriate. Site-specific source terms may be different than the source terms presented herein. However, the source terms presented in this chapter were developed to bound most used fuels and will result in reasonably bounding dose rates.

Fuel types that are authorized for storage are provided in Chapter 2. These fuel types may be divided into PWR and BWR fuel types. The list of authorized fuels is summarized below.

PWR

- Westinghouse (WE) 14x14 class
- WE 15x15 class
- WE 17x17 class
- Babcock & Wilcox (B&W) 15x15 class
- Combustion Engineering (CE) 14x14 class
- CE 15x15 class
- CE 16x16 class

BWR

- 7x7 lattice array type
- 8x8 lattice array type
- 9x9 lattice array type
- 10x10 lattice array type

[

]

[

]

6.2.1 Computer Programs

Source terms are generated using the ORIGEN-ARP module of SCALE6.0. ORIGEN-ARP is a control module for the ORIGEN-S computer program. ORIGEN-ARP allows a simplified input description that can rapidly compute source terms and decay heat compared to a full two-dimensional SCALE6.0/TRITON calculation.

Prior to using ORIGEN-ARP, detailed two-dimensional models of the design basis PWR and BWR FAs are developed in TRITON using the FA design data in Chapter 2. TRITON is used to generate ORIGEN-ARP data libraries as a function of burnup and enrichment. These libraries are collapsed from the ENDF/B-VII 238-group cross section library and are used by ORIGEN-ARP to compute the source terms.

ORIGEN-ARP uses interpolated cross section libraries to generate source terms that are essentially equivalent to the detailed TRITON runs. TRITON has been benchmarked against experimentally measured isotopes and results in excellent agreement with the measured data in ORNL/TM-2010 SCALE 5.1 [6-2]. As part of the code validation, the TRITON benchmark cases from SCALE 5.1 are rerun using the ENDF/B-VII 238-group cross section library. The isotopes important for shielding for which benchmark data are available include Cs-137/Ba-137m, Cs-134, Eu-154, Ce-144/Pr-144, Ru-106/Rh-106, Sr-90/Y-90, and Cm-244. The average ratio of the measured to calculated concentration for these nuclides is close to unity, indicating that TRITON/ORIGEN-ARP is an acceptable program for source term generation.

6.2.2 PWR and BWR Source Terms

[

]

Sources are developed for a variety of different enrichments. For a particular U-235 enrichment, the uranium fuel loading is distributed according to the following relationship from the SCALE 6.0 manual:

- wt. % U-234 = 0.0089 * wt. % U-235
- wt. % U-236 = 0.0046 * wt. % U-235
- wt. % U-238 = 100 – wt. % U-234 – wt. % U-235 – wt. % U-236

The EOS-DSC baskets are zoned by heat load. Heat load zoning allows hotter FAs, which generally have larger neutron and gamma source terms, to be placed in the inner zones and be shielded by FAs in the outer zone. The heat load zoning configurations conservative for shielding analysis for the EOS-37PTH and EOS-89BTH DSCs are shown in Figure 6-1 and Figure 6-2, respectively. The EOS-TC108 and EOS-TC125/135 have different heat load zone configurations because the EOS-TC125/135 is more heavily shielded than the EOS-TC108 and can therefore be loaded with stronger sources.

Because the FAs are zoned by heat load, it is necessary to develop source terms for each zone. Candidate sources are developed for high burnup (62 GWd/MTU), medium burnup (50 GWd/MTU) and lower burnup (40 GWd/MTU) fuel. Cooling time is selected so that the decay heat meets or exceeds the heat load limit for each zone. Because the cooling time required at these burnups is generally much larger than the minimum allowed cooling time for each zone, the burnup that results in a cooling time that matches the minimum cooling time for each zone is also determined. From these four candidate burnup/cooling time combinations, a bounding source for each zone is selected.

The EOS-TC108 and EOS-TC125/135 feature reduced lead thickness next to the top nozzle region of the fuel assembly. For this reason, the maximum dose rate at the side of the EOS-TC occurs next to the top nozzle rather than the active fuel. The dose rate at this location is due almost entirely to Co-60 in the top nozzle and plenum regions of the FA. Therefore, to be conservative, the burnup/enrichment/cooling time combination that maximizes Co-60 activity is used to develop the top nozzle, plenum, and bottom nozzle sources. The computed Co-60 activity for each burnup/enrichment/cooling time is provided in the last column of Table 6-8 and Table 6-9 and represents the total Co-60 present in the FA. These Co-60 activities are only used for ranking the sources. For the active fuel region, the burnup/enrichment/cooling time combination that maximizes dose rate next to the active fuel is used to develop the active fuel region sources. The final "hybrid" sources are very conservative because the hardware is integral to the FA and the hardware and active fuel cannot be at different burnups/cooling times.

Based on EOS-TC and EOS-HSM dose rates (for the active fuel) and Co-60 activity (for the end hardware), reasonably bounding burnup/enrichment/cooling time combinations are determined. For these burnup/enrichment/cooling time combinations, the sources in the bottom nozzle, active fuel, plenum, and top nozzle are computed using the appropriate light elements from Table 6-5 and Table 6-6.

During an EOS-TC accident, it is postulated that the water in the neutron shield is lost. In this scenario, there is no hydrogenous neutron shield and the neutron dose rate dominates the primary gamma dose rate. Therefore, the highest allowed burnup (62 GWd/MTU) is used in accident calculations with no neutron shield because the neutron source is maximized for high-burnup fuel. In many cases, the normal condition and accident condition sources are the same.

PWR source terms are reported in the following tables:

- PWR sources terms for EOS-TC108: Table 6-10 through Table 6-13
- PWR source terms for EOS-TC125/135: Table 6-14 through Table 6-16
- PWR source terms for EOS-HSM: Table 6-17 through Table 6-19

BWR source terms are reported in the following tables:

- BWR sources terms for EOS-TC108: Table 6-20 through Table 6-22
- BWR source terms for EOS-TC125/135: Table 6-23 through Table 6-26
- BWR source terms for EOS-HSM: Table 6-27 through Table 6-29

In these tables, the "raw" neutron source computed by ORIGEN-ARP is provided, as well as neutron sources that include neutron peaking factors and subcritical neutron multiplication. These factors are derived in Section 6.2.3. The scaled neutron sources are used in the detailed MCNP dose rate calculations. Only the total neutron source magnitude is reported because the Cm-244 spectrum is used in all dose rate calculations for simplicity because the neutron source is almost entirely due to Cm-244 decay. For example, for the 62 GWd/MTU, 10.25 year cooled PWR source, 95% of the neutron source is due to spontaneous fission of Cm-244. Cm-244 is also the dominant neutron source for shorter cooling times. For instance, for a 36.178 GWd/MTU, three-year cooled PWR source, Cm-244 represents 97% of the total neutron source. The effect on the neutron spectrum of neutron source isotopes with shorter half-lives, such as Cm-242 and Cf-252, is negligible.

6.2.3 Axial Source Distributions and Subcritical Neutron Multiplication

ORIGEN-ARP is used to compute source terms for the average assembly burnup. However, an FA will exhibit an axial burnup profile in which the fuel is more highly burned near the axial center of the fuel assembly and less burned near the ends. This axial burnup profile must be taken into account when performing dose rate calculations, as the dose rate will typically peak near the maximum of this distribution.

The PWR axial burnup profile is taken from NUREG/CR-6801 [6-6] for fuel in the burnup range 26-30 GWd/MTU and is provided in Table 6-30. As fuel is more highly peaked for lower burnups, this distribution is more conservative than a flatter high-burnup distribution. The gamma source term varies proportionally to axial burnup, while neutron source terms vary exponentially with burnup by a power of 4.0 to 4.2 [6-7]. Therefore, the burnup profile is used as the gamma axial source distribution, while the neutron axial source distribution is derived as the burnup profile raised to the power of 4.2.

The average value of the neutron source distribution is 1.215, as shown in Table 6-30. This value has a physical meaning, as it is the ratio of the total neutron source from an FA with the given axial burnup profile to an assembly with a flat burnup profile. The neutron source term as computed by ORIGEN-ARP is for a flat burnup profile (average assembly burnup). Therefore, the "raw" PWR neutron source computed by ORIGEN-ARP is scaled by the factor 1.215 to account for the burnup profile.

For clarity, both the gamma and neutron axial source distributions are renormalized to sum to 1.0, as shown in Table 6-30. When normalized in this manner, the source distribution is the fraction of the source in each axial segment. For example, the fraction of the neutron source in axial segment 10 is 0.0781, or 7.81%.

The BWR axial burnup profile is taken from [6-8] for fuel with a burnup of 40.2 GWd/MTU and is provided in Table 6-31. This distribution is highly peaked and is conservative. The BWR gamma and neutron source distributions are derived using the same method used for the PWR source distributions. The average value of the BWR neutron source distribution is 1.232, and the "raw" neutron sources computed by ORIGEN-ARP are increased by this factor to account for the burnup profile.

ORIGEN-ARP does not account for subcritical neutron multiplication. Subcritical neutron multiplication is taken into account by multiplying the neutron source by 1/(1-k), where k is the multiplication factor for the system. When the system is dry, k is low due to the lack of moderation as well as burnup of the fuel. For dry analysis, k is assumed to be 0.40. When the system is wet, such as during decontamination of the EOS-TC, k is larger. For wet analysis, k is assumed to be 0.65. This value of k is reasonable for shielding calculations because the fuel is burned and heavily poisoned. Fresh or lightly burned fuel would have a higher value for k, but fresh or lightly burned FAs have a small neutron source. Because the neutron source increases proportional to the 4.2 power of the burnup, large neutron sources occur only at high burnups, and for such burnups a k of 0.65 is reasonable.

The effect on the neutron source of both the axial source distribution and subcritical neutron multiplication are combined, as shown in the source term tables (Table 6-10 and Table 6-29). For PWR sources, the "raw" ORIGEN-ARP neutron sources are scaled by 1.215/(1-0.40) = 2.025 for dry analysis and 1.215/(1-0.65) = 3.471 for wet analysis. For BWR sources, the "raw" ORIGEN-ARP neutron sources are scaled by 1.232/(1-0.40) = 2.053 for dry analysis and 1.232/(1-0.65) = 3.520 for wet analysis.

The only analysis that uses the wet neutron source term is the loading/decontamination stage of the EOS-TCs. After loading/decontamination the EOS-TCs are modeled as dry. No wet neutron sources are provided in the EOS-HSM source term tables because the DSC is always dry when inside the EOS-HSM.

6.2.4 Control Components

Control components may also be included with the PWR FAs. For BWR fuel, the fuel channel and associated attachment hardware is included in the BWR source presented in Section 6.2.2, so it will not be discussed in this section. While CCs do not contain fuel, these items result in a source term, primarily due to activation of the Co-59 impurity in the metal. Allowed CCs are identified in section 2.1 of the Technical Specifications [6-11].

Any other CC type is acceptable if it can be demonstrated that the source term is bounded by the source terms presented in this analysis. Also, the total as-loaded decay heat of the system, including CCs, must be less that the heat load zoning configurations defined in Figure 6-1.

Control components may be grouped into two categories: (1) those that extend into the top, plenum and active fuel regions of the fuel assembly, and (2) those that essentially extend only into the top and plenum regions of the FA. The BPRA is used as a representative CC for category (1) and the TPA is used as a representative CC for category (2). The objective is to use these representative CC types to develop Co-60 activity limits for CCs.

The BPRAs are assumed to be burned in two cycles to a total host FA burnup of 50 GWd/MTU. This represents a limiting burnup because the absorber material is completely depleted for this burnup. TPAs do not contain burnable poisons and may be used in multiple host FAs for very long burnups. A cumulative host FA burnup of 300 GWd/MTU is assumed. However, a TPA is primarily located in the top nozzle and plenum region of the core where the flux is depressed and the “effective” burnup of a TPA is significantly less.

A neutron source may be included in CCs, such as an NSA. Typically, the neutron source from an NSA is negligible compared to the neutron source from spent fuel. However, some neutron sources could have comparable source strength relative to the fuel assemblies. For this purpose, the loading of neutron sources is limited to the interior locations of the EOS-37PTH basket to maximize self shielding; i. e., neutron sources can be loaded in Zone 1 locations only (13 locations per Figure 1).

Representative BPRA hardware masses are available for three BPRA types:

- B&W 15x15
- WE 17x17 Pyrex
- WE 17x17 WABA

The BPRA hardware masses are provided in Table 6-32.

Representative TPA hardware masses are available for three TPA hardware types:

- Westinghouse 17x17
- Westinghouse 14x14 Type 1 and 2

The TPA hardware masses are provided in Table 6-33.

Elemental compositions for Zircaloy-4, Inconel-718, Inconel X-750, and 304 stainless steel are provided in Table 6-3. Note that the source term and dose rate are driven by Co-60, which arises primarily from Co-59 activation and to a much lesser extent from Ni-60 activation via an (n,p) reaction. The remaining light elements have little effect on the source term at the decay times of interest.

The poison is assumed to be Pyrex® (borosilicate glass). The choice of poison material has little effect on the source term or decay heat and is included for completeness. The elemental composition is obtained from [6-9] and is reproduced in Table 6-34.

The plenum and top regions are outside the active core and experience a reduced flux. The ratio of the flux in each region to the active fuel flux is provided in Table 6-4.

The source term and decay heat for the decay times of interest are dominated by Co-60. Co-60 primarily arises through activation of the Co-59 impurity present in the metal. Therefore, the BPRA and TPA hardware that has the largest Co-59 mass in each region is used to prepare the light element inputs. For the BPRA, B&W 15x15 is used for the top and WE 17x17 Pyrex is used for the plenum and active fuel regions. For the TPA, the WE 17x17 is used for all regions.

The source terms are computed using ORIGEN-ARP and the B&W 15x15 library. A separate ORIGEN-ARP input file is developed for each hardware type and region.

For the BPRA, the host FA is burned to 50 GWd/MTU in two cycles. The minimum enrichment is 3.1% based on Table 6-7. The FA loading is 0.492 MTU. The assembly power is 19.68 MW, the irradiation time per cycle is 625 days, and the down time between cycles is 30 days. Decay heat, Co-60 activity, and the gamma source term is requested for a decay time of 10 years.

To account for the reduced flux in the plenum and top regions, the BPRA input masses are scaled by the appropriate flux scaling factor. The ORIGEN-ARP inputs for the three BPRA regions are summarized in Table 6-35.

The methodology for TPAs is slightly different than for BPRAs. The reason is that a TPA may reside in several host FAs for a total host fuel assembly burnup of 300 GWd/MTU. ORIGEN-ARP cannot burn a single FA to such a high burnup. Therefore, rather than apply the flux scaling factors to the input masses, the true masses are input and the flux scaling factors are applied to the FA burnup. The TPA input masses are summarized in Table 6-33. These masses do not include flux scaling factors and are therefore larger than the BPRA input masses.

For the TPA plenum, the effective burnup is 300*0.2 = 60 GWd/MTU, while for the TPA top the effective burnup is 300*0.1 = 30 GWd/MTU. This reduces the cumulative burnup in each region to a value within the bounds of a typical ORIGEN-ARP model.

The TPA irradiation time is input to match the true irradiation time to properly credit Co-60 decay during the irradiation. Assuming a reactor assembly power of 19.68 MW and fuel loading of 0.492 MTU, the irradiation time to achieve a cumulative fuel assembly burnup of 300,000 GWd/MTU is 7,500 days. Because the irradiation time is fixed at 7,500 days, the FA power is selected to give the desired effective burnup in the plenum and top regions. For the top, the assembly power is 1.968 MW to achieve an effective burnup of 30 GWd/MTU. For the plenum, the assembly power is 3.936 MW to achieve an effective burnup of 60 GWd/MTU.

For simplicity of input preparation in the TPA calculation, no credit is taken for down time between cycles (typically assumed to be 30 days). Using approximately 12 cycles to achieve a burnup of 300 GWd/MTU, the conservatism of this assumption is 11*30 = 330 days of uncredited decay time.

Results for Co-60 activity and decay heat for both the BPRA and TPA are summarized in Table 6-36 for a cooling time of 10 years. It is observed that the BPRA source may be used in the active fuel region, as the TPA does not extend into this region. However, the TPA has a larger source than the BPRA in the plenum and top regions due to the high TPA burnup. Decay heat for both is small compared to SFA but must be accounted for during loading. The CC source used in the detailed PWR dose rate calculations is a hybrid CC source that combines the active fuel source of the BPRA with the top/plenum source of the TPA in Zones 1 and 2, but limits Zone 3 to the lower BPRA source. This source is provided in Table 6-37.

The CC source significantly impacts the peak dose rates on the side of the EOS-TC, due to the reduced lead thickness near the top nozzle. Site-specific calculations by the general licensee of CC source terms should limit the computed Co-60 activity to values bounded by the results of this analysis, as follows:

- Zones 1, 2, and 3: 308 Ci Co-60 per CC in the active fuel region
- Zones 1 and 2: 63.0 Ci Co-60 per CC in the combined plenum/top region
- Zone 3: 24.3 Ci Co-60 per CC in the combined plenum/top region

While the specific CC source term presented in Table 6-37 is computed for a decay time of 10 years, this is not a minimum decay time requirement for licensing purposes. The actual CC to be loaded may have a shorter decay time as long as the as-loaded Co-60 activity is less than the limits provided above, and the total EOS-DSC decay heat remains below the applicable limit.

6.2.5 Blended Low Enriched Uranium Fuel

6.2.6 Reconstituted Fuel

Proprietary Information on This Page
Withheld Pursuant to 10 CFR 2.390

6.2.7 Irradiation Gases

During irradiation in a reactor, a FA will generate gases due to fission, alpha decay, and light element activation. The moles of gas generated are needed for subsequent pressure calculations documented in Chapter 4, Section 4.7, and are computed using ORIGEN-ARP. The noble gases (He, Ne, Ar, Kr, Xe, and Rn) are of primary interest as these gases do not react with other elements. The elements H, N, F, and Cl are conservatively assumed to be present in a gaseous state, although these elements may have formed solid compounds and may not be present as a gas. Bromine and iodine are also assumed to be present as a gas because the boiling points of these elements are low. Oxygen is not treated as a gas because it is present primarily in the compound UO_2.

The quantities of irradiation gases increase with burnup. Therefore, the quantity of gas is maximized for a burnup of 62 GWd/MTU. Most of the gases generated are stable isotopes. However, due to alpha decay of actinides present in spent fuel, the quantity of helium slowly increases with time. To obtain a bounding value for helium buildup due to alpha decay, 100 years of decay is assumed.

Integral fuel burnable absorber rods (IFBA) are used in some Westinghouse PWR designs. IFBA contains B-10, which results in helium gas generation due to the reaction B-10 + n → Li-7 + He-4. While the design basis B&W 15x15 FA does not contain IFBA, the effect of an IFBA FA is conservatively included by adding 450 g boron to the PWR input file.

Control components also may result in helium gas generation, primarily due to B-10 activation. No actinides or fission products are present in the CCs, so the quantity of gas is smaller than spent fuel. Because the BPRA contains boron while the TPA does not, the BPRA bounds the TPA for gas generation. BPRA data is summarized in Table 6-32. The B&W 15x15 BPRA contains poison in the form B_4C-Al_2O_3, typically up to 5% B_4C, while the WE 17x17 Pyrex design utilizes Pyrex poison. To conservatively bound these designs and potentially other designs, the boron mass is input as 450 g.

Irradiation gases are computed for (1) the design basis PWR fuel including CCs (without IFBA), (2) the design basis PWR fuel with IFBA (without CCs), and (3) the design basis BWR fuel. The moles of each isotope of interest are reported in Table 6-40 for a decay time of 100 years. The PWR FA with CCs (without IFBA) has 59.0 moles of gas (49.4 moles from the FA and 9.6 moles from CCs). For a PWR fuel assembly with IFBA (without CCs), there are 57.7 moles of gas. Therefore, the bounding PWR value is 59.0 moles of gas. For BWR fuel, the total gas is 20.6 moles.

Due to the helium generated from B-10 activation, the following restrictions are in effect for PWR fuel in order to limit the total moles of gas generated:

- If a FA does not contain IFBA, it may include any CC type.

- If a FA contains IFBA, it cannot include CCs that had an initial boron loading (e.g., BPRAs). Control components that do not contain initial boron (e.g., TPAs) may be included with an IFBA assembly.

The quantity of fission gas generated in a FA is proportional to the fuel loading. The moles of gas for the design basis PWR FA are based on a fuel loading of 0.492 MTU. However, there are shorter FAs with smaller fuel loadings and longer FAs with larger fuel loadings. The EOS-DSC may be shorter or longer depending on the length of fuel, and thus the free volume within the DSC changes with fuel length/loading. For the pressure calculation (Section 4.7), FAs are binned into short, medium, and long groups.

The short group has an unirradiated FA length < 157 inches. The medium group has an unirradiated FA length between 157 and 190 inches, while the long group has an unirradiated FA length > 190 inches. The design basis PWR fuel has an unirradiated fuel length of 165.76 inches, which places it in the medium group.

For the pressure calculation the medium length FAs bound the long fuel assemblies. There are three short PWR FAs, CE 14x14 Fort Calhoun, CE 15x15 Palisades, and Exxon/ANF 15x15 CE. The maximum fuel loading for the three short FAs is 0.450 MTU. Therefore, the irradiation gas result for the design basis assembly (49.4 moles) may be scaled by 0.450/0.492 = 0.915. The gas from CCs (9.6 moles) is conservatively assumed to be unchanged for the shorter FAs. The bounding quantity of gas for the short PWR assemblies is then 49.4 moles*0.915 + 9.6 moles = 54.8 moles.

Note that the moles of gas presented are only gases generated due to irradiation. Both fuel and CCs will be pre-pressurized with gas (typically helium) when fabricated and the moles of this initial gas is not included.

6.3 Model Specification

MCNP5 is used to perform detailed three-dimensional near-field dose rate calculations for EOS-TCs and EOS-HSMs. All relevant details of the EOS-37PTH DSC, EOS-89BTH DSC, EOS-TC108, EOS-TC125/135, and EOS-HSM are modeled explicitly.

Separate primary gamma and neutron models are developed. The EOS-TC and EOS-HSM neutron models are run in coupled neutron-photon mode so that the secondary gamma dose rate from (n,γ) reactions may be computed. The secondary gamma dose rate from the EOS-TC arises primarily from neutron absorption in the water neutron shield. Secondary gammas from the EOS-HSM are negligible but are computed for completeness.

The treatment of subcritical neutron multiplication is suppressed in MCNP by using the NONU card. This is done because the fuel assemblies are modeled as fresh fuel and homogenized for simplicity, which would cause inaccurate treatment of subcritical neutron multiplication by MCNP. Subcritical neutron multiplication is accounted for in the neutron source magnitude, as discussed in Section 6.2.3.

6.3.1 Material Properties

Basic materials used in the models, such as 304 stainless steel, carbon steel, and concrete, are obtained from PNNL-15870 [6-9] and are summarized in Table 6-41. Not all materials are used in every model. The density of concrete has been conservatively reduced to 2.243 g/cm^3. Simple materials consisting of one element are not listed in Table 6-41. Such materials include lead, which is modeled with a reduced density of 11.18 g/cm^3. Aluminum is used in the basket plates with a density of 2.7 g/cm^3. The metal matrix composite (MMC) poison is modeled as pure aluminum (no boron) with a reduced density of 2.56 g/cm^3.

Borated polyethylene is used at the bottom of the EOS-TC for neutron shielding. Approximately 16% boric acid by weight (B_2O_3) is added to polyethylene so that the material is 5% boron by weight. The atom density of hydrogen is conservatively reduced by 15% to account for potential hydrogen loss due to aging. The borated polyethylene composition used in the EOS-TC models is provided in Table 6-42.

The FAs are homogenized for simplicity. Fuel assemblies are modeled as fresh with a U-235 enrichment of 3%. The enrichment used is arbitrary because fission has been suppressed with the NONU card. Separate homogenization is performed for the bottom nozzle, active fuel, plenum, and top nozzle regions of the FA for both wet and dry conditions. The masses used for the homogenization are obtained from Table 6-1 and Table 6-2 for PWR and BWR fuel, respectively.

Table 6-1 does not include CC masses. For PWR fuel, the CC mass is also included in the plenum and bottom nozzle homogenizations because the CC source is always included in the MCNP models (no CC mass is credited in the active fuel region). As discussed in Section 6.2.4, the CC source is based on the BPRA B&W 15x15 in the top region (Zone 3), BPRA WE 17x17 Pyrex in the plenum region (Zone 3), and TPA WE 17x17 in both the top and plenum regions (Zones 1 and 2). The additional CC mass to be homogenized with the fuel is the minimum masses when comparing these CC types. This results in an additional 2.468 kg SS304 and 0.358 kg Inconel-718 in the top nozzle and an additional 2.85 kg SS304 in the plenum.

For BWR fuel, the mass of the channel is conservatively ignored because the channel may not be present. In the wet models, water with a density of 0.958 g/cm^3 fills the void space within the FA. The homogenized PWR fuel compositions are provided in Table 6-43 and Table 6-44 for dry and wet analysis, respectively. The homogenized BWR fuel compositions are provided in Table 6-45 and Table 6-46 for dry and wet analysis, respectively.

Concrete used in the EOS-HSM is modeled without steel rebar at a conservatively low density of 140 pcf (2.243 g/cm^3).

6.3.2 MCNP Model Geometry for the EOS-TC

Detailed EOS-TC MCNP models are developed for the following four configurations:

- EOS-TC108 with EOS-37PTH DSC
- EOS-TC108 with EOS-89BTH DSC
- EOS-TC125/135 with EOS-37PTH DSC
- EOS-TC125/135 with EOS-89BTH DSC

The EOS-37PTH DSC and EOS-89BTH DSC are modeled explicitly, including the steel basket structure, aluminum plates, MMC (conservatively modeled without boron), transition rails, and shield plugs. Key dimensions used to develop the DSC models are summarized in Table 6-47, and figures illustrating the basic MCNP model are provided in Figure 6-3 through Figure 6-6. The figures illustrate the EOS-TC108 with the EOS-89BTH DSC, although the other EOS-TC and EOS-DSC combinations are similar.

[

]

Proprietary Information on This Page
Withheld Pursuant to 10 CFR 2.390

Three model configurations are used to simulate the EOS System during the various stages from loading to transfer. These configurations are loading/decontamination, welding/drying, and downending/transfer, and are described below.

- Loading/Decontamination. The shield plug is in place while the ITCP, OTCP, and top cover plate (lid) are not installed. The neutron shield is off (for the EOS-TC108) or drained (for the EOS-TC125/135), simulating the configuration when the EOS-TC is first removed from the pool. (The actual decontamination operation is performed with the neutron shield full.) Due to crane weight constraints, the EOS-TC108 is modeled with the DSC cavity drained to the top of the active fuel for the EOS-37PTH DSC and drained to the top of the plenum for the EOS-89BTH DSC. The top nozzle of BWR fuel is sufficiently long that draining the plenum region is not anticipated. For the EOS-TC125/135, the DSC cavity is completely filled with water at all times because there is no constraint on crane capacity. The annulus between the EOS-DSC and EOS-TC is filled with water.
- Welding/Drying. The ITCP is installed but the OTCP and top cover plate (lid) are not installed. The neutron shield is filled with water and the DSC is dry. The water height in the annulus is reduced by 12 inches.
- Downending/Transfer. The TC is fully assembled for the transfer operation. The OTCP and top cover plate (lid) are installed. The neutron shield is filled with water and all TC cavities are dry. The EOS-TC108 is modeled with the intermediate aluminum lid rather than the final steel lid.

These three configurations are also summarized in Table 6-49.

The EOS-TC108 has a removable neutron shield. The shield is formed of three panels that are connected with hinges on two joints and latches on the third joint. The interface joint between the three panels features 1.5 inches of aluminum, which allows limited neutron streaming through these three joints along the length of the EOS-TC108. The EOS-TC108 models do not include this streaming path, i.e., the neutron shield is modeled as continuous around the circumference. However, the neutron shield joints are modeled explicitly in a supplementary model, and the dose rates in the vicinity of the joints do not exceed the reported peak dose rates. In addition, the dose rates used in the dose assessment are essentially unchanged when the neutron shield joints are modeled. Therefore, it is acceptable to model the EOS-TC108 neutron shield as continuous around the circumference.

No temporary shielding is modeled, which would be used in practice to shield penetrations or localized areas of high dose rate. Therefore, the computed dose rates are larger than the dose rates that would be observed in actual practice.

The source terms used in the EOS-37PTH DSC models are the combined fuel and CC source terms. The CC source term from Table 6-37 is simply added to the fuel source term from Table 6-10 through Table 6-16. The CC source is added to every FA in the EOS-37PTH DSC. The EOS-89BTH DSC source terms are provided in Table 6-20 through Table 6-26. Note that the source term tables provide dry and wet neutron sources. Wet neutron sources are used only in the loading/decontamination models, while dry neutron sources are used in all other models. For the active fuel regions, an axial source distribution is applied per Table 6-30 and Table 6-31 for PWR and BWR fuel, respectively. For the top nozzle, plenum, and bottom nozzle regions, the source is evenly distributed throughout the region.

For each TC/DSC combination, dose rates are calculated on the surface, 30 cm, and 100 cm from the surfaces of the EOS-TC. Dose rates are also computed 300 cm from the side surface. All side dose rates are computed in 18 axial bins. The general tally locations are shown in Figure 6-7. In addition, for the final transfer configuration, dose rates are computed on the bottom and top surface in six radial segments (see Figure 6-8 and Figure 6-9) and on the side surface in 18 radial segments and 24 angular segments (see Figure 6-10).

Accident models are also developed for the four transfer configurations. In the accident models, the water neutron shield, neutron shield panel, and borated polyethylene bottom neutron shield are replaced with void, and the accident source terms are used. The dose rate is calculated at a distance of 100 m from the EOS-TC. Ground is modeled to account for ground scatter at large distances.

6.3.3 MCNP Model Geometry for the EOS-HSM

Detailed EOS-HSM MCNP models are developed for the following two configurations:

- EOS-HSM-Short with EOS-37PTH DSC

- EOS-HSM-Medium with EOS-89BTH DSC

The EOS-37PTH DSC and EOS-89BTH DSC models developed in Section 6.3.2 are used in the EOS-HSM models. Consistent with the EOS-DSC models, the Z-axis in the EOS-HSM models is along the length of the EOS-DSC. Because the DSC cavity has been reduced in length to match the length of the fuel, the EOS-37PTH DSC model is shorter than the EOS-89BTH DSC model. Short, medium, and long versions of the EOS-HSM may be used, depending on the length of EOS-DSC to be stored. The EOS-HSM modeled is the smallest EOS-HSM that fits the EOS-DSC. Therefore, the EOS-HSM-Short is modeled with the EOS-37PTH DSC and the EOS-HSM-Medium is modeled with the EOS-89BTH DSC.

PWR source terms (without CCs) are provided in Table 6-17 through Table 6-19, and the CC source provided in Table 6-37 is added to these PWR source terms for all FAs. BWR source terms are provided in Table 6-27 through Table 6-29. For the active fuel regions, an axial source distribution is applied per Table 6-30 and Table 6-31 for PWR and BWR fuel, respectively. For the top nozzle, plenum, and bottom nozzle regions, the source is evenly distributed throughout the region.

The EOS-HSMs are modeled explicitly, including the inlet (front) and outlet (roof) vents. Key dimensions used to develop the EOS-HSM models are summarized in Table 6-50, and figures illustrating the basic MCNP model are provided in Figure 6-11 through Figure 6-13. The figures illustrate the EOS-HSM-Medium with the EOS-89BTH DSC, although the geometry of the EOS-HSM-Short with the EOS-37PTH DSC is similar.

The EOS-HSM design consists of a base module that includes the door and 1-foot thick shield walls on the sides and rear. A 3-foot-8-inch thick roof block that matches the length and width of the base rests on the base module. The modules may be positioned either side-by-side in a single row or back-to-back in a double row. When positioned in a single row the rear of the base module is shielded by a 3-foot thick rear shield wall. An end (side) shield wall, which is also 3 feet thick, is placed beside the last module in the row. The end shield wall is comprised of two pieces mated with a Z-joint to prevent direct streaming through the joint. A corner shield wall is placed at the interface of the rear and end shield walls. When the modules are positioned back-to-back, no rear or corner shield walls are used.

Air inlet vents are located on the front and air outlet vents are located on the roof. Because little radiation directly penetrates the thick concrete shielding, essentially all of the dose rate is due to gamma radiation streaming from the vents. Radiation streaming through the outlet vents is mitigated by the use of vent covers. The vent covers feature a 1-inch thick steel plate and approximately 11 inches of concrete. The vent covers are 4 feet wide and are placed between adjacent EOS-HSMs or between an EOS-HSM and the end shield wall. Under normal and off-normal conditions the vent covers are always in place.

[

]

The baseline MCNP model consists of an EOS-HSM with a rear shield wall. On the right side (+x direction) an end shield wall is modeled, while on the left side (-x direction) a mirror boundary is modeled. The mirror boundary simulates an adjacent EOS-HSM so that the model is effectively a 2x1 array of EOS-HSMs. Modeling a 2x1 array significantly increases the vent dose rates compared to simply modeling a single EOS-HSM because a significant source of radiation at a vent is from the EOS-DSC in an adjacent EOS-HSM. The mirror boundary is placed 0.75 inch from the left face of the module to simulate a total gap of 1.5 inches. This model is referred to as the "single reflection model." Dose rates are computed at the inlet and outlet vents and at the 1.5-inch gaps between the base module and shield walls.

The average fluxes and dose rates on the faces of the EOS-HSM are used as input to a generic site dose calculation that is documented in Chapter 11. These average fluxes and dose rates are computed on the surface of a box that envelops the EOS-HSM model, including the vent covers, door, and fabrication gaps. The average end shield wall dose rates are computed with the 2x1 EOS-HSM "single reflection" model described above. However, to capture the contribution from side-by-side or back-to-back EOS-HSMs, additional "double reflection" and "triple reflection" models are developed.

In the "double reflection" model, the end shield wall and corner shield wall are removed and a reflective boundary is added on the right side. The double reflection model simulates an EOS-HSM with an adjacent EOS-HSM on each side. Gaps are included between the modules. This model is only used to compute the average fluxes and dose rate on the rear shield wall used as input to the site dose calculation.

In the "triple reflection" model, all shield walls are removed and replaced with reflective boundaries. This model is illustrated in Figure 6-14. The triple reflection model simulates an EOS-HSM with an adjacent EOS-HSM on each side and back-to-back. The triple reflection model is used to compute the average dose rates on the front and roof used as input to the site dose calculation. The triple reflection model is also used to compute vent and gap dose rates.

In an accident condition, the vent covers are assumed to be absent. This will cause the average roof dose rate to increase substantially but will have negligible effect on the front, rear, or side dose rates. A triple reflection accident model is developed to compute the average flux and dose rate on the roof when the vent covers are removed.

A simple model of an EOS-89BTH DSC with 44 inches of cylindrical concrete shielding and no vents is used to demonstrate the bulk shielding effectiveness of the EOS-HSM in the absence of penetrations. This model is illustrated in Figure 6-15. The outer three and six inches of this model is also replaced with low-density grout (100 pcf versus the 140 pcf concrete used in the EOS-HSM model) to demonstrate that concrete that has spalled may be patched with grout with a negligible impact on the dose rates.

6.4 Shielding Analysis

6.4.1 Computer Codes

MCNP5 v1.40 is used in the shielding analysis [6-5]. MCNP5 is a Monte Carlo transport program that allows full three-dimensional modeling of the EOS-TC and EOS-HSM. Therefore, no geometrical approximations are necessary when developing the shielding models.

6.4.2 Flux-to-Dose Rate Conversion

MCNP5 is used to compute the neutron or gamma flux at the location of interest and the flux is converted to a dose rate using ANSI/ANS-6.1.1-1977 flux-to-dose rate conversion factors [6-10]. These factors are provided in Table 6-51. Results are computed in the units mrem/hr.

6.4.3 EOS-TC Dose Rates

[

]

Proprietary Information on Pages 6-29 through 6-31
Withheld Pursuant to 10 CFR 2.390

The results are presented in Table 6-59. With no grout, the dose rate is 1.4 mrem/hr, while with 6 inches of grout, the dose rate is 2.2 mrem/hr. Therefore, the use of lower density grout to repair concrete is acceptable because the localized dose rate remains small. For example, the average dose rate on the end shield wall of the EOS-HSM is 0.544 mrem/hr (see Table 6-55), and if 6 inches of grout were used, the dose rate would increase to only 0.544*2.2/1.4 = 0.85 mrem/hr. Dose rates are dominated by streaming from the vents because little radiation penetrates the thick concrete shield walls, and repairing the EOS-HSM with grout in localized areas will have no effect on worker exposure or site dose rates.

6.5 Supplemental Information

6.5.1 References

6-1 Oak Ridge National Laboratory, "A Modular Code System for Performing Standardized Computer Analyses for Licensing Evaluation," ORNL/TM-2005/39, Version 6, SCALE, January 2009.

6-2 Oak Ridge National Laboratory, "Predictions of PWR Spent Nuclear Fuel Isotopic Compositions," ORNL/TM-2010/44, SCALE 5.1, March 2010.

6-3 Oak Ridge National Laboratory, "Standard- and Extended-Burnup PWR and BWR Reactor Models for the ORIGEN2 Code," ORNL/TM-11018, December 1989.

6-4 Pacific Northwest Laboratory, "Spent Fuel Assembly Hardware: Characterization and 10 CFR 61 Classification for Waste Disposal, Volume 1 – Activation Measurements and Comparison with Calculations for Spent Fuel Assembly Hardware," PNL-6906, Vol. 1, June 1989.

6-5 Oak Ridge National Laboratory, "MCNP/MCNPX – Monte Carlo N-Particle Transport Code System Including MCNP5 1.40 and MCNPX 2.5.0 and Data Libraries," CCC-730, RSICC Computer Code Collection, January 2006.

6-6 NUREG/CR-6801, "Recommendations for Addressing Axial Burnup in PWR Burnup Credit Analyses," March 2003.

6-7 NUREG-1536, Rev. 1, "Standard Review Plan for Spent Fuel Dry Storage Systems at a General License Facility," July 2010.

6-8 Design Data Document DI-81001-02, NOK Document, "Technical Specification for the Supply of Transportable Casks for the Storage of Kernkraftwerk Leibstardt (KKL) Spent Fuel in ZWILAG," TS 07/01, Rev. 1.

6-9 Pacific Northwest National Laboratory, "Compendium of Material Composition Data for Radiation Transport Modeling," PNNL-15870, Rev. 1, March 2011.

6-10 ANSI/ANS-6.1.1-1977, "American National Standard Neutron and Gamma-Ray Flux-to-Dose-Rate Factors," American National Standards Institute, Inc., New York, New York.

6-11 Proposed CoC 1042 Appendix A, NUHOMS® EOS System Generic Technical Specifications, Amendment 0.

Table 6-1
PWR (BW 15x15) Hardware Characteristics

Fuel Assembly Region and Length	Fuel Assembly Part	Material	Mass (kg)
Top Nozzle, 6.23 in.	Top nozzle/misc. steel	SS304	9.180
	Hold down spring	Inconel-718	1.800
Plenum, 8.73 in.	Upper spring	Inconel-718	4.344
	Upper end cap	Zircaloy-4	1.039
	Encompassing cladding	Zircaloy-4	5.763
	Upper end grid	Inconel-718	1.067
	Encompassing guide tube	Zircaloy-4	0.004
Active Fuel, 142.29 in.	Encompassing cladding	Zircaloy-4	101.1
	Encompassing guide tube	Zircaloy-4	6.328
	Six spacer grids	Inconel-718	4.985
	Grid Supports	Zircaloy-4	0.640
Bottom Nozzle, 8.38 in.	Lower end plug	Zircaloy-4	8.877
	Encompassing guide tube	Zircaloy-4	0.140
	Lower guide tube plugs	Zircaloy-4	1.439
	Lower end fitting	SS304	8.172
	Lower end grid	Inconel-718	1.067

Table 6-2
BWR (GE 7x7) Hardware Characteristics

Fuel Assembly Region and Length	Fuel Assembly Part	Material	Mass (kg)
Top Nozzle, 12.62 in.	Upper tie plate	SS304	2.08
	Lock tab washers and nuts	SS304	0.05
	Expansion springs	Inconel X-750	0.43
	End plugs	Zircaloy-2	1.26
Plenum, 12.93 in.	Cladding	Zircaloy-2	4.89
	Springs	SS304	1.05
Active Fuel, 144 in.	Cladding	Zircaloy-2	49.2
	Spacers	Zircaloy-2	1.95
	Spacer springs	Inconel X-750	0.36
	Channel sleeve	Zircaloy-2	37.1
	Channel spacer and rivet	SS304	0.13
	Channel fastener guard	SS304	0.46
	Channel fastener spring and bolt	Inconel X-750	0.13
Bottom Nozzle, 6.65 in.	Finger springs	Inconel X-750	0.05
	End plugs	Zircaloy-2	1.26
	Lower tie plate	SS304	4.70

Table 6-3
Fuel Assembly Material Compositions
2 Pages

Element	Zircaloy-4 (ppm)	Inconel-718 (ppm)	Inconel X-750 (ppm)	SS304 (ppm)	UO_2 (g/MTU)
Hydrogen	13	0	0	0	0
Lithium	0	0	0	0	1
Boron	0.33	0	0	0	1
Carbon	120	400	399	800	89.4
Nitrogen	80	1300	1300	1300	25
Oxygen	950	0	0	0	134454
Fluorine	0	0	0	0	10.7
Sodium	0	0	0	0	15
Magnesium	0	0	0	0	2
Aluminum	24	5992	7982	0	16.7
Silicon	0	1997	2993	10000	12.1
Phosphorous	0	0	0	450	35
Sulfur	35	70	70	300	0
Chlorine	0	0	0	0	5.3
Calcium	0	0	0	0	2
Titanium	20	7990	24943	0	1
Vanadium	20	0	0	0	3
Chromium	1250	189753	149660	190000	4
Manganese	20	1997	6984	20000	1.7
Iron	2250	179766	67846	688440	18
Cobalt	10	500	500	500	1
Nickel	20	519625	721861	89200	24
Copper	20	999	499	0	1
Zinc	0	0	0	0	40.3
Zirconium	979110	0	0	0	0
Niobium	0	55458	8980	0	0
Molybdenum	0	29961	0	0	10
Silver	0	0	0	0	0.1
Cadmium	0.25	0	0	0	25
Indium	0	0	0	0	2
Tin	16000	0	0	0	4
Gadolinium	0	0	0	0	2.5

Table 6-3
Fuel Assembly Material Compositions
2 Pages

Element	Zircaloy-4 (ppm)	Inconel-718 (ppm)	Inconel X-750 (ppm)	SS304 (ppm)	UO_2 (g/MTU)
Hafnium	78	0	0	0	0
Tungsten	20	0	0	0	2
Lead	0	0	0	0	1
Bismuth	0	0	0	0	0.4
Uranium	0.2	0	0	0	1000000

Table 6-4
Flux Scaling Factors

Region	PWR	BWR
Top Nozzle	0.1	0.1
Plenum	0.2	0.2
Active Fuel	1.0	1.0
Bottom Nozzle	0.2	0.15

Table 6-5
PWR Light Elements by Fuel Assembly Region (ORIGEN-ARP Input, grams)
2 Pages

Element	Bottom Nozzle	Active Fuel	Plenum	Top Nozzle	Total
H	2.718E-02	1.405E+00	1.769E-02	0.000E+00	1.450E+00
Li	0.000E+00	4.919E-01	0.000E+00	0.000E+00	4.919E-01
B	6.901E-04	5.275E-01	4.492E-04	0.000E+00	5.287E-01
C	1.642E+00	5.894E+01	5.962E-01	8.055E-01	6.198E+01
N	2.567E+00	2.742E+01	1.516E+00	1.426E+00	3.293E+01
O	1.987E+00	6.623E+04	1.293E+00	0.000E+00	6.624E+04
F	0.000E+00	5.263E+00	0.000E+00	0.000E+00	5.263E+00
Na	0.000E+00	7.378E+00	0.000E+00	0.000E+00	7.378E+00
Mg	0.000E+00	9.837E-01	0.000E+00	0.000E+00	9.837E-01
Al	1.329E+00	4.068E+01	6.517E+00	1.079E+00	4.960E+01
Si	1.675E+01	1.591E+01	2.161E+00	9.528E+00	4.434E+01
P	7.345E-01	1.721E+01	0.000E+00	4.126E-01	1.836E+01
S	5.778E-01	4.132E+00	1.234E-01	2.876E-01	5.121E+00
Cl	0.000E+00	2.607E+00	0.000E+00	0.000E+00	2.607E+00
Ca	0.000E+00	9.837E-01	0.000E+00	0.000E+00	9.837E-01
Ti	1.747E+00	4.248E+01	8.674E+00	1.438E+00	5.434E+01
V	4.182E-02	3.637E+00	2.722E-02	0.000E+00	3.706E+00
Cr	3.532E+02	1.083E+03	2.071E+02	2.084E+02	1.852E+03
Mn	3.311E+01	1.295E+01	2.188E+00	1.870E+01	6.695E+01
Fe	1.167E+03	1.148E+03	1.976E+02	6.635E+02	3.176E+03
Co	9.448E-01	4.065E+00	5.547E-01	5.490E-01	6.114E+00
Ni	2.565E+02	2.604E+03	5.624E+02	1.753E+02	3.598E+03
Cu	2.550E-01	7.633E+00	1.108E+00	1.798E-01	9.177E+00
Zn	0.000E+00	1.982E+01	0.000E+00	0.000E+00	1.982E+01
Zr	2.047E+03	1.058E+05	1.333E+03	0.000E+00	1.092E+05
Nb	1.183E+01	2.765E+02	6.002E+01	9.982E+00	3.583E+02
Mo	6.394E+00	1.543E+02	3.242E+01	5.393E+00	1.985E+02
Ag	0.000E+00	4.919E-02	0.000E+00	0.000E+00	4.919E-02
Cd	5.228E-04	1.232E+01	3.403E-04	0.000E+00	1.232E+01
In	0.000E+00	9.837E-01	0.000E+00	0.000E+00	9.837E-01
Sn	3.346E+01	1.731E+03	2.178E+01	0.000E+00	1.787E+03
Gd	0.000E+00	1.230E+00	0.000E+00	0.000E+00	1.230E+00

Table 6-5
PWR Light Elements by Fuel Assembly Region (ORIGEN-ARP Input, grams)
2 Pages

Element	Bottom Nozzle	Active Fuel	Plenum	Top Nozzle	Total
Hf	1.631E-01	8.430E+00	1.062E-01	0.000E+00	8.700E+00
W	4.182E-02	3.145E+00	2.722E-02	0.000E+00	3.214E+00
Pb	0.000E+00	4.919E-01	0.000E+00	0.000E+00	4.919E-01
Bi	0.000E+00	1.967E-01	0.000E+00	0.000E+00	1.967E-01

Table 6-6
BWR Light Elements by Fuel Assembly Region (ORIGEN-ARP Input, grams)
2 Pages

Element	Bottom Nozzle	Active Fuel	Plenum	Top Nozzle	Total
H	2.457E-03	1.147E+00	1.271E-02	1.638E-03	1.164E+00
Li	0.000E+00	1.980E-01	0.000E+00	0.000E+00	1.980E-01
B	6.237E-05	2.271E-01	3.227E-04	4.158E-05	2.275E-01
C	5.889E-01	2.896E+01	2.851E-01	2.025E-01	3.003E+01
N	9.402E-01	1.341E+01	3.509E-01	3.425E-01	1.505E+01
O	1.795E-01	2.671E+04	9.291E-01	1.197E-01	2.671E+04
F	0.000E+00	2.119E+00	0.000E+00	0.000E+00	2.119E+00
Na	0.000E+00	2.970E+00	0.000E+00	0.000E+00	2.970E+00
Mg	0.000E+00	3.960E-01	0.000E+00	0.000E+00	3.960E-01
Al	6.440E-02	9.336E+00	2.347E-02	3.462E-01	9.770E+00
Si	7.063E+00	9.755E+00	2.097E+00	2.256E+00	2.117E+01
P	3.168E-01	7.195E+00	9.438E-02	9.573E-02	7.702E+00
S	2.184E-01	3.300E+00	9.715E-02	7.124E-02	3.686E+00
Cl	0.000E+00	1.049E+00	0.000E+00	0.000E+00	1.049E+00
Ca	0.000E+00	3.960E-01	0.000E+00	0.000E+00	3.960E-01
Ti	1.909E-01	1.418E+01	1.956E-02	1.075E+00	1.547E+01
V	3.780E-03	2.359E+00	1.956E-02	2.520E-03	2.385E+00
Cr	1.351E+02	2.964E+02	4.107E+01	4.701E+01	5.196E+02
Mn	1.414E+01	1.731E+01	4.214E+00	4.557E+00	4.022E+01
Fe	4.859E+02	6.441E+02	1.466E+02	1.500E+02	1.427E+03
Co	3.577E-01	1.620E+00	1.146E-01	1.291E-01	2.222E+00
Ni	6.822E+01	4.128E+02	1.873E+01	5.002E+01	5.498E+02
Cu	7.522E-03	2.207E+00	1.956E-02	2.398E-02	2.258E+00
Zn	0.000E+00	7.979E+00	0.000E+00	0.000E+00	7.979E+00
Zr	1.850E+02	8.640E+04	9.575E+02	1.234E+02	8.767E+04
Nb	6.735E-02	4.400E+00	0.000E+00	3.861E-01	4.854E+00
Mo	0.000E+00	1.980E+00	0.000E+00	0.000E+00	1.980E+00
Ag	0.000E+00	1.980E-02	0.000E+00	0.000E+00	1.980E-02
Cd	4.725E-05	4.972E+00	2.445E-04	3.150E-05	4.972E+00
In	0.000E+00	3.960E-01	0.000E+00	0.000E+00	3.960E-01
Sn	3.024E+00	1.413E+03	1.565E+01	2.016E+00	1.433E+03
Gd	0.000E+00	4.950E-01	0.000E+00	0.000E+00	4.950E-01

Table 6-6
BWR Light Elements by Fuel Assembly Region (ORIGEN-ARP Input, grams)
2 Pages

Element	Bottom Nozzle	Active Fuel	Plenum	Top Nozzle	Total
Hf	1.474E-02	6.883E+00	7.628E-02	9.828E-03	6.984E+00
W	3.780E-03	2.161E+00	1.956E-02	2.520E-03	2.187E+00
Pb	0.000E+00	1.980E-01	0.000E+00	0.000E+00	1.980E-01
Bi	0.000E+00	7.920E-02	0.000E+00	0.000E+00	7.920E-02

Proprietary Information on Pages 6-43 through 6-45
Withheld Pursuant to 10 CFR 2.390

Table 6-10
PWR Source Term for the EOS-TC108, Zone 1 (Normal and Accident)

Burnup (GWd/MTU)			33.086	62	33.086	33.086
Enrichment (wt. % U-235)			2.0	3.8	2.0	2.0
Cooling Time (years)			5.00	20.13	5.00	5.00
Gamma Source Term, γ/(sec*FA)						
E_{min}, MeV	**to**	**E_{max}, MeV**	**Bottom Nozzle**	**In-core**	**Plenum**	**Top Nozzle**
1.00E-02	to	5.00E-02	2.168E+11	9.547E+14	1.468E+11	4.999E+10
5.00E-02	to	1.00E-01	1.735E+10	2.705E+14	1.125E+10	9.697E+09
1.00E-01	to	2.00E-01	1.626E+10	1.798E+14	1.055E+10	2.375E+09
2.00E-01	to	3.00E-01	1.067E+09	5.387E+13	6.968E+08	1.170E+08
3.00E-01	to	4.00E-01	3.136E+09	3.493E+13	2.042E+09	1.519E+08
4.00E-01	to	6.00E-01	6.461E+10	3.725E+13	4.206E+10	1.072E+07
6.00E-01	to	8.00E-01	3.483E+10	1.829E+15	2.764E+10	9.512E+08
8.00E-01	to	1.00E+00	1.144E+11	2.667E+13	2.477E+10	6.536E+10
1.00E+00	to	1.33E+00	4.803E+12	3.972E+13	3.109E+12	2.810E+12
1.33E+00	to	1.66E+00	1.356E+12	4.235E+12	8.780E+11	7.935E+11
1.66E+00	to	2.00E+00	7.184E+02	9.029E+10	1.354E+03	3.931E+02
2.00E+00	to	2.50E+00	3.245E+07	4.694E+09	2.101E+07	1.899E+07
2.50E+00	to	3.00E+00	2.773E+04	9.233E+08	1.795E+04	1.622E+04
3.00E+00	to	4.00E+00	8.044E-06	8.009E+07	3.995E-05	6.624E-06
4.00E+00	to	5.00E+00	2.247E-28	2.690E+07	1.463E-28	0.000E+00
5.00E+00	to	6.50E+00	6.475E-29	1.080E+07	4.215E-29	0.000E+00
6.50E+00	to	8.00E+00	8.236E-30	2.118E+06	5.361E-30	0.000E+00
8.00E+00	to	1.00E+01	1.099E-30	4.496E+05	7.154E-31	0.000E+00
Total Gamma, g/(sec*FA)			6.627E+12	3.431E+15	4.253E+12	3.732E+12
Total Neutron Source Term, n/(sec*FA)						
Raw ORIGEN-ARP source for uniform burnup						7.848E+08
Treated with peaking factor 1.215 and k_{eff}=0.4 (dry)						1.589E+09
Treated with peaking factor 1.215 and k_{eff}=0.65 (wet)						2.724E+09

Table 6-11
PWR Source Term for the EOS-TC108, Zone 2 (Normal and Accident)

Burnup (GWd/MTU)			40	62	40	40
Enrichment (wt. % U-235)			2.5	3.8	2.5	2.5
Cooling Time (years)			4.148	7.817	4.148	4.148
Gamma Source Term, γ/(sec*FA)						
E_{min}, MeV	**to**	**E_{max}, MeV**	**Bottom Nozzle**	**In-core**	**Plenum**	**Top Nozzle**
1.00E-02	to	5.00E-02	2.994E+11	1.461E+15	2.025E+11	5.956E+10
5.00E-02	to	1.00E-01	2.082E+10	3.943E+14	1.368E+10	1.156E+10
1.00E-01	to	2.00E-01	2.165E+10	3.065E+14	1.410E+10	2.835E+09
2.00E-01	to	3.00E-01	1.434E+09	8.619E+13	9.387E+08	1.394E+08
3.00E-01	to	4.00E-01	4.321E+09	5.399E+13	2.816E+09	1.810E+08
4.00E-01	to	6.00E-01	8.906E+10	5.984E+14	5.798E+10	1.317E+07
6.00E-01	to	8.00E-01	4.774E+10	3.023E+15	3.674E+10	1.084E+09
8.00E-01	to	1.00E+00	2.401E+11	3.007E+14	4.680E+10	1.369E+11
1.00E+00	to	1.33E+00	5.720E+12	1.305E+14	3.757E+12	3.350E+12
1.33E+00	to	1.66E+00	1.615E+12	2.943E+13	1.061E+12	9.460E+11
1.66E+00	to	2.00E+00	1.273E+04	3.558E+11	2.738E+04	8.465E+03
2.00E+00	to	2.50E+00	3.865E+07	3.138E+11	2.538E+07	2.264E+07
2.50E+00	to	3.00E+00	3.302E+04	1.992E+10	2.169E+04	1.934E+04
3.00E+00	to	4.00E+00	1.009E-05	1.910E+09	5.011E-05	8.309E-06
4.00E+00	to	5.00E+00	5.952E-28	4.275E+07	3.874E-28	0.000E+00
5.00E+00	to	6.50E+00	1.715E-28	1.716E+07	1.116E-28	0.000E+00
6.50E+00	to	8.00E+00	2.181E-29	3.366E+06	1.420E-29	0.000E+00
8.00E+00	to	1.00E+01	2.911E-30	7.146E+05	1.895E-30	0.000E+00
Total Gamma, g/(sec*FA)			8.060E+12	6.385E+15	5.193E+12	4.508E+12
Total Neutron Source Term, n/(sec*FA)						
Raw ORIGEN-ARP source for uniform burnup						1.247E+09
Treated with peaking factor 1.215 and k_{eff}=0.4 (dry)						2.525E+09
Treated with peaking factor 1.215 and k_{eff}=0.65 (wet)						4.329E+09

Table 6-12
PWR Source Term for the EOS-TC108, Zone 3 (Normal)

Burnup (GWd/MTU)			33.086	61.536	33.086	33.086
Enrichment (wt. % U-235)			2.0	3.8	2.0	2.0
Cooling Time (years)			5.00	10.00	5.00	5.00
Gamma Source Term, γ/(sec*FA)						
E_{min}, MeV	**to**	**E_{max}, MeV**	**Bottom Nozzle**	**In-core**	**Plenum**	**Top Nozzle**
1.00E-02	to	5.00E-02	2.168E+11	1.289E+15	1.468E+11	4.999E+10
5.00E-02	to	1.00E-01	1.735E+10	3.490E+14	1.125E+10	9.697E+09
1.00E-01	to	2.00E-01	1.626E+10	2.627E+14	1.055E+10	2.375E+09
2.00E-01	to	3.00E-01	1.067E+09	7.484E+13	6.968E+08	1.170E+08
3.00E-01	to	4.00E-01	3.136E+09	4.663E+13	2.042E+09	1.519E+08
4.00E-01	to	6.00E-01	6.461E+10	3.000E+14	4.206E+10	1.072E+07
6.00E-01	to	8.00E-01	3.483E+10	2.574E+15	2.764E+10	9.512E+08
8.00E-01	to	1.00E+00	1.144E+11	1.629E+14	2.477E+10	6.536E+10
1.00E+00	to	1.33E+00	4.803E+12	1.001E+14	3.109E+12	2.810E+12
1.33E+00	to	1.66E+00	1.356E+12	1.794E+13	8.780E+11	7.935E+11
1.66E+00	to	2.00E+00	7.184E+02	1.685E+11	1.354E+03	3.931E+02
2.00E+00	to	2.50E+00	3.245E+07	6.186E+10	2.101E+07	1.899E+07
2.50E+00	to	3.00E+00	2.773E+04	5.154E+09	1.795E+04	1.622E+04
3.00E+00	to	4.00E+00	8.044E-06	5.137E+08	3.995E-05	6.624E-06
4.00E+00	to	5.00E+00	2.247E-28	3.836E+07	1.463E-28	0.000E+00
5.00E+00	to	6.50E+00	6.475E-29	1.540E+07	4.215E-29	0.000E+00
6.50E+00	to	8.00E+00	8.236E-30	3.020E+06	5.361E-30	0.000E+00
8.00E+00	to	1.00E+01	1.099E-30	6.412E+05	7.154E-31	0.000E+00
Total Gamma, g/(sec*FA)			6.627E+12	5.177E+15	4.253E+12	3.732E+12
Total Neutron Source Term, n/(sec*FA)						
Raw ORIGEN-ARP source for uniform burnup						1.117E+09
Treated with peaking factor 1.215 and k_{eff}=0.4 (dry)						2.262E+09
Treated with peaking factor 1.215 and k_{eff}=0.65 (wet)						3.878E+09

Table 6-13
PWR Source Term for the EOS-TC108, Zone 3 (Accident)

Burnup (GWd/MTU)			33.086	62	33.086	33.086
Enrichment (wt. % U-235)			2.0	3.8	2.0	2.0
Cooling Time (years)			5.00	10.25	5.00	5.00
Gamma Source Term, γ/(sec*FA)						
E_{min}, MeV	**to**	**E_{max}, MeV**	**Bottom Nozzle**	**In-core**	**Plenum**	**Top Nozzle**
1.00E-02	to	5.00E-02	2.168E+11	1.283E+15	1.468E+11	4.999E+10
5.00E-02	to	1.00E-01	1.735E+10	3.475E+14	1.125E+10	9.697E+09
1.00E-01	to	2.00E-01	1.626E+10	2.608E+14	1.055E+10	2.375E+09
2.00E-01	to	3.00E-01	1.067E+09	7.440E+13	6.968E+08	1.170E+08
3.00E-01	to	4.00E-01	3.136E+09	4.635E+13	2.042E+09	1.519E+08
4.00E-01	to	6.00E-01	6.461E+10	2.813E+14	4.206E+10	1.072E+07
6.00E-01	to	8.00E-01	3.483E+10	2.557E+15	2.764E+10	9.512E+08
8.00E-01	to	1.00E+00	1.144E+11	1.542E+14	2.477E+10	6.536E+10
1.00E+00	to	1.33E+00	4.803E+12	9.823E+13	3.109E+12	2.810E+12
1.33E+00	to	1.66E+00	1.356E+12	1.721E+13	8.780E+11	7.935E+11
1.66E+00	to	2.00E+00	7.184E+02	1.605E+11	1.354E+03	3.931E+02
2.00E+00	to	2.50E+00	3.245E+07	5.228E+10	2.101E+07	1.899E+07
2.50E+00	to	3.00E+00	2.773E+04	4.525E+09	1.795E+04	1.622E+04
3.00E+00	to	4.00E+00	8.044E-06	4.548E+08	3.995E-05	6.624E-06
4.00E+00	to	5.00E+00	2.247E-28	3.895E+07	1.463E-28	0.000E+00
5.00E+00	to	6.50E+00	6.475E-29	1.563E+07	4.215E-29	0.000E+00
6.50E+00	to	8.00E+00	8.236E-30	3.067E+06	5.361E-30	0.000E+00
8.00E+00	to	1.00E+01	1.099E-30	6.511E+05	7.154E-31	0.000E+00
Total Gamma, g/(sec*FA)			6.627E+12	5.120E+15	4.253E+12	3.732E+12
Total Neutron Source Term, n/(sec*FA)						
Raw ORIGEN-ARP source for uniform burnup						1.135E+09
Treated with peaking factor 1.215 and k_{eff}=0.4 (dry)						2.298E+09
Treated with peaking factor 1.215 and k_{eff}=0.65 (wet)						3.940E+09

Table 6-14
PWR Source Term for the EOS-TC125/135, Zone 1 (Normal and Accident)

Burnup (GWd/MTU)			33.086	62	33.086	33.086
Enrichment (wt. % U-235)			2.0	3.8	2.0	2.0
Cooling Time (years)			5.00	20.13	5.00	5.00
Gamma Source Term, γ/(sec*FA)						
E_{min}, MeV	**to**	**E_{max}, MeV**	**Bottom Nozzle**	**In-core**	**Plenum**	**Top Nozzle**
1.00E-02	to	5.00E-02	2.168E+11	9.547E+14	1.468E+11	4.999E+10
5.00E-02	to	1.00E-01	1.735E+10	2.705E+14	1.125E+10	9.697E+09
1.00E-01	to	2.00E-01	1.626E+10	1.798E+14	1.055E+10	2.375E+09
2.00E-01	to	3.00E-01	1.067E+09	5.387E+13	6.968E+08	1.170E+08
3.00E-01	to	4.00E-01	3.136E+09	3.493E+13	2.042E+09	1.519E+08
4.00E-01	to	6.00E-01	6.461E+10	3.725E+13	4.206E+10	1.072E+07
6.00E-01	to	8.00E-01	3.483E+10	1.829E+15	2.764E+10	9.512E+08
8.00E-01	to	1.00E+00	1.144E+11	2.667E+13	2.477E+10	6.536E+10
1.00E+00	to	1.33E+00	4.803E+12	3.972E+13	3.109E+12	2.810E+12
1.33E+00	to	1.66E+00	1.356E+12	4.235E+12	8.780E+11	7.935E+11
1.66E+00	to	2.00E+00	7.184E+02	9.029E+10	1.354E+03	3.931E+02
2.00E+00	to	2.50E+00	3.245E+07	4.694E+09	2.101E+07	1.899E+07
2.50E+00	to	3.00E+00	2.773E+04	9.233E+08	1.795E+04	1.622E+04
3.00E+00	to	4.00E+00	8.044E-06	8.009E+07	3.995E-05	6.624E-06
4.00E+00	to	5.00E+00	2.247E-28	2.690E+07	1.463E-28	0.000E+00
5.00E+00	to	6.50E+00	6.475E-29	1.080E+07	4.215E-29	0.000E+00
6.50E+00	to	8.00E+00	8.236E-30	2.118E+06	5.361E-30	0.000E+00
8.00E+00	to	1.00E+01	1.099E-30	4.496E+05	7.154E-31	0.000E+00
Total Gamma, g/(sec*FA)			6.627E+12	3.431E+15	4.253E+12	3.732E+12
Total Neutron Source Term, n/(sec*FA)						
Raw ORIGEN-ARP source for uniform burnup						7.848E+08
Treated with peaking factor 1.215 and k_{eff}=0.4 (dry)						1.589E+09
Treated with peaking factor 1.215 and k_{eff}=0.65 (wet)						2.724E+09

Table 6-15
PWR Source Term for the EOS-TC125/135, Zone 2 (Normal and Accident)

Burnup (GWd/MTU)			50	62	50	50
Enrichment (wt. % U-235)			3.1	3.8	3.1	3.1
Cooling Time (years)			3.959	5.131	3.959	3.959
Gamma Source Term, γ/(sec*FA)						
E_{min}, MeV	**to**	**E_{max}, MeV**	**Bottom Nozzle**	**In-core**	**Plenum**	**Top Nozzle**
1.00E-02	to	5.00E-02	3.521E+11	2.057E+15	2.398E+11	6.714E+10
5.00E-02	to	1.00E-01	2.348E+10	5.785E+14	1.574E+10	1.302E+10
1.00E-01	to	2.00E-01	2.546E+10	4.777E+14	1.666E+10	3.190E+09
2.00E-01	to	3.00E-01	1.693E+09	1.332E+14	1.112E+09	1.569E+08
3.00E-01	to	4.00E-01	5.145E+09	8.924E+13	3.358E+09	2.038E+08
4.00E-01	to	6.00E-01	1.061E+11	1.492E+15	6.904E+10	1.529E+07
6.00E-01	to	8.00E-01	5.685E+10	4.078E+15	4.371E+10	1.283E+09
8.00E-01	to	1.00E+00	2.984E+11	6.795E+14	5.780E+10	1.701E+11
1.00E+00	to	1.33E+00	6.430E+12	1.973E+14	4.315E+12	3.772E+12
1.33E+00	to	1.66E+00	1.816E+12	6.062E+13	1.219E+12	1.065E+12
1.66E+00	to	2.00E+00	2.582E+04	1.630E+12	5.554E+04	1.717E+04
2.00E+00	to	2.50E+00	4.345E+07	2.680E+12	2.916E+07	2.549E+07
2.50E+00	to	3.00E+00	3.712E+04	1.205E+11	2.491E+04	2.177E+04
3.00E+00	to	4.00E+00	1.313E-05	1.126E+10	6.518E-05	1.081E-05
4.00E+00	to	5.00E+00	2.027E-27	4.746E+07	1.319E-27	0.000E+00
5.00E+00	to	6.50E+00	5.840E-28	1.905E+07	3.801E-28	0.000E+00
6.50E+00	to	8.00E+00	7.427E-29	3.737E+06	4.834E-29	0.000E+00
8.00E+00	to	1.00E+01	9.912E-30	7.934E+05	6.452E-30	0.000E+00
Total Gamma, g/(sec*FA)			9.115E+12	9.848E+15	5.981E+12	5.092E+12
Total Neutron Source Term, n/(sec*FA)						
Raw ORIGEN-ARP source for uniform burnup						1.386E+09
Treated with peaking factor 1.215 and k_{eff}=0.4 (dry)						2.807E+09
Treated with peaking factor 1.215 and k_{eff}=0.65 (wet)						4.811E+09

Table 6-16
PWR Source Term for the EOS-TC125/135, Zone 3 (Normal and Accident)

Burnup (GWd/MTU)			40	62	40	40
Enrichment (wt. % U-235)			2.5	3.8	2.5	2.5
Cooling Time (years)			4.698	10.25	4.698	4.698
Gamma Source Term, γ/(sec*FA)						
E_{min}, MeV	**to**	**E_{max}, MeV**	**Bottom Nozzle**	**In-core**	**Plenum**	**Top Nozzle**
1.00E-02	to	5.00E-02	2.553E+11	1.283E+15	1.736E+11	5.548E+10
5.00E-02	to	1.00E-01	1.929E+10	3.475E+14	1.268E+10	1.075E+10
1.00E-01	to	2.00E-01	1.912E+10	2.608E+14	1.246E+10	2.633E+09
2.00E-01	to	3.00E-01	1.260E+09	7.440E+13	8.254E+08	1.297E+08
3.00E-01	to	4.00E-01	3.742E+09	4.635E+13	2.440E+09	1.684E+08
4.00E-01	to	6.00E-01	7.744E+10	2.813E+14	5.041E+10	1.187E+07
6.00E-01	to	8.00E-01	4.168E+10	2.557E+15	3.279E+10	1.084E+09
8.00E-01	to	1.00E+00	1.542E+11	1.542E+14	3.225E+10	8.801E+10
1.00E+00	to	1.33E+00	5.321E+12	9.823E+13	3.494E+12	3.116E+12
1.33E+00	to	1.66E+00	1.503E+12	1.721E+13	9.868E+11	8.800E+11
1.66E+00	to	2.00E+00	1.926E+03	1.605E+11	3.930E+03	1.187E+03
2.00E+00	to	2.50E+00	3.595E+07	5.228E+10	2.361E+07	2.106E+07
2.50E+00	to	3.00E+00	3.072E+04	4.525E+09	2.017E+04	1.799E+04
3.00E+00	to	4.00E+00	9.973E-06	4.548E+08	4.953E-05	8.212E-06
4.00E+00	to	5.00E+00	5.952E-28	3.895E+07	3.874E-28	0.000E+00
5.00E+00	to	6.50E+00	1.715E-28	1.563E+07	1.116E-28	0.000E+00
6.50E+00	to	8.00E+00	2.181E-29	3.067E+06	1.420E-29	0.000E+00
8.00E+00	to	1.00E+01	2.911E-30	6.511E+05	1.895E-30	0.000E+00
Total Gamma, g/(sec*FA)			7.395E+12	5.120E+15	4.799E+12	4.154E+12
Total Neutron Source Term, n/(sec*FA)						
Raw ORIGEN-ARP source for uniform burnup						1.135E+09
Treated with peaking factor 1.215 and k_{eff}=0.4 (dry)						2.298E+09
Treated with peaking factor 1.215 and k_{eff}=0.65 (wet)						3.940E+09

Table 6-17
PWR Source Term for the EOS-HSM, Zone 1 (Normal and Accident)

Burnup (GWd/MTU)			33.086	33.086	33.086	33.086
Enrichment (wt. % U-235)			2.0	2.0	2.0	2.0
Cooling Time (years)			5.00	5.00	5.00	5.00
Gamma Source Term, γ/(sec*FA)						
E_{min}, MeV	**to**	**E_{max}, MeV**	**Bottom Nozzle**	**In-core**	**Plenum**	**Top Nozzle**
1.00E-02	to	5.00E-02	2.168E+11	1.271E+15	1.468E+11	4.999E+10
5.00E-02	to	1.00E-01	1.735E+10	3.698E+14	1.125E+10	9.697E+09
1.00E-01	to	2.00E-01	1.626E+10	3.082E+14	1.055E+10	2.375E+09
2.00E-01	to	3.00E-01	1.067E+09	8.618E+13	6.968E+08	1.170E+08
3.00E-01	to	4.00E-01	3.136E+09	6.061E+13	2.042E+09	1.519E+08
4.00E-01	to	6.00E-01	6.461E+10	7.503E+14	4.206E+10	1.072E+07
6.00E-01	to	8.00E-01	3.483E+10	2.131E+15	2.764E+10	9.512E+08
8.00E-01	to	1.00E+00	1.144E+11	3.162E+14	2.477E+10	6.536E+10
1.00E+00	to	1.33E+00	4.803E+12	1.083E+14	3.109E+12	2.810E+12
1.33E+00	to	1.66E+00	1.356E+12	3.206E+13	8.780E+11	7.935E+11
1.66E+00	to	2.00E+00	7.184E+02	1.371E+12	1.354E+03	3.931E+02
2.00E+00	to	2.50E+00	3.245E+07	2.541E+12	2.101E+07	1.899E+07
2.50E+00	to	3.00E+00	2.773E+04	1.030E+11	1.795E+04	1.622E+04
3.00E+00	to	4.00E+00	8.044E-06	9.562E+09	3.995E-05	6.624E-06
4.00E+00	to	5.00E+00	2.247E-28	1.253E+07	1.463E-28	0.000E+00
5.00E+00	to	6.50E+00	6.475E-29	5.029E+06	4.215E-29	0.000E+00
6.50E+00	to	8.00E+00	8.236E-30	9.866E+05	5.361E-30	0.000E+00
8.00E+00	to	1.00E+01	1.099E-30	2.095E+05	7.154E-31	0.000E+00
Total Gamma, g/(sec*FA)			6.627E+12	5.438E+15	4.253E+12	3.732E+12
Total Neutron Source Term, n/(sec*FA)						
Raw ORIGEN-ARP source for uniform burnup						3.599E+08
Treated with peaking factor 1.215 and k_{eff}=0.4 (dry)						7.288E+08

Table 6-18
PWR Source Term for the EOS-HSM, Zone 2 (Normal and Accident)

Burnup (GWd/MTU)			50	50	50	50
Enrichment (wt. % U-235)			3.1	3.1	3.1	3.1
Cooling Time (years)			3.959	3.959	3.959	3.959
Gamma Source Term, γ/(sec*FA)						
E_{min}, MeV	**to**	**E_{max}, MeV**	**Bottom Nozzle**	**In-core**	**Plenum**	**Top Nozzle**
1.00E-02	to	5.00E-02	3.521E+11	2.449E+15	2.398E+11	6.714E+10
5.00E-02	to	1.00E-01	2.348E+10	7.302E+14	1.574E+10	1.302E+10
1.00E-01	to	2.00E-01	2.546E+10	6.328E+14	1.666E+10	3.190E+09
2.00E-01	to	3.00E-01	1.693E+09	1.754E+14	1.112E+09	1.569E+08
3.00E-01	to	4.00E-01	5.145E+09	1.257E+14	3.358E+09	2.038E+08
4.00E-01	to	6.00E-01	1.061E+11	1.808E+15	6.904E+10	1.529E+07
6.00E-01	to	8.00E-01	5.685E+10	3.918E+15	4.371E+10	1.283E+09
8.00E-01	to	1.00E+00	2.984E+11	7.609E+14	5.780E+10	1.701E+11
1.00E+00	to	1.33E+00	6.430E+12	2.058E+14	4.315E+12	3.772E+12
1.33E+00	to	1.66E+00	1.816E+12	7.017E+13	1.219E+12	1.065E+12
1.66E+00	to	2.00E+00	2.582E+04	3.289E+12	5.554E+04	1.717E+04
2.00E+00	to	2.50E+00	4.345E+07	6.769E+12	2.916E+07	2.549E+07
2.50E+00	to	3.00E+00	3.712E+04	2.480E+11	2.491E+04	2.177E+04
3.00E+00	to	4.00E+00	1.313E-05	2.297E+10	6.518E-05	1.081E-05
4.00E+00	to	5.00E+00	2.027E-27	3.151E+07	1.319E-27	0.000E+00
5.00E+00	to	6.50E+00	5.840E-28	1.265E+07	3.801E-28	0.000E+00
6.50E+00	to	8.00E+00	7.427E-29	2.481E+06	4.834E-29	0.000E+00
8.00E+00	to	1.00E+01	9.912E-30	5.268E+05	6.452E-30	0.000E+00
Total Gamma, g/(sec*FA)			9.115E+12	1.089E+16	5.981E+12	5.092E+12
Total Neutron Source Term, n/(sec*FA)						
Raw ORIGEN-ARP source for uniform burnup						9.107E+08
Treated with peaking factor 1.215 and k_{eff}=0.4 (dry)						1.844E+09

Table 6-19
PWR Source Term for the EOS-HSM, Zone 3 (Normal and Accident)

Burnup (GWd/MTU)			40	40	40	40
Enrichment (wt. % U-235)			2.5	2.5	2.5	2.5
Cooling Time (years)			4.698	4.698	4.698	4.698
Gamma Source Term, γ/(sec*FA)						
E_{min}, MeV	**to**	**E_{max}, MeV**	**Bottom Nozzle**	**In-core**	**Plenum**	**Top Nozzle**
1.00E-02	to	5.00E-02	2.553E+11	1.621E+15	1.736E+11	5.548E+10
5.00E-02	to	1.00E-01	1.929E+10	4.734E+14	1.268E+10	1.075E+10
1.00E-01	to	2.00E-01	1.912E+10	3.991E+14	1.246E+10	2.633E+09
2.00E-01	to	3.00E-01	1.260E+09	1.112E+14	8.254E+08	1.297E+08
3.00E-01	to	4.00E-01	3.742E+09	7.827E+13	2.440E+09	1.684E+08
4.00E-01	to	6.00E-01	7.744E+10	1.052E+15	5.041E+10	1.187E+07
6.00E-01	to	8.00E-01	4.168E+10	2.730E+15	3.279E+10	1.084E+09
8.00E-01	to	1.00E+00	1.542E+11	4.477E+14	3.225E+10	8.801E+10
1.00E+00	to	1.33E+00	5.321E+12	1.393E+14	3.494E+12	3.116E+12
1.33E+00	to	1.66E+00	1.503E+12	4.315E+13	9.868E+11	8.800E+11
1.66E+00	to	2.00E+00	1.926E+03	1.817E+12	3.930E+03	1.187E+03
2.00E+00	to	2.50E+00	3.595E+07	3.468E+12	2.361E+07	2.106E+07
2.50E+00	to	3.00E+00	3.072E+04	1.364E+11	2.017E+04	1.799E+04
3.00E+00	to	4.00E+00	9.973E-06	1.266E+10	4.953E-05	8.212E-06
4.00E+00	to	5.00E+00	5.952E-28	1.869E+07	3.874E-28	0.000E+00
5.00E+00	to	6.50E+00	1.715E-28	7.501E+06	1.116E-28	0.000E+00
6.50E+00	to	8.00E+00	2.181E-29	1.472E+06	1.420E-29	0.000E+00
8.00E+00	to	1.00E+01	2.911E-30	3.124E+05	1.895E-30	0.000E+00
Total Gamma, g/(sec*FA)			7.395E+12	7.100E+15	4.799E+12	4.154E+12
Total Neutron Source Term, n/(sec*FA)						
Raw ORIGEN-ARP source for uniform burnup						5.376E+08
Treated with peaking factor 1.215 and k_{eff}=0.4 (dry)						1.089E+09

Table 6-20
BWR Source Term for the EOS-TC108, Zone 1 (Normal and Accident)

Burnup (GWD/MTU)			17.07	62	17.07	17.07
Enrichment (wt. % U-235)			0.9	3.8	0.9	0.9
Cooling Time (years)			3.000	16.490	3.000	3.000
Gamma Source Term, γ/(sec*FA)						
E_{min}, MeV	**to**	**E_{max}, MeV**	**Bottom Nozzle**	**In-core**	**Plenum**	**Top Nozzle**
1.00E-02	to	5.00E-02	5.478E+10	4.235E+14	1.045E+11	2.552E+10
5.00E-02	to	1.00E-01	7.401E+09	1.171E+14	2.736E+09	2.729E+09
1.00E-01	to	2.00E-01	2.931E+09	8.105E+13	6.338E+09	1.404E+09
2.00E-01	to	3.00E-01	1.691E+08	2.424E+13	4.480E+08	8.636E+07
3.00E-01	to	4.00E-01	4.376E+08	1.589E+13	1.711E+09	2.576E+08
4.00E-01	to	6.00E-01	5.899E+09	2.407E+13	3.045E+10	3.932E+09
6.00E-01	to	8.00E-01	3.122E+09	8.094E+14	1.613E+10	2.101E+09
8.00E-01	to	1.00E+00	1.515E+11	1.462E+13	4.572E+10	4.680E+10
1.00E+00	to	1.33E+00	2.111E+12	1.787E+13	6.749E+11	7.732E+11
1.33E+00	to	1.66E+00	5.961E+11	2.287E+12	1.906E+11	2.184E+11
1.66E+00	to	2.00E+00	1.388E+05	4.114E+10	4.210E+04	1.017E+05
2.00E+00	to	2.50E+00	1.426E+07	2.301E+09	4.561E+06	5.225E+06
2.50E+00	to	3.00E+00	1.219E+04	3.129E+08	3.897E+03	4.464E+03
3.00E+00	to	4.00E+00	3.040E-07	3.411E+07	3.117E-08	1.713E-06
4.00E+00	to	5.00E+00	4.928E-31	1.087E+07	2.553E-30	3.289E-31
5.00E+00	to	6.50E+00	1.420E-31	4.362E+06	7.356E-31	9.477E-32
6.50E+00	to	8.00E+00	1.806E-32	8.557E+05	9.356E-32	1.205E-32
8.00E+00	to	1.00E+01	2.410E-33	1.817E+05	1.249E-32	1.609E-33
Total Gamma, g/(sec*FA)			2.933E+12	1.530E+15	1.074E+12	1.074E+12
Total Neutron Source Term, n/(sec*FA)						
Raw ORIGEN-ARP source for uniform burnup						3.168E+08
Treated with peaking factor 1.232 and k_{eff}=0.4 (dry)						6.505E+08
Treated with peaking factor 1.232 and k_{eff}=0.65 (wet)						1.115E+09

Table 6-21
BWR Source Term for the EOS-TC108, Zone 2 (Normal and Accident)

Burnup (GWD/MTU)			23.4	62	23.4	23.4
Enrichment (wt. % U-235)			1.2	3.8	1.2	1.2
Cooling Time (years)			3.000	8.515	3.000	3.000
Gamma Source Term, γ/(sec*FA)						
E_{min}, MeV	**to**	**E_{max}, MeV**	**Bottom Nozzle**	**In-core**	**Plenum**	**Top Nozzle**
1.00E-02	to	5.00E-02	6.519E+10	5.613E+14	1.271E+11	3.062E+10
5.00E-02	to	1.00E-01	8.701E+09	1.516E+14	3.243E+09	3.225E+09
1.00E-01	to	2.00E-01	3.546E+09	1.136E+14	7.976E+09	1.721E+09
2.00E-01	to	3.00E-01	2.057E+08	3.258E+13	5.628E+08	1.063E+08
3.00E-01	to	4.00E-01	5.307E+08	2.101E+13	2.097E+09	3.140E+08
4.00E-01	to	6.00E-01	7.473E+09	1.819E+14	3.859E+10	4.981E+09
6.00E-01	to	8.00E-01	3.945E+09	1.137E+15	2.038E+10	2.655E+09
8.00E-01	to	1.00E+00	1.803E+11	8.994E+13	5.441E+10	5.569E+10
1.00E+00	to	1.33E+00	2.480E+12	4.038E+13	7.924E+11	9.128E+11
1.33E+00	to	1.66E+00	7.005E+11	9.234E+12	2.238E+11	2.578E+11
1.66E+00	to	2.00E+00	1.463E+05	1.069E+11	4.623E+04	1.071E+05
2.00E+00	to	2.50E+00	1.676E+07	7.362E+10	5.355E+06	6.167E+06
2.50E+00	to	3.00E+00	1.432E+04	4.972E+09	4.575E+03	5.270E+03
3.00E+00	to	4.00E+00	4.768E-07	4.831E+08	4.888E-08	2.687E-06
4.00E+00	to	5.00E+00	3.049E-30	1.469E+07	1.579E-29	2.035E-30
5.00E+00	to	6.50E+00	8.785E-31	5.896E+06	4.551E-30	5.863E-31
6.50E+00	to	8.00E+00	1.117E-31	1.157E+06	5.788E-31	7.458E-32
8.00E+00	to	1.00E+01	1.491E-32	2.456E+05	7.725E-32	9.953E-33
Total Gamma, g/(sec*FA)			3.451E+12	2.339E+15	1.270E+12	1.270E+12
Total Neutron Source Term, n/(sec*FA)						
Raw ORIGEN-ARP source for uniform burnup						4.285E+08
Treated with peaking factor 1.232 and k_{eff}=0.4 (dry)						8.799E+08
Treated with peaking factor 1.232 and k_{eff}=0.65 (wet)						1.508E+09

Table 6-22
BWR Source Term for the EOS-TC108, Zone 3 (Normal and Accident)

Burnup (GWD/MTU)			62	62	62	62
Enrichment (wt. % U-235)			3.8	3.8	3.8	3.8
Cooling Time (years)			9.699	9.699	9.699	9.699
Gamma Source Term, γ/(sec*FA)						
E_{min}, MeV	**to**	**E_{max}, MeV**	**Bottom Nozzle**	**In-core**	**Plenum**	**Top Nozzle**
1.00E-02	to	5.00E-02	2.884E+10	5.285E+14	2.939E+10	1.222E+10
5.00E-02	to	1.00E-01	4.888E+09	1.430E+14	1.692E+09	1.848E+09
1.00E-01	to	2.00E-01	1.638E+09	1.056E+14	2.718E+09	7.473E+08
2.00E-01	to	3.00E-01	9.060E+07	3.051E+13	1.849E+08	4.356E+07
3.00E-01	to	4.00E-01	1.826E+08	1.963E+13	5.747E+08	9.977E+07
4.00E-01	to	6.00E-01	2.401E+09	1.263E+14	1.240E+10	1.600E+09
6.00E-01	to	8.00E-01	1.262E+09	1.053E+15	6.468E+09	8.900E+08
8.00E-01	to	1.00E+00	1.158E+09	6.453E+13	3.478E+08	4.128E+08
1.00E+00	to	1.33E+00	1.411E+12	3.500E+13	4.489E+11	5.314E+11
1.33E+00	to	1.66E+00	3.985E+11	7.091E+12	1.268E+11	1.501E+11
1.66E+00	to	2.00E+00	2.084E+01	7.384E+10	1.078E+02	1.390E+01
2.00E+00	to	2.50E+00	9.535E+06	3.080E+10	3.033E+06	3.591E+06
2.50E+00	to	3.00E+00	8.147E+03	2.376E+09	2.592E+03	3.068E+03
3.00E+00	to	4.00E+00	1.264E-06	2.379E+08	1.295E-07	7.119E-06
4.00E+00	to	5.00E+00	4.257E-28	1.404E+07	2.205E-27	2.840E-28
5.00E+00	to	6.50E+00	1.227E-28	5.634E+06	6.352E-28	8.184E-29
6.50E+00	to	8.00E+00	1.560E-29	1.105E+06	8.080E-29	1.041E-29
8.00E+00	to	1.00E+01	2.082E-30	2.347E+05	1.078E-29	1.389E-30
Total Gamma, g/(sec*FA)			1.850E+12	2.113E+15	6.295E+11	6.993E+11
Total Neutron Source Term, n/(sec*FA)						
Raw ORIGEN-ARP source for uniform burnup						4.094E+08
Treated with peaking factor 1.232 and k_{eff}=0.4 (dry)						8.406E+08
Treated with peaking factor 1.232 and k_{eff}=0.65 (wet)						1.441E+09

Table 6-23
BWR Source Term for the EOS-TC125/135, Zone 1 (Normal and Accident)

Burnup (GWD/MTU)			17.07	62	17.07	17.07
Enrichment (wt. % U-235)			0.9	3.8	0.9	0.9
Cooling Time (years)			3.000	16.490	3.000	3.000
Gamma Source Term, γ/(sec*FA)						
E_{min}, MeV	**to**	**E_{max}, MeV**	**Bottom Nozzle**	**In-core**	**Plenum**	**Top Nozzle**
1.00E-02	to	5.00E-02	5.478E+10	4.235E+14	1.045E+11	2.552E+10
5.00E-02	to	1.00E-01	7.401E+09	1.171E+14	2.736E+09	2.729E+09
1.00E-01	to	2.00E-01	2.931E+09	8.105E+13	6.338E+09	1.404E+09
2.00E-01	to	3.00E-01	1.691E+08	2.424E+13	4.480E+08	8.636E+07
3.00E-01	to	4.00E-01	4.376E+08	1.589E+13	1.711E+09	2.576E+08
4.00E-01	to	6.00E-01	5.899E+09	2.407E+13	3.045E+10	3.932E+09
6.00E-01	to	8.00E-01	3.122E+09	8.094E+14	1.613E+10	2.101E+09
8.00E-01	to	1.00E+00	1.515E+11	1.462E+13	4.572E+10	4.680E+10
1.00E+00	to	1.33E+00	2.111E+12	1.787E+13	6.749E+11	7.732E+11
1.33E+00	to	1.66E+00	5.961E+11	2.287E+12	1.906E+11	2.184E+11
1.66E+00	to	2.00E+00	1.388E+05	4.114E+10	4.210E+04	1.017E+05
2.00E+00	to	2.50E+00	1.426E+07	2.301E+09	4.561E+06	5.225E+06
2.50E+00	to	3.00E+00	1.219E+04	3.129E+08	3.897E+03	4.464E+03
3.00E+00	to	4.00E+00	3.040E-07	3.411E+07	3.117E-08	1.713E-06
4.00E+00	to	5.00E+00	4.928E-31	1.087E+07	2.553E-30	3.289E-31
5.00E+00	to	6.50E+00	1.420E-31	4.362E+06	7.356E-31	9.477E-32
6.50E+00	to	8.00E+00	1.806E-32	8.557E+05	9.356E-32	1.205E-32
8.00E+00	to	1.00E+01	2.410E-33	1.817E+05	1.249E-32	1.609E-33
Total Gamma, g/(sec*FA)			2.933E+12	1.530E+15	1.074E+12	1.074E+12
Total Neutron Source Term, n/(sec*FA)						
Raw ORIGEN-ARP source for uniform burnup						3.168E+08
Treated with peaking factor 1.232 and k_{eff}=0.4 (dry)						6.505E+08
Treated with peaking factor 1.232 and k_{eff}=0.65 (wet)						1.115E+09

Table 6-24
BWR Source Term for the EOS-TC125/135, Zone 2 (Normal and Accident)

Burnup (GWD/MTU)			26.59	62	26.59	26.59
Enrichment (wt. % U-235)			1.3	3.8	1.3	1.3
Cooling Time (years)			3.000	6.971	3.000	3.000
Gamma Source Term, γ/(sec*FA)						
E_{min}, MeV	**to**	**E_{max}, MeV**	**Bottom Nozzle**	**In-core**	**Plenum**	**Top Nozzle**
1.00E-02	to	5.00E-02	6.951E+10	6.304E+14	1.360E+11	3.271E+10
5.00E-02	to	1.00E-01	9.256E+09	1.714E+14	3.458E+09	3.438E+09
1.00E-01	to	2.00E-01	3.805E+09	1.315E+14	8.658E+09	1.855E+09
2.00E-01	to	3.00E-01	2.210E+08	3.742E+13	6.104E+08	1.147E+08
3.00E-01	to	4.00E-01	5.690E+08	2.449E+13	2.254E+09	3.371E+08
4.00E-01	to	6.00E-01	8.127E+09	3.004E+14	4.197E+10	5.417E+09
6.00E-01	to	8.00E-01	4.287E+09	1.294E+15	2.214E+10	2.885E+09
8.00E-01	to	1.00E+00	1.905E+11	1.421E+14	5.750E+10	5.885E+10
1.00E+00	to	1.33E+00	2.638E+12	4.996E+13	8.425E+11	9.729E+11
1.33E+00	to	1.66E+00	7.451E+11	1.353E+13	2.379E+11	2.747E+11
1.66E+00	to	2.00E+00	1.487E+05	2.171E+11	4.786E+04	1.089E+05
2.00E+00	to	2.50E+00	1.783E+07	2.445E+11	5.694E+06	6.574E+06
2.50E+00	to	3.00E+00	1.523E+04	1.377E+10	4.865E+03	5.617E+03
3.00E+00	to	4.00E+00	5.566E-07	1.306E+09	5.706E-08	3.136E-06
4.00E+00	to	5.00E+00	6.020E-30	1.560E+07	3.119E-29	4.018E-30
5.00E+00	to	6.50E+00	1.735E-30	6.260E+06	8.986E-30	1.158E-30
6.50E+00	to	8.00E+00	2.206E-31	1.228E+06	1.143E-30	1.473E-31
8.00E+00	to	1.00E+01	2.945E-32	2.608E+05	1.525E-31	1.965E-32
Total Gamma, g/(sec*FA)			3.670E+12	2.796E+15	1.353E+12	1.353E+12
Total Neutron Source Term, n/(sec*FA)						
Raw ORIGEN-ARP source for uniform burnup						4.553E+08
Treated with peaking factor 1.232 and k_{eff}=0.4 (dry)						9.349E+08
Treated with peaking factor 1.232 and k_{eff}=0.65 (wet)						1.603E+09

Table 6-25
BWR Source Term for the EOS-TC125/135, Zone 3 (Normal)

Burnup (GWD/MTU)			21.72	21.72	21.72	21.72
Enrichment (wt. % U-235)			1.1	1.1	1.1	1.1
Cooling Time (years)			3.000	3.000	3.000	3.000
Gamma Source Term, γ/(sec*FA)						
E_{min}, MeV	**to**	**E_{max}, MeV**	**Bottom Nozzle**	**In-core**	**Plenum**	**Top Nozzle**
1.00E-02	to	5.00E-02	6.284E+10	8.933E+14	1.217E+11	2.945E+10
5.00E-02	to	1.00E-01	8.418E+09	2.854E+14	3.130E+09	3.116E+09
1.00E-01	to	2.00E-01	3.404E+09	2.626E+14	7.575E+09	1.646E+09
2.00E-01	to	3.00E-01	1.971E+08	7.166E+13	5.346E+08	1.016E+08
3.00E-01	to	4.00E-01	5.085E+08	5.544E+13	2.003E+09	3.004E+08
4.00E-01	to	6.00E-01	7.084E+09	4.152E+14	3.658E+10	4.722E+09
6.00E-01	to	8.00E-01	3.742E+09	7.410E+14	1.933E+10	2.518E+09
8.00E-01	to	1.00E+00	1.736E+11	1.317E+14	5.239E+10	5.363E+10
1.00E+00	to	1.33E+00	2.400E+12	4.950E+13	7.669E+11	8.822E+11
1.33E+00	to	1.66E+00	6.778E+11	1.676E+13	2.166E+11	2.491E+11
1.66E+00	to	2.00E+00	1.443E+05	1.788E+12	4.516E+04	1.057E+05
2.00E+00	to	2.50E+00	1.622E+07	4.468E+12	5.183E+06	5.961E+06
2.50E+00	to	3.00E+00	1.386E+04	1.335E+11	4.428E+03	5.093E+03
3.00E+00	to	4.00E+00	4.305E-07	1.226E+10	4.413E-08	2.426E-06
4.00E+00	to	5.00E+00	2.020E-30	2.004E+06	1.046E-29	1.348E-30
5.00E+00	to	6.50E+00	5.820E-31	8.044E+05	3.015E-30	3.884E-31
6.50E+00	to	8.00E+00	7.403E-32	1.578E+05	3.835E-31	4.941E-32
8.00E+00	to	1.00E+01	9.879E-33	3.350E+04	5.118E-32	6.594E-33
Total Gamma, g/(sec*FA)			3.338E+12	2.929E+15	1.227E+12	1.227E+12
Total Neutron Source Term, n/(sec*FA)						
Raw ORIGEN-ARP source for uniform burnup						5.743E+07
Treated with peaking factor 1.232 and k_{eff}=0.4 (dry)						1.179E+08
Treated with peaking factor 1.232 and k_{eff}=0.65 (wet)						2.022E+08

Table 6-26
BWR Source Term for the EOS-TC125/135, Zone 3 (Accident)

Burnup (GWD/MTU)			21.72	62	21.72	21.72
Enrichment (wt. % U-235)			1.1	3.8	1.1	1.1
Cooling Time (years)			3.000	9.699	3.000	3.000
Gamma Source Term, γ/(sec*FA)						
E_{min}, MeV	**to**	**E_{max}, MeV**	**Bottom Nozzle**	**In-core**	**Plenum**	**Top Nozzle**
1.00E-02	to	5.00E-02	6.284E+10	5.285E+14	1.217E+11	2.945E+10
5.00E-02	to	1.00E-01	8.418E+09	1.430E+14	3.130E+09	3.116E+09
1.00E-01	to	2.00E-01	3.404E+09	1.056E+14	7.575E+09	1.646E+09
2.00E-01	to	3.00E-01	1.971E+08	3.051E+13	5.346E+08	1.016E+08
3.00E-01	to	4.00E-01	5.085E+08	1.963E+13	2.003E+09	3.004E+08
4.00E-01	to	6.00E-01	7.084E+09	1.263E+14	3.658E+10	4.722E+09
6.00E-01	to	8.00E-01	3.742E+09	1.053E+15	1.933E+10	2.518E+09
8.00E-01	to	1.00E+00	1.736E+11	6.453E+13	5.239E+10	5.363E+10
1.00E+00	to	1.33E+00	2.400E+12	3.500E+13	7.669E+11	8.822E+11
1.33E+00	to	1.66E+00	6.778E+11	7.091E+12	2.166E+11	2.491E+11
1.66E+00	to	2.00E+00	1.443E+05	7.384E+10	4.516E+04	1.057E+05
2.00E+00	to	2.50E+00	1.622E+07	3.080E+10	5.183E+06	5.961E+06
2.50E+00	to	3.00E+00	1.386E+04	2.376E+09	4.428E+03	5.093E+03
3.00E+00	to	4.00E+00	4.305E-07	2.379E+08	4.413E-08	2.426E-06
4.00E+00	to	5.00E+00	2.020E-30	1.404E+07	1.046E-29	1.348E-30
5.00E+00	to	6.50E+00	5.820E-31	5.634E+06	3.015E-30	3.884E-31
6.50E+00	to	8.00E+00	7.403E-32	1.105E+06	3.835E-31	4.941E-32
8.00E+00	to	1.00E+01	9.879E-33	2.347E+05	5.118E-32	6.594E-33
Total Gamma, g/(sec*FA)			3.338E+12	2.113E+15	1.227E+12	1.227E+12
Total Neutron Source Term, n/(sec*FA)						
Raw ORIGEN-ARP source for uniform burnup						4.094E+08
Treated with peaking factor 1.232 and k_{eff}=0.4 (dry)						8.406E+08
Treated with peaking factor 1.232 and k_{eff}=0.65 (wet)						1.441E+09

Table 6-27
BWR Source Term for the EOS-HSM, Zone 1 (Normal and Accident)

Burnup (GWD/MTU)			17.07	40	17.07	17.07
Enrichment (wt. % U-235)			0.9	2.5	0.9	0.9
Cooling Time (years)			3.000	5.955	3.000	3.000
Gamma Source Term, γ/(sec*FA)						
E_{min}, MeV	**to**	**E_{max}, MeV**	**Bottom Nozzle**	**In-core**	**Plenum**	**Top Nozzle**
1.00E-02	to	5.00E-02	5.478E+10	4.862E+14	1.045E+11	2.552E+10
5.00E-02	to	1.00E-01	7.401E+09	1.362E+14	2.736E+09	2.729E+09
1.00E-01	to	2.00E-01	2.931E+09	1.074E+14	6.338E+09	1.404E+09
2.00E-01	to	3.00E-01	1.691E+08	3.041E+13	4.480E+08	8.636E+07
3.00E-01	to	4.00E-01	4.376E+08	2.076E+13	1.711E+09	2.576E+08
4.00E-01	to	6.00E-01	5.899E+09	2.518E+14	3.045E+10	3.932E+09
6.00E-01	to	8.00E-01	3.122E+09	9.138E+14	1.613E+10	2.101E+09
8.00E-01	to	1.00E+00	1.515E+11	1.114E+14	4.572E+10	4.680E+10
1.00E+00	to	1.33E+00	2.111E+12	3.914E+13	6.749E+11	7.732E+11
1.33E+00	to	1.66E+00	5.961E+11	1.125E+13	1.906E+11	2.184E+11
1.66E+00	to	2.00E+00	1.388E+05	3.161E+11	4.210E+04	1.017E+05
2.00E+00	to	2.50E+00	1.426E+07	4.963E+11	4.561E+06	5.225E+06
2.50E+00	to	3.00E+00	1.219E+04	2.265E+10	3.897E+03	4.464E+03
3.00E+00	to	4.00E+00	3.040E-07	2.113E+09	3.117E-08	1.713E-06
4.00E+00	to	5.00E+00	4.928E-31	6.042E+06	2.553E-30	3.289E-31
5.00E+00	to	6.50E+00	1.420E-31	2.425E+06	7.356E-31	9.477E-32
6.50E+00	to	8.00E+00	1.806E-32	4.757E+05	9.356E-32	1.205E-32
8.00E+00	to	1.00E+01	2.410E-33	1.010E+05	1.249E-32	1.609E-33
Total Gamma, g/(sec*FA)			2.933E+12	2.109E+15	1.074E+12	1.074E+12
Total Neutron Source Term, n/(sec*FA)						
Raw ORIGEN-ARP source for uniform burnup						1.738E+08
Treated with peaking factor 1.232 and k_{eff}=0.4 (dry)						3.569E+08

Table 6-28
BWR Source Term for the EOS-HSM, Zone 2 (Normal and Accident)

Burnup (GWD/MTU)			26.59	50	26.59	26.59
Enrichment (wt. % U-235)			1.3	3.1	1.3	1.3
Cooling Time (years)			3.000	5.031	3.000	3.000
Gamma Source Term, γ/(sec*FA)						
E_{min}, MeV	**to**	**E_{max}, MeV**	**Bottom Nozzle**	**In-core**	**Plenum**	**Top Nozzle**
1.00E-02	to	5.00E-02	6.951E+10	7.110E+14	1.360E+11	3.271E+10
5.00E-02	to	1.00E-01	9.256E+09	2.029E+14	3.458E+09	3.438E+09
1.00E-01	to	2.00E-01	3.805E+09	1.652E+14	8.658E+09	1.855E+09
2.00E-01	to	3.00E-01	2.210E+08	4.652E+13	6.104E+08	1.147E+08
3.00E-01	to	4.00E-01	5.690E+08	3.244E+13	2.254E+09	3.371E+08
4.00E-01	to	6.00E-01	8.127E+09	4.596E+14	4.197E+10	5.417E+09
6.00E-01	to	8.00E-01	4.287E+09	1.298E+15	2.214E+10	2.885E+09
8.00E-01	to	1.00E+00	1.905E+11	1.997E+14	5.750E+10	5.885E+10
1.00E+00	to	1.33E+00	2.638E+12	5.772E+13	8.425E+11	9.729E+11
1.33E+00	to	1.66E+00	7.451E+11	1.872E+13	2.379E+11	2.747E+11
1.66E+00	to	2.00E+00	1.487E+05	6.343E+11	4.786E+04	1.089E+05
2.00E+00	to	2.50E+00	1.783E+07	1.122E+12	5.694E+06	6.574E+06
2.50E+00	to	3.00E+00	1.523E+04	4.695E+10	4.865E+03	5.617E+03
3.00E+00	to	4.00E+00	5.566E-07	4.371E+09	5.706E-08	3.136E-06
4.00E+00	to	5.00E+00	6.020E-30	1.044E+07	3.119E-29	4.018E-30
5.00E+00	to	6.50E+00	1.735E-30	4.191E+06	8.986E-30	1.158E-30
6.50E+00	to	8.00E+00	2.206E-31	8.222E+05	1.143E-30	1.473E-31
8.00E+00	to	1.00E+01	2.945E-32	1.746E+05	1.525E-31	1.965E-32
Total Gamma, g/(sec*FA)			3.670E+12	3.194E+15	1.353E+12	1.353E+12
Total Neutron Source Term, n/(sec*FA)						
Raw ORIGEN-ARP source for uniform burnup						3.018E+08
Treated with peaking factor 1.232 and k_{eff}=0.4 (dry)						6.197E+08

Table 6-29
BWR Source Term for the EOS-HSM, Zone 3 (Normal and Accident)

Burnup (GWD/MTU)			21.72	40	21.72	21.72
Enrichment (wt. % U-235)			1.1	2.5	1.1	1.1
Cooling Time (years)			3.000	4.715	3.000	3.000
Gamma Source Term, γ/(sec*FA)						
E_{min}, MeV	**to**	**E_{max}, MeV**	**Bottom Nozzle**	**In-core**	**Plenum**	**Top Nozzle**
1.00E-02	to	5.00E-02	6.284E+10	6.488E+14	1.217E+11	2.945E+10
5.00E-02	to	1.00E-01	8.418E+09	1.891E+14	3.130E+09	3.116E+09
1.00E-01	to	2.00E-01	3.404E+09	1.571E+14	7.575E+09	1.646E+09
2.00E-01	to	3.00E-01	1.971E+08	4.404E+13	5.346E+08	1.016E+08
3.00E-01	to	4.00E-01	5.085E+08	3.146E+13	2.003E+09	3.004E+08
4.00E-01	to	6.00E-01	7.084E+09	3.971E+14	3.658E+10	4.722E+09
6.00E-01	to	8.00E-01	3.742E+09	1.069E+15	1.933E+10	2.518E+09
8.00E-01	to	1.00E+00	1.736E+11	1.654E+14	5.239E+10	5.363E+10
1.00E+00	to	1.33E+00	2.400E+12	5.020E+13	7.669E+11	8.822E+11
1.33E+00	to	1.66E+00	6.778E+11	1.629E+13	2.166E+11	2.491E+11
1.66E+00	to	2.00E+00	1.443E+05	7.080E+11	4.516E+04	1.057E+05
2.00E+00	to	2.50E+00	1.622E+07	1.375E+12	5.183E+06	5.961E+06
2.50E+00	to	3.00E+00	1.386E+04	5.282E+10	4.428E+03	5.093E+03
3.00E+00	to	4.00E+00	4.305E-07	4.897E+09	4.413E-08	2.426E-06
4.00E+00	to	5.00E+00	2.020E-30	6.334E+06	1.046E-29	1.348E-30
5.00E+00	to	6.50E+00	5.820E-31	2.542E+06	3.015E-30	3.884E-31
6.50E+00	to	8.00E+00	7.403E-32	4.987E+05	3.835E-31	4.941E-32
8.00E+00	to	1.00E+01	9.879E-33	1.059E+05	5.118E-32	6.594E-33
Total Gamma, g/(sec*FA)			3.338E+12	2.771E+15	1.227E+12	1.227E+12
Total Neutron Source Term, n/(sec*FA)						
Raw ORIGEN-ARP source for uniform burnup						1.821E+08
Treated with peaking factor 1.232 and k_{eff}=0.4 (dry)						3.739E+08

Table 6-30
PWR Axial Source Distributions

Axial Segment	Percentage of In-core Height (top of segment)	Burnup Profile (Gamma Profile)	Normalized Gamma Profile(1)	Neutron Profile(2)	Normalized Neutron Profile(3)
1	5.6	0.619	0.0344	0.133	0.0061
2	11.1	0.924	0.0513	0.718	0.0328
3	16.7	1.056	0.0587	1.257	0.0575
4	22.2	1.097	0.0609	1.475	0.0675
5	27.8	1.103	0.0613	1.509	0.0690
6	33.3	1.101	0.0612	1.498	0.0685
7	38.9	1.103	0.0613	1.509	0.0690
8	44.4	1.112	0.0618	1.562	0.0714
9	50.0	1.125	0.0625	1.640	0.0750
10	55.6	1.136	0.0631	1.708	0.0781
11	61.1	1.143	0.0635	1.753	0.0802
12	66.7	1.143	0.0635	1.753	0.0802
13	72.2	1.136	0.0631	1.708	0.0781
14	77.8	1.115	0.0619	1.580	0.0722
15	83.3	1.047	0.0582	1.213	0.0555
16	88.9	0.882	0.0490	0.590	0.0270
17	94.4	0.701	0.0389	0.225	0.0103
18	100.0	0.456	0.0253	0.037	0.0017
-	Sum	17.999	1.000	21.869	1.000
-	Average	1.0	-	1.215	-

Notes:

(1) The normalized gamma profile is the gamma profile divided by the sum of the gamma profile (sum=17.999).

(2) The neutron profile is the burnup profile raised to the 4.2 power.

(3) The normalized neutron profile is the neutron profile divided by the sum of the neutron profile (sum=21.869).

Table 6-31
BWR Axial Source Distributions

Axial Segment	Percentage of In-core Height (top of segment)	Burnup Profile (Gamma Profile)	Normalized Gamma Profile(1)	Neutron Profile(2)	Normalized Neutron Profile(3)
1	4	0.7144	0.0288	0.244	0.0079
2	8	1.0993	0.0443	1.488	0.0483
3	12	1.2185	0.0491	2.293	0.0745
4	16	1.2312	0.0496	2.395	0.0778
5	20	1.2200	0.0492	2.305	0.0748
6	24	1.1799	0.0475	2.003	0.0650
7	28	1.1528	0.0465	1.817	0.0590
8	32	1.1306	0.0456	1.675	0.0544
9	36	1.1140	0.0449	1.574	0.0511
10	40	1.1192	0.0451	1.605	0.0521
11	44	1.1070	0.0446	1.533	0.0498
12	48	1.0807	0.0436	1.385	0.0450
13	52	1.0722	0.0432	1.340	0.0435
14	56	1.0579	0.0426	1.267	0.0411
15	60	1.0313	0.0416	1.138	0.0370
16	64	1.0180	0.0410	1.078	0.0350
17	68	1.0180	0.0410	1.078	0.0350
18	72	1.0212	0.0412	1.092	0.0355
19	76	1.0140	0.0409	1.060	0.0344
20	80	0.9789	0.0394	0.914	0.0297
21	84	0.9169	0.0370	0.695	0.0226
22	88	0.8430	0.0340	0.488	0.0158
23	92	0.7185	0.0290	0.249	0.0081
24	96	0.5540	0.0223	0.084	0.0027
25	100	0.2025	0.0082	0.001	0.0000
-	Sum	24.814	1.000	30.801	1.000
-	Average	1.0	-	1.232	-

Notes:

(1) The normalized gamma profile is the gamma profile divided by the sum of the gamma profile (sum=24.814).

(2) The neutron profile is the burnup profile raised to the 4.2 power.

(3) The normalized neutron profile is the neutron profile divided by the sum of the neutron profile (sum=30.801).

Table 6-32
BPRA Hardware Masses

Region	SS304 (kg)	Inconel X-750 (kg)	Inconel 718 (kg)	Poison (kg)	Zr-4 (kg)
BW 15x15					
Top	3.602	0.058	0	0	0
Plenum	1.068	0	0	0.724	1.197
Core	2.468	0	0	9.146	11.98
WE 17x17 Pyrex					
Top	2.62	0	0.42	0	0
Plenum	2.85	0	0	0	0
Core	11.9	0	0	5.08	0
WE 17x17 WABA					
Top	2.95	0	0	0	0
Plenum	2.76	0	0	0	2.61
Core	0	0	0	2.5	14.8

Table 6-33
TPA Hardware Masses

Region	SS304 (kg)	Inconel X-750 (kg)	Inconel 718 (kg)	Poison (kg)	Zr-4 (kg)
WE 17x17					
Top	2.468	0	0.358	0	0
Plenum	3.266	0	0	0	0
WE 14x14 Type 1					
Top	2.03	0	0.417	0	0
Plenum	2.69	0	0	0	0
WE 14x14 Type 2					
Top	2.03	0.363	0	0	0
Plenum	2.69	0	0	0	0

Table 6-34
Elemental Constituents of Pyrex Poison

Element	Pyrex (wt. fraction)
B	0.040064
O	0.539562
Na	0.028191
Al	0.011644
Si	0.377220
K	0.003321

Table 6-35
CC ORIGEN-ARP Input Mass

Element	BPRA			TPA	
	Active Fuel (g)	Plenum (g)	Top (g)	Plenum (g)	Top (g)
B	203.525	0.000	0.000	0.000	0.000
C	9.508	0.455	0.290	2.609	2.115
N	15.450	0.740	0.475	4.240	3.670
O	2740.969	0.000	0.000	0.000	0.000
Na	143.210	0.000	0.000	0.000	0.000
Al	59.151	0.000	0.046	0.000	2.145
Si	2035.120	5.693	3.615	32.618	25.363
P	5.348	0.256	0.162	1.468	1.109
S	3.565	0.171	0.108	0.979	0.765
K	16.871	0.000	0.000	0.000	0.000
Ti	0.000	0.000	0.145	0.000	2.860
V	0.000	0.000	0.000	0.000	0.000
Cr	2258.087	108.160	69.218	619.741	536.247
Mn	237.693	11.385	7.235	65.236	50.011
Fe	8181.881	391.905	248.050	2245.548	1761.237
Co	5.950	0.285	0.183	1.633	1.413
Ni	1060.112	50.778	36.275	290.952	405.887
Cu	0.000	0.000	0.003	0.000	0.358
Zr	0.000	0.000	0.000	0.000	0.000
Nb	0.000	0.000	0.052	0.000	19.854
Mo	0.000	0.000	0.000	0.000	10.726

Note: For the BPRA ORIGEN-ARP inputs, the flux scaling factors are applied to the constituent masses. For the TPA inputs, the true masses are used in the inputs and the flux scaling factors are applied to the burnup.

Table 6-36
CC Co-60 Activity and Decay Heat

Parameter	BPRA			TPA	
	Active Fuel	Plenum	Top	Plenum	Top
Co-60 (Ci)	308	14.8	9.5	44.1	18.9
Decay Heat (watts)	4.8	0.2	0.1	0.7	0.3

Table 6-37
CC Source Term

E_{min} (MeV)	Zone	Zones 1, 2, 3	Zones 1, 2	Zone 3	Zones 1, 2	Zone 3
	Co-60 (Ci)	308	44.1	14.8	18.9	9.5
	E_{max} (MeV)	Active Fuel (γ/s-CC)	Plenum (γ/s-CC)	Plenum (γ/s-CC)	Top (γ/s-CC)	Top (γ/s-CC)
1.00E-02	5.00E-02	3.133E+11	4.540E+10	1.502E+10	2.061E+10	9.702E+09
5.00E-02	1.00E-01	6.183E+10	8.841E+09	2.965E+09	3.795E+09	1.911E+09
1.00E-01	2.00E-01	1.504E+10	2.145E+09	7.211E+08	9.226E+08	4.648E+08
2.00E-01	3.00E-01	7.435E+08	1.068E+08	3.565E+07	4.682E+07	2.300E+07
3.00E-01	4.00E-01	9.718E+08	1.397E+08	4.660E+07	6.024E+07	3.005E+07
4.00E-01	6.00E-01	7.218E+07	1.113E+07	3.288E+06	5.563E+06	2.144E+06
6.00E-01	8.00E-01	2.770E+07	5.117E+06	1.328E+06	1.497E+09	7.527E+06
8.00E-01	1.00E+00	1.640E+10	1.172E+09	7.865E+08	1.849E+09	5.047E+08
1.00E+00	1.33E+00	1.798E+13	2.573E+12	8.624E+11	1.100E+12	5.559E+11
1.33E+00	1.66E+00	5.078E+12	7.267E+11	2.435E+11	3.106E+11	1.570E+11
1.66E+00	2.00E+00	3.510E+00	3.100E-05	1.936E-05	2.716E-03	2.344E-04
2.00E+00	2.50E+00	1.215E+08	1.739E+07	5.827E+06	7.432E+06	3.756E+06
2.50E+00	3.00E+00	1.038E+05	1.486E+04	4.979E+03	6.350E+03	3.210E+03
3.00E+00	4.00E+00	1.322E-02	3.488E-11	1.102E-11	1.051E-06	9.764E-07
4.00E+00	5.00E+00	0.000E+00	0.000E+00	0.000E+00	0.000E+00	0.000E+00
5.00E+00	6.50E+00	0.000E+00	0.000E+00	0.000E+00	0.000E+00	0.000E+00
6.50E+00	8.00E+00	0.000E+00	0.000E+00	0.000E+00	0.000E+00	0.000E+00
8.00E+00	1.00E+01	0.000E+00	0.000E+00	0.000E+00	0.000E+00	0.000E+00
	Total	2.347E+13	3.358E+12	1.125E+12	1.439E+12	7.256E+11

Proprietary Information on Pages 6-73 through 6-74
Withheld Pursuant to 10 CFR 2.390

Table 6-40
Irradiation Gases

Element	PWR with CC (no IFBA) (moles)[1]	PWR with IFBA (no CC) (moles)[1]	BWR (moles)[1]
H	1.63E+00	1.58E+00	1.19E+00
He	1.17E+01	1.16E+01	1.08E+00
N	3.52E+00	2.33E+00	1.06E+00
F	2.77E-01	2.77E-01	1.12E-01
Ne	2.27E-04	1.63E-04	7.03E-05
Cl	7.35E-02	7.34E-02	2.96E-02
Ar	6.52E-04	2.60E-05	1.38E-05
Br	2.15E-01	2.15E-01	8.80E-02
Kr	3.25E+00	3.25E+00	1.34E+00
I	1.51E+00	1.51E+00	5.90E-01
Xe	3.69E+01	3.68E+01	1.51E+01
Rn	6.15E-13	6.14E-13	2.21E-13
Total	59.0[2][3]	57.7	20.6

Notes:

(1) These gases represent gas generated by irradiation and do not include any gas present when the fuel or CC was originally fabricated.

(2) The 59.0 moles of gas includes 49.4 moles from the PWR FA and 9.6 moles from CC.

(3) For fuel with a total unirradiated fuel length < 157 inches, this value is 54.8 moles.

Table 6-41
MCNP Material Compositions (wt. %)

Element	Carbon Steel	Stainless Steel	Dry Air	Water	Regular Concrete	Soil
Hydrogen	-	-	-	11.1894	1.0	-
Helium	-	-	-	-	-	-
Boron	-	-	-	-	-	-
Carbon	0.5	0.04	0.0124	-	-	-
Nitrogen	-	-	75.5268	-	-	-
Oxygen	-	-	23.1781	88.8106	53.2	51.37
Sodium	-	-	-	-	2.9	0.614
Magnesium	-	-	-	-	-	1.33
Aluminum	-	-	-	-	3.4	6.856
Silicon	-	0.5	-	-	33.7	27.118
Phosphorous	-	0.023	-	-	-	-
Sulfur	-	0.015	-	-	-	-
Argon	-	-	1.2827	-	-	-
Potassium	-	-	-	-	-	1.433
Calcium	-	-	-	-	4.4	5.117
Titanium	-	-	-	-	-	0.461
Chromium	-	19	-	-	-	-
Manganese	-	1	-	-	-	0.0716
Iron	99.5	70.173	-	-	1.4	5.629
Cobalt	-	-	-	-	-	-
Nickel	-	9.25	-	-	-	-
Copper	-	-	-	-	-	-
Zirconium	-	-	-	-	-	-
Niobium	-	-	-	-	-	-
Molybdenum	-	-	-	-	-	-
Tin	-	-	-	-	-	-
Lead	-	-	-	-	-	-
Density (g/cm^3)	7.82	8.00	0.001205	(1)	2.243	1.52

Note: (1) 0.958 g/cm^3 inside the DSC and 0.9982 g/cm^3 inside the neutron shield.

Table 6-42
MCNP Borated Polyethylene Composition

Element	Atom Density (atom/b-cm)
Hydrogen	6.1848E-02
Boron-10	5.5978E-04
Boron-11	2.2532E-03
Carbon	3.6381E-02
Oxygen	4.2195E-03
Total	1.0526E-01

Table 6-43
MCNP PWR Dry Fuel Compositions (wt. fraction)

Material	Bottom Nozzle	Active Fuel	Plenum	Top Nozzle
Boron	2.7088E-06	3.7133E-07	1.7956E-05	7.8154E-06
Carbon	2.0552E-04	5.4215E-06	3.3783E-04	4.5158E-04
Oxygen	6.3495E-04	9.8758E-02	5.4025E-04	-
Aluminum	2.7088E-04	3.7133E-05	1.7956E-03	7.8154E-04
Silicon	2.2469E-03	2.3617E-05	2.0878E-03	4.7155E-03
Phosphorous	1.0302E-04	1.0397E-06	9.3784E-05	2.1593E-04
Sulfur	6.9824E-05	1.0397E-06	7.8651E-05	1.4844E-04
Titanium	4.8759E-04	6.6840E-05	3.2322E-03	1.4068E-03
Chromium	8.9659E-02	1.5716E-03	1.0462E-01	1.9000E-01
Manganese	4.3216E-03	2.3617E-05	3.0336E-03	8.9340E-03
Iron	3.0144E-01	1.5836E-03	1.9469E-01	6.1862E-01
Cobalt	4.9300E-04	6.7583E-05	3.2681E-03	1.4224E-03
Nickel	6.6661E-02	3.8767E-03	2.0496E-01	1.5963E-01
Copper	1.4790E-04	2.0275E-05	9.8042E-04	4.2672E-04
Zirconium	5.2126E-01	1.5811E-01	4.4352E-01	-
Niobium	2.7765E-03	3.8062E-04	1.8405E-02	8.0108E-03
Molybdenum	1.6524E-03	2.2651E-04	1.0953E-02	4.7674E-03
Tin	7.4087E-03	2.2471E-03	6.3037E-03	-
U-234	-	1.9571E-04	-	-
U-235	-	2.1989E-02	-	-
U-236	-	1.0115E-04	-	-
U-238	-	7.1069E-01	-	-
Total	1.0	1.0	1.0	1.0
Density (g/cm^3)	1.9683	3.9508	1.4454	1.8560

Table 6-44
MCNP PWR Wet Fuel Compositions (wt. fraction)

Material	Bottom Nozzle	Active Fuel	Plenum	Top Nozzle
Hydrogen	2.9202E-02	1.4216E-02	3.8863E-02	3.1790E-02
Boron	2.0019E-06	3.2415E-07	1.1720E-05	5.5950E-06
Carbon	1.5188E-04	4.7326E-06	2.2049E-04	3.2328E-04
Oxygen	2.3225E-01	1.9905E-01	3.0881E-01	2.5232E-01
Aluminum	2.0019E-04	3.2415E-05	1.1720E-03	5.5950E-04
Silicon	1.6605E-03	2.0616E-05	1.3627E-03	3.3758E-03
Phosphorous	7.6132E-05	9.0763E-07	6.1211E-05	1.5458E-04
Sulfur	5.1601E-05	9.0763E-07	5.1334E-05	1.0626E-04
Titanium	3.6033E-04	5.8348E-05	2.1096E-03	1.0071E-03
Chromium	6.6260E-02	1.3719E-03	6.8286E-02	1.3602E-01
Manganese	3.1937E-03	2.0616E-05	1.9800E-03	6.3958E-03
Iron	2.2277E-01	1.3824E-03	1.2707E-01	4.4286E-01
Cobalt	3.6434E-04	5.8996E-05	2.1330E-03	1.0183E-03
Nickel	4.9263E-02	3.3842E-03	1.3377E-01	1.1428E-01
Copper	1.0930E-04	1.7699E-05	6.3990E-04	3.0549E-04
Zirconium	3.8522E-01	1.3802E-01	2.8948E-01	-
Niobium	2.0519E-03	3.3226E-04	1.2013E-02	5.7349E-03
Molybdenum	1.2211E-03	1.9773E-04	7.1491E-03	3.4130E-03
Tin	5.4751E-03	1.9616E-03	4.1143E-03	-
U-234	-	1.7084E-04	-	-
U-235	-	1.9196E-02	-	-
U-236	-	8.8300E-05	-	-
U-238	-	6.2040E-01	-	-
Total	1.0	1.0	1.0	1.0
Density (g/cm^3)	2.6635	4.5258	2.2146	2.5925

Table 6-45
MCNP BWR Dry Fuel Compositions (wt. fraction)

Material	Bottom Nozzle	Active Fuel	Plenum	Top Nozzle
Boron	-	-	-	6.0000E-06
Carbon	3.1900E-04	9.6424E-02	7.1000E-05	3.0500E-04
Oxygen	2.5100E-04	2.2200E-04	9.8500E-04	3.9400E-04
Aluminum	4.2000E-05	7.0000E-06	-	5.6300E-04
Silicon	3.9370E-03	4.0000E-06	8.8400E-04	3.1460E-03
Phosphorus	1.8100E-04	-	4.1000E-05	1.4400E-04
Sulfur	1.1800E-04	-	2.7000E-05	9.9000E-05
Titanium	7.5000E-05	1.2000E-05	-	1.0130E-03
Chromium	1.5037E-01	4.3200E-04	3.4406E-02	1.2766E-01
Manganese	7.8470E-03	4.0000E-06	1.7680E-03	5.9340E-03
Iron	5.5060E-01	5.9100E-04	1.2568E-01	4.1107E-01
Cobalt	7.6000E-05	1.2000E-05	-	1.0240E-03
Nickel	7.6705E-02	6.8400E-04	1.6351E-02	1.1067E-01
Copper	2.3000E-05	4.0000E-06	-	3.0700E-04
Zirconium	2.0585E-01	1.8186E-01	8.0830E-01	3.2386E-01
Niobium	4.2600E-04	6.7000E-05	-	5.7690E-03
Molybdenum	2.5400E-04	4.0000E-05	-	3.4330E-03
Tin	2.9260E-03	2.5850E-03	1.1488E-02	4.6030E-03
U-234	-	1.9100E-04	-	-
U-235	-	2.1511E-02	-	-
U-236	-	9.9000E-05	-	-
U-238	-	6.9525E-01	-	-
Total	1.0	1.0	1.0	1.0
Density (g/cm^3)	1.980	4.201	1.006	0.663

Table 6-46
MCNP BWR Wet Fuel Compositions (wt. fraction)

Material	Bottom Nozzle	Active Fuel	Plenum	Top Nozzle
Hydrogen	2.9538E-02	1.2850E-02	5.0093E-02	6.3595E-02
Boron	-	-	-	2.0000E-06
Carbon	2.3500E-04	8.5351E-02	3.9000E-05	1.3200E-04
Oxygen	2.3463E-01	1.0219E-01	3.9814E-01	5.0492E-01
Aluminum	3.1000E-05	6.0000E-06	-	2.4300E-04
Silicon	2.8970E-03	4.0000E-06	4.8800E-04	1.3580E-03
Phosphorus	1.3300E-04	-	2.2000E-05	6.2000E-05
Sulfur	8.7000E-05	-	1.5000E-05	4.3000E-05
Titanium	5.5000E-05	1.0000E-05	-	4.3700E-04
Chromium	1.1068E-01	3.8300E-04	1.9003E-02	5.5104E-02
Manganese	5.7750E-03	4.0000E-06	9.7600E-04	2.5610E-03
Iron	4.0525E-01	5.2300E-04	6.9417E-02	1.7744E-01
Cobalt	5.6000E-05	1.1000E-05	-	4.4200E-04
Nickel	5.6456E-02	6.0600E-04	9.0310E-03	4.7773E-02
Copper	1.7000E-05	3.0000E-06	-	1.3300E-04
Zirconium	1.5151E-01	1.6098E-01	4.4643E-01	1.3980E-01
Niobium	3.1400E-04	5.9000E-05	0.0000E+00	2.4900E-03
Molybdenum	1.8700E-04	3.5000E-05	0.0000E+00	1.4820E-03
Tin	2.1530E-03	2.2880E-03	6.3450E-03	1.9870E-03
U-234	-	1.6900E-04	-	-
U-235	-	1.9041E-02	-	-
U-236	-	8.8000E-05	-	-
U-238	-	6.1541E-01	-	-
Total	1.0	1.0	1.0	1.0
Density (g/cm^3)	2.690	4.746	1.822	1.536

Table 6-47
EOS-37PTH DSC and EOS-89BTH DSC Key As-Modeled Dimensions
(Inches)

Item	EOS-37PTH DSC	EOS-89BTH DSC
Carbon steel shield plug thickness	6.0	6.0
Stainless steel inner top cover plate thickness	2.0	2.0
Stainless steel outer top cover plate thickness	2.0	2.0
Stainless steel shell thickness	0.5	0.5
Stainless steel shell outer diameter	75.5	75.5
Stainless steel outer bottom cover thickness	2.0	2.0
Carbon steel inner bottom shield thickness	4.0	4.0
Stainless steel inner bottom cover thickness	2.0	2.0
Basket compartment inner width	8.86	5.85
Carbon steel basket plate thickness(1)	0.281	0.1875
Aluminum basket plate thickness	0.250	0
MMC basket plate thickness	0.164	0.175

Note:

(1) The EOS-89BTH DSC carbon steel basket plates are modeled as stainless steel. This has no effect on the results.

Table 6-48
EOS-TC108 and EOS-TC125/135 Key As-Modeled Dimensions (Inches)

Item	EOS-TC108	EOS-TC125/135
Cask inner diameter	76.25	76.25
Carbon steel inner shell thickness	0.75	0.75
Stainless steel side lead minimum thickness	2.4	3.51
Carbon steel outer shell thickness	1.0	1.0
Neutron shield water thickness	2.5	4.0
Ram port inner diameter	22.0	22.0
Carbon steel ram plate thickness	1.25	1.25
Carbon steel bottom panel thickness	0.75	0.75
Borated polyethylene thickness	2.13	2.13
Carbon steel bottom end plate thickness	2.0	2.0
Carbon steel bottom ring height	9.0	9.0
Carbon steel top ring height	16.25	16.25
Top ring lead height	5.65	5.65
Top ring lead minimum thickness	0.85	0.85
Top ring thickness (at top nozzle)	4.63	5.38
Top cover plate (lid) thickness	2.0 (Aluminum)	3.2 (Carbon Steel)

Table 6-49
EOS-TC Model Configurations

EOS-TC108							
Configuration	**Water Fill**	**Shield Plug**	**ITCP**	**OTCP**	**Annulus Water Fill**	**Neutron Shield**	**Top Cover Plate (Lid)**
Decontamination	Partial(1)	On	Off	Off	Full	Off	Off
Welding/Drying	Empty	On	On	Off	-12 inches	On/Full	Off
Downending/Transfer	Empty	On	On	On	Empty	On/Full	On
EOS-TC125/135							
Configuration	**Water Fill**	**Shield Plug**	**ITCP**	**OTCP**	**Annulus Water Fill**	**Neutron Shield**	**Top Cover Plate (Lid)**
Decontamination	Full	On	Off	Off	Full	Empty	Off
Welding/Drying	Empty	On	On	Off	-12 inches	Full	Off
Downending/Transfer	Empty	On	On	On	Empty	Full	On

Note: (1) Top nozzle and plenum are dry for EOS-37PTH DSC, top nozzle is dry for EOS-89BTH DSC.

Table 6-50
EOS-HSM Key As-Modeled Dimensions (Inches)

Item	EOS-HSM-Short	EOS-HSM-Medium
Base/roof width	116	116
Base height	178	178
Base/roof length	228	248
Base upper side wall thickness	12	12
Base upper rear wall thickness	12	12
Roof thickness	44	44
Rear/end (side) shield wall thickness	36	36
Rear/end (side)/corner shield wall height	222	222
End (side) shield wall length	117	127
Corner shield wall width (square)	36	36
Door inner steel plate thickness	1	1
Door concrete thickness (centerline)	30.5	30.5
Door outer concrete width (square)	100.375	100.375
Inlet vent height	30	30
Inlet vent width	10	10
Base outlet vent height	8	8
Base outlet vent length	128	148
Roof outlet vent opening width	8	8
Roof outlet vent opening length	132 max./116 min. (trapezoidal)	152 max./136 min. (trapezoidal)
Outlet vent cover width	48	48
Outlet vent cover length	156	176
Outlet vent cover concrete thickness	10.625	10.625
Outlet vent cover steel plate thickness	1	1
Outlet vent cover opening height	6.25	6.25
Outlet vent cover opening length	132	152
Gaps between base and shield walls	1.5	1.5

Table 6-51
ANSI/ANS-6.1.1-1977 Flux-to-Dose-Rate Conversion Factors

E (MeV)	Neutron Factors (mrem/hr)/(n/cm^2-s)	E (MeV)	Neutron Factors (mrem/hr)/(n/cm^2-s)
2.50E-08	3.67E-03	0.5	9.26E-02
1.00E-07	3.67E-03	1.0	1.32E-01
1.00E-06	4.46E-03	2.5	1.25E-01
1.00E-05	4.54E-03	5.0	1.56E-01
1.00E-04	4.18E-03	7.0	1.47E-01
0.001	3.76E-03	10.0	1.47E-01
0.01	3.56E-03	14.0	2.08E-01
0.1	2.17E-02	20.0	2.27E-01
E (MeV)	**Gamma Factors (mrem/hr)/(γ/cm^2-s)**	**E (MeV)**	**Gamma Factors (mrem/hr)/(γ/cm^2-s)**
0.01	3.96E-03	1.4	2.51E-03
0.03	5.82E-04	1.8	2.99E-03
0.05	2.90E-04	2.2	3.42E-03
0.07	2.58E-04	2.6	3.82E-03
0.1	2.83E-04	2.8	4.01E-03
0.15	3.79E-04	3.25	4.41E-03
0.2	5.01E-04	3.75	4.83E-03
0.25	6.31E-04	4.25	5.23E-03
0.3	7.59E-04	4.75	5.60E-03
0.35	8.78E-04	5.0	5.80E-03
0.4	9.85E-04	5.25	6.01E-03
0.45	1.08E-03	5.75	6.37E-03
0.5	1.17E-03	6.25	6.74E-03
0.55	1.27E-03	6.75	7.11E-03
0.6	1.36E-03	7.5	7.66E-03
0.65	1.44E-03	9.0	8.77E-03
0.7	1.52E-03	11.0	1.03E-02
0.8	1.68E-03	13.0	1.18E-02
1.0	1.98E-03	15.0	1.33E-02

Proprietary Information on Pages 6-87 through 6-94
Withheld Pursuant to 10 CFR 2.390

Table 6-58
EOS-HSM Neutron Average Fluxes and Dose Rates, EOS-89BTH DSC

Table 6-59
EOS-HSM Grout Study Results, EOS-89BTH DSC

Configuration	Side Gamma Dose Rate (mrem/hr)
No grout	1.40
3 in. grout	1.78
6 in. grout	2.20

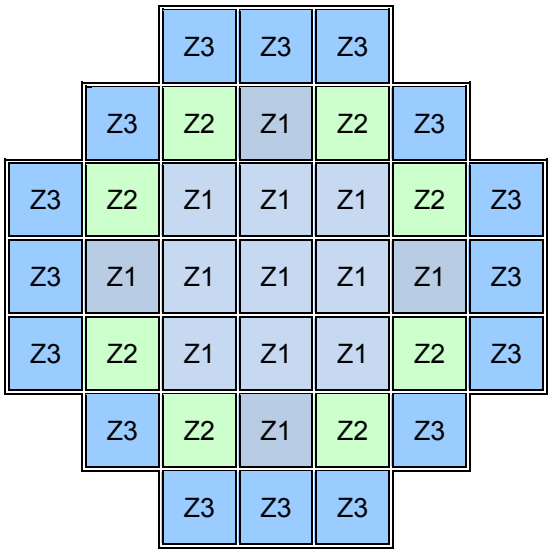

Heat Load Zone Configuration for the EOS-37PTH in the EOS-TC125/135

Zone No.	1	2	3
Maximum Decay Heat (kW/FA plus CCs if any)	1.0	2.0	1.3125
Minimum Cooling Time, Standard (years)	3.0	3.0	3.0
Minimum Cooling Time, SS304 Reconstituted (years)	15.0	15.0	15.0
Number of Fuel Assemblies	13	8	16
Maximum Decay Heat per DSC (kW)	50.0		

Heat Load Zone Configuration for the EOS-37PTH in the EOS-TC108

Zone No.	1	2	3	
Maximum Decay Heat (kW/FA plus CCs if any)	1.0	1.5	≤ 1.0	$1.0 < H \leq 1.05$
Minimum Cooling Time, Standard (years)	3.0	3.0	5.0	8.0
Minimum Cooling Time, SS304 Reconstituted (years)	15.0	15.0	15.0	15.0
Number of Fuel Assemblies	13	8	16	16
Maximum Decay Heat per DSC (kW)	41.8			

Figure 6-1
EOS-37PTH Heat Load Zone Configurations

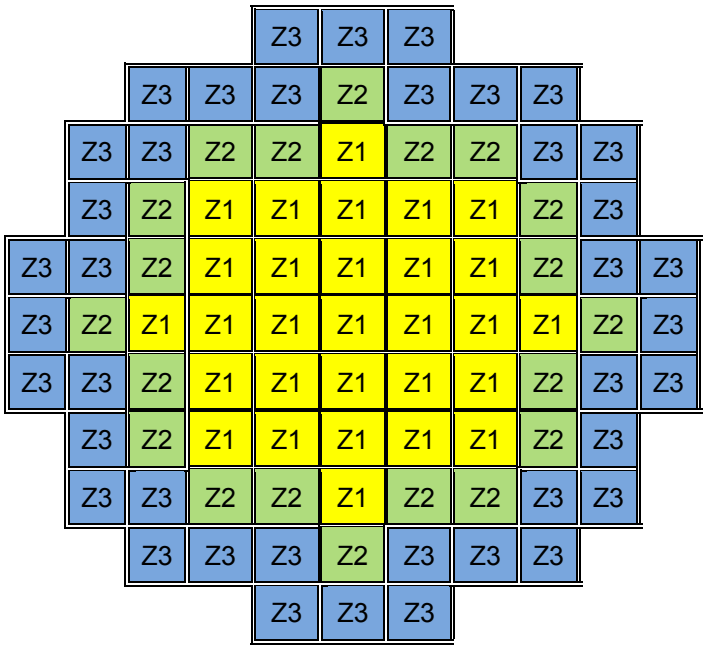

Heat Load Zone Configuration for the EOS-89BTH in the EOS-TC125

Zone Number	1	2	3
Minimum Cooling Time, Standard (years)	3.0	3.0	3.0
Minimum Cooling Time, SS304 Reconstituted (years)	15.0	15.0	15.0
Maximum Decay Heat per SFA plus channel (kW)	0.4	0.6	0.5
Number of Fuel Assemblies	29	20	40
Maximum Decay Heat per DSC (kW)	43.6		

Heat Load Zone Configuration for the EOS-89BTH in the EOS-TC108

Zone Number	1	2	3
Minimum Cooling Time, Standard (years)	3.0	3.0	9.7
Minimum Cooling Time, SS304 Reconstituted (years)	15.0	15.0	15.0
Maximum Decay Heat per SFA plus channel (kW)	0.4	0.5	0.5
Number of Fuel Assemblies	29	20	40
Maximum Decay Heat per DSC (kW)	41.6		

Figure 6-2
EOS-89BTH Heat Load Zone Configurations

Proprietary Information
Withheld Pursuant to 10

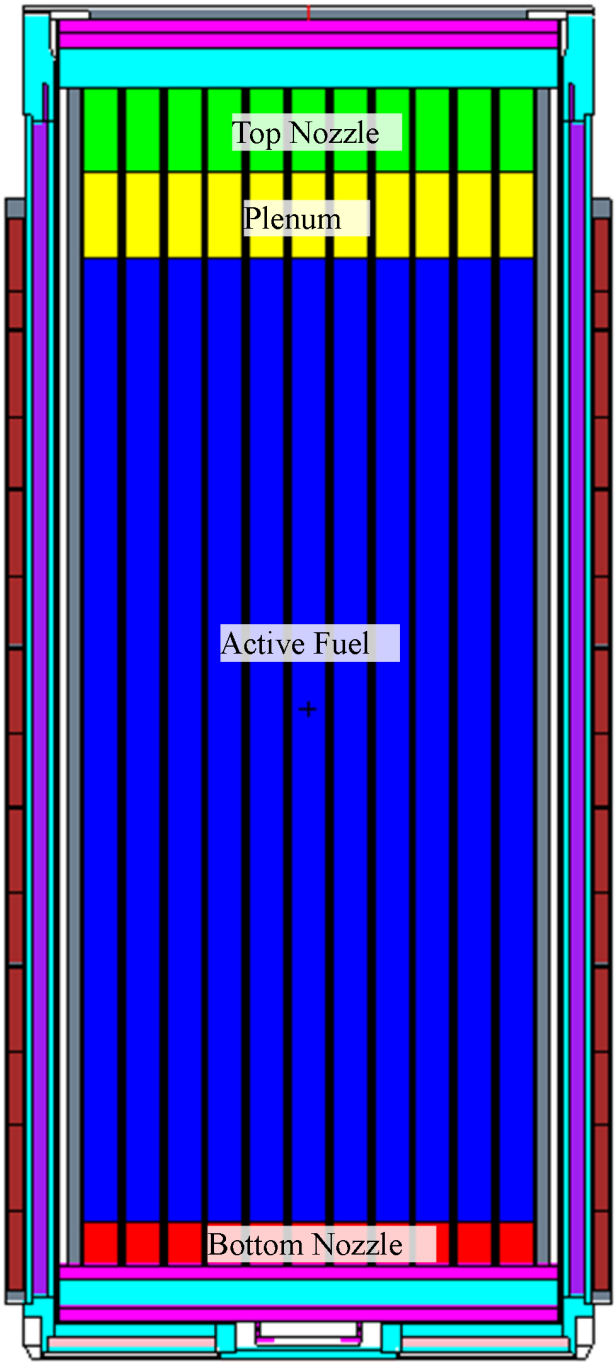

EOS-89BTH DSC in EOS-TC108 depicted; other configurations are similar.

Figure 6-4
General EOS-TC MCNP Model, x-z View

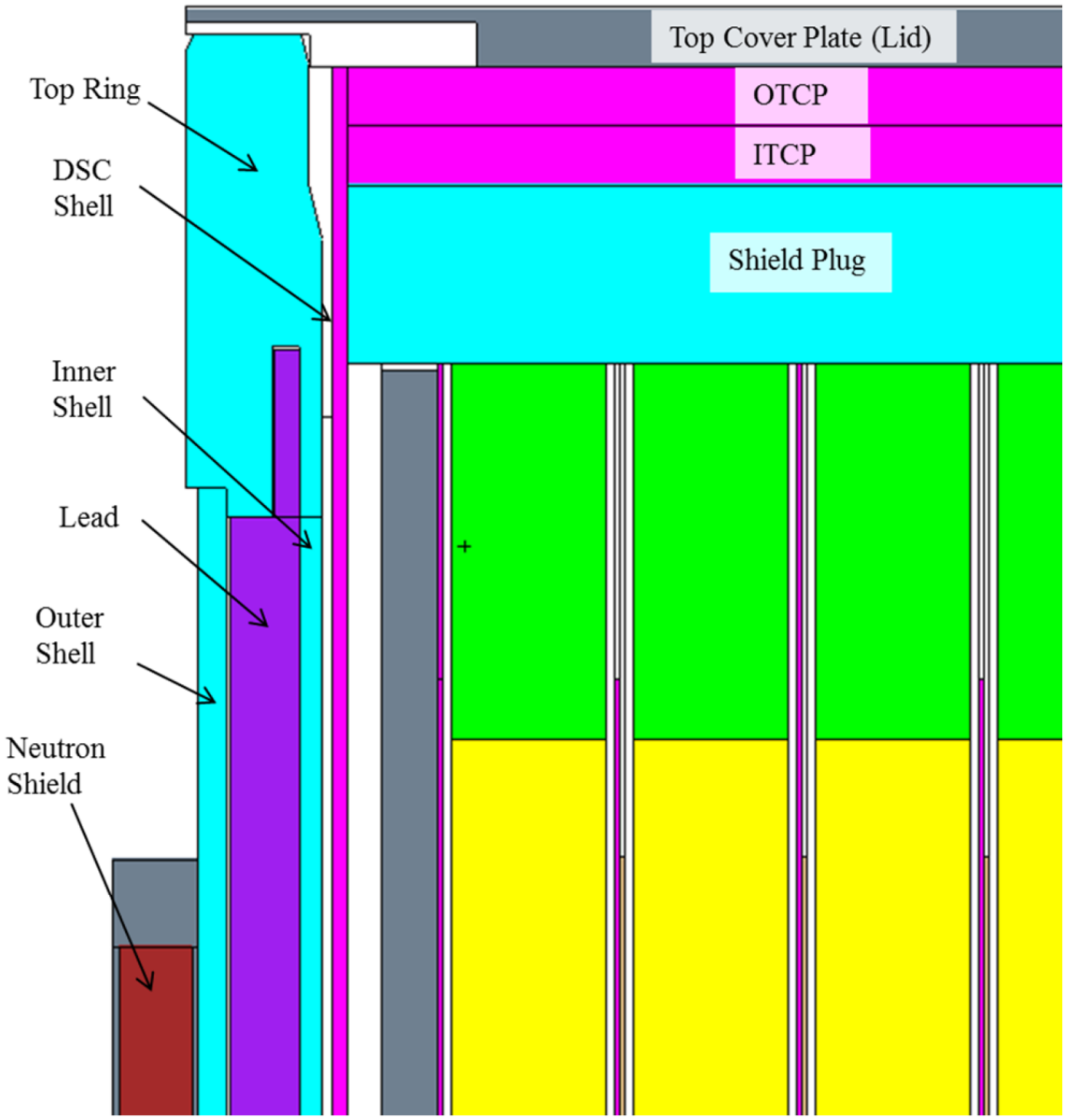

EOS-89BTH DSC in EOS-TC108 depicted; other configurations are similar.

Figure 6-5
Detailed Upper View of EOS-TC MCNP Model

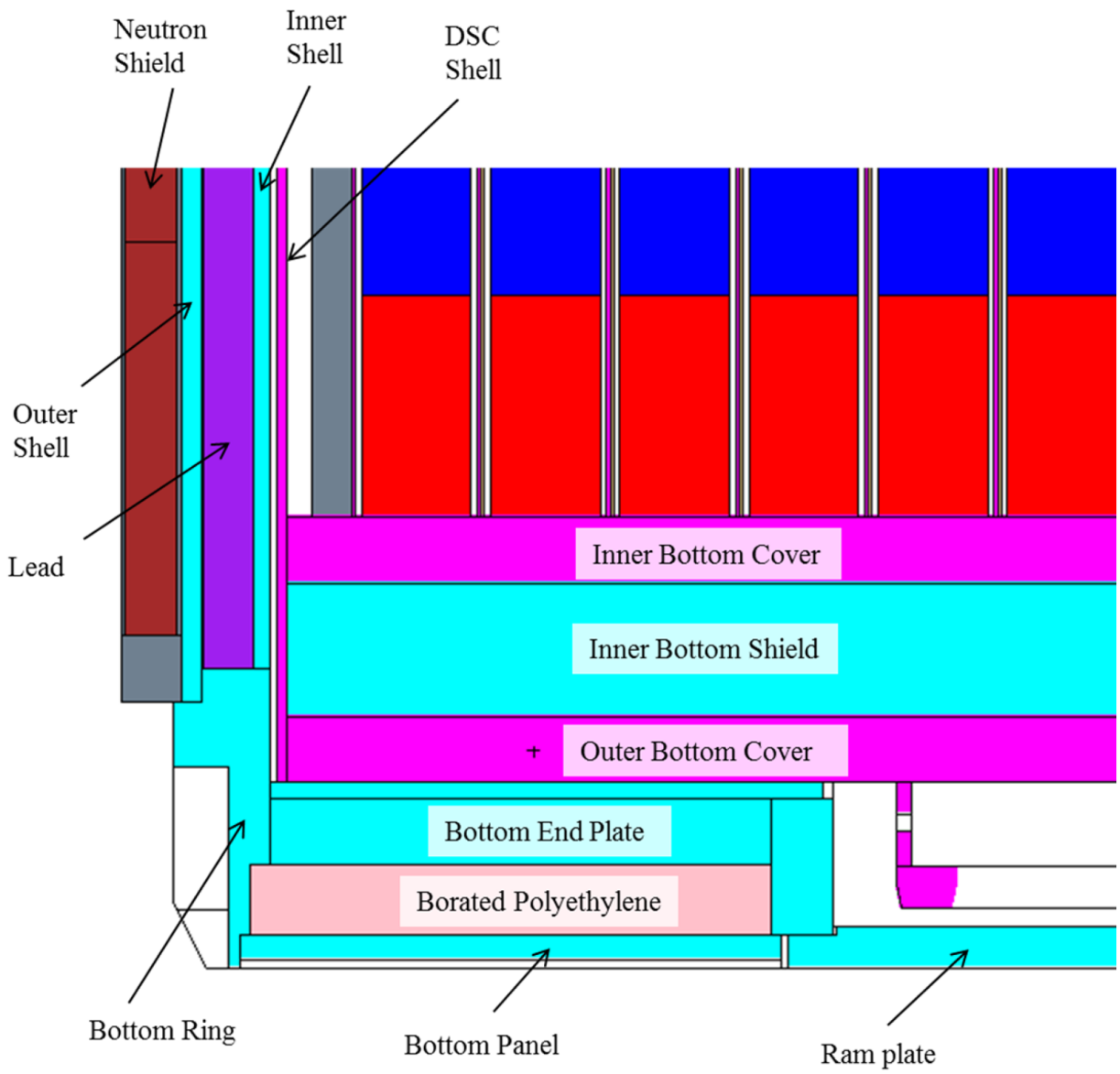

Figure 6-6
Detailed Lower View of EOS-TC MCNP Model

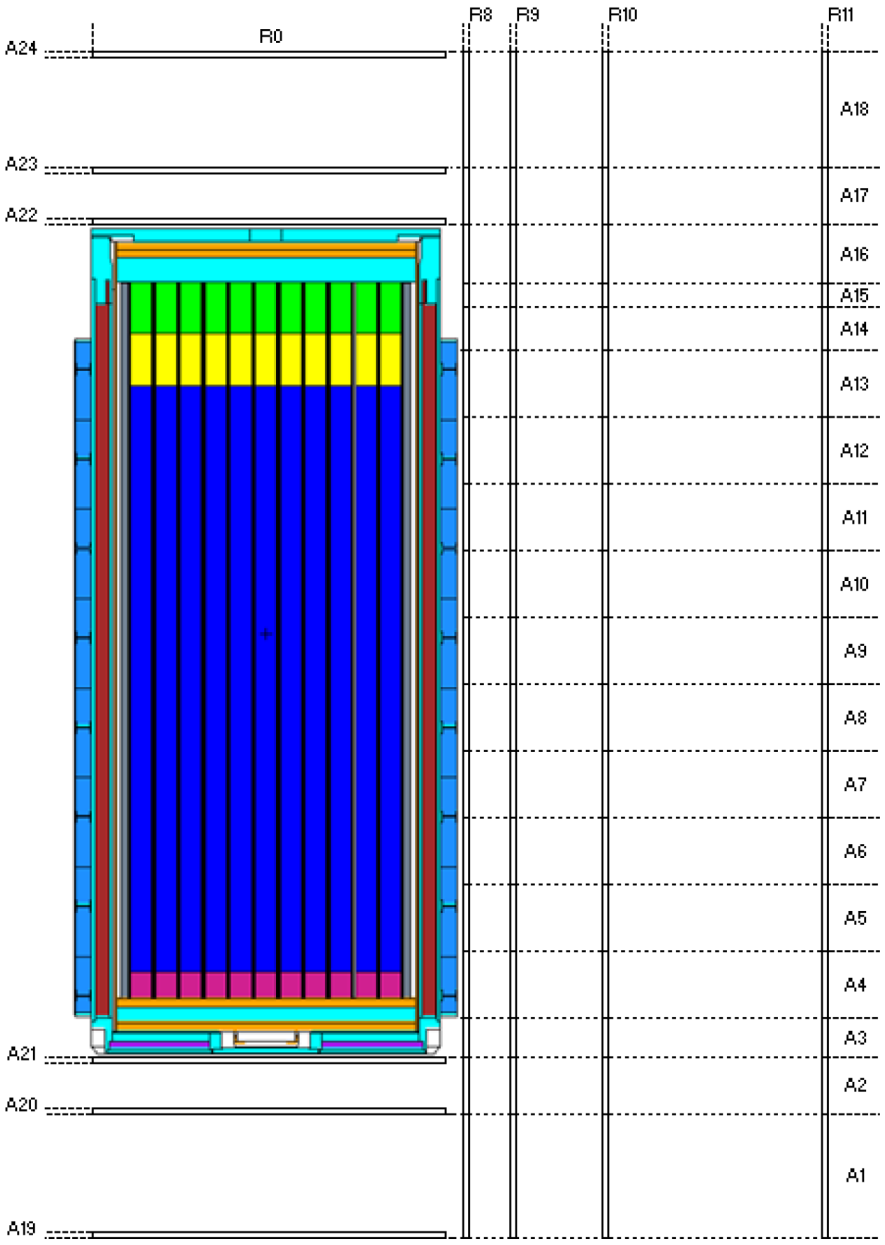

EOS-89BTH DSC in EOS-TC125/135 depicted; other configurations are similar.

Figure 6-7
EOS-TC General Dose Rate Tally Locations

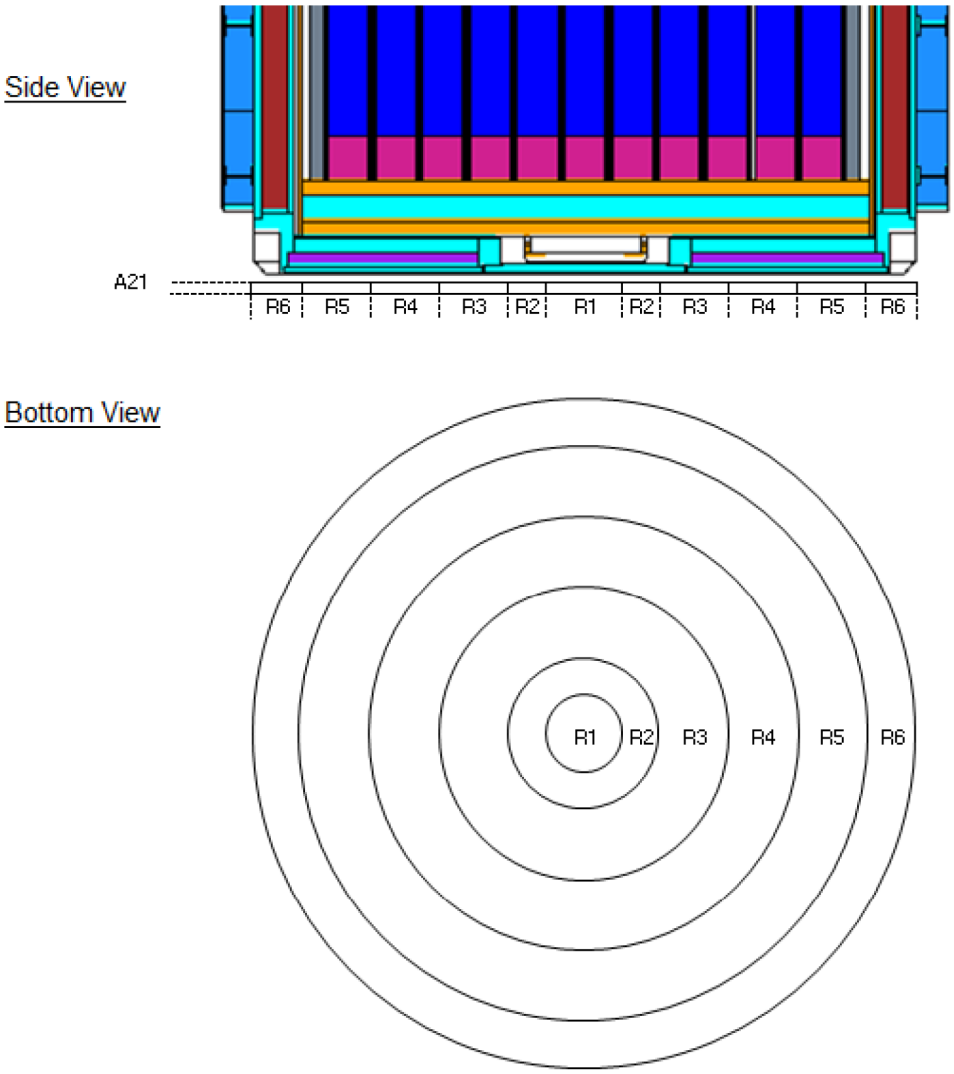

EOS-89BTH DSC in EOS-TC125/135 depicted; other configurations are similar.

Figure 6-8
EOS-TC Bottom Dose Rate Tally Locations, Transfer Configuration

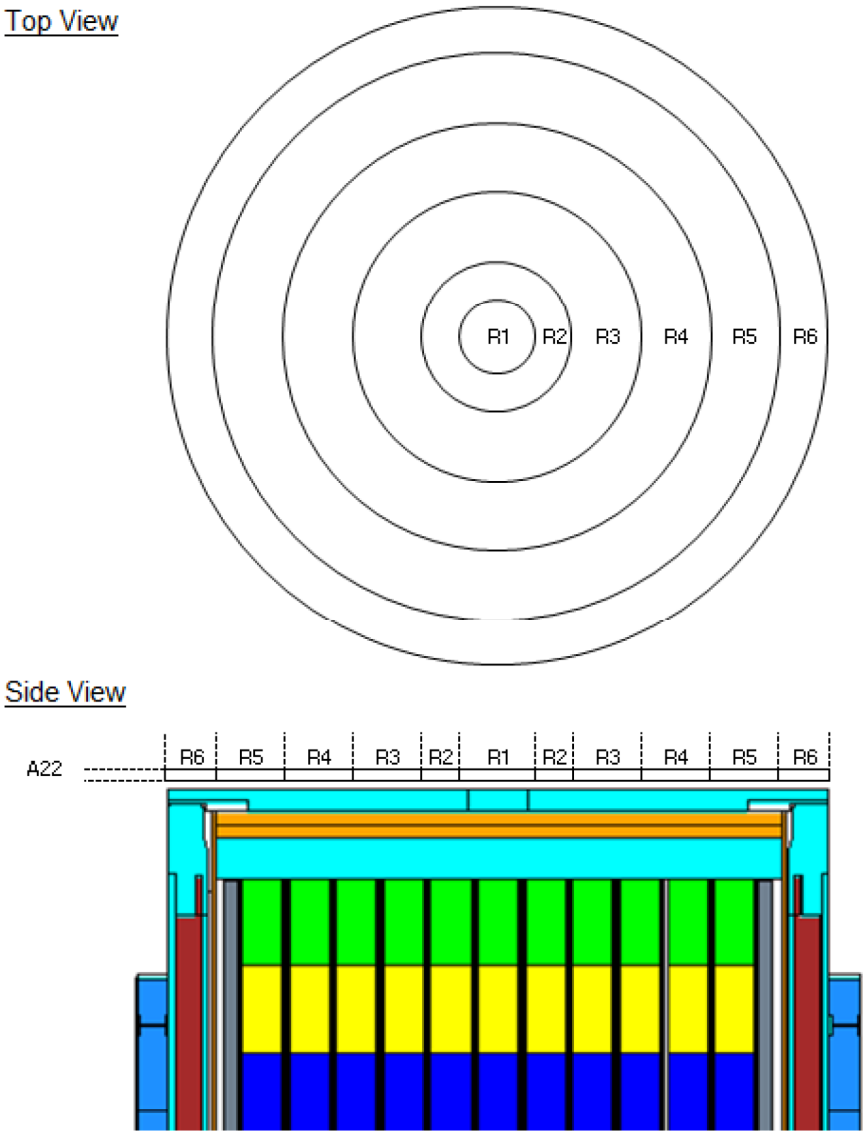

EOS-89BTH DSC in EOS-TC125/135 depicted; other configurations are similar.

Figure 6-9
EOS-TC Top Dose Rate Tally Locations, Transfer Configuration

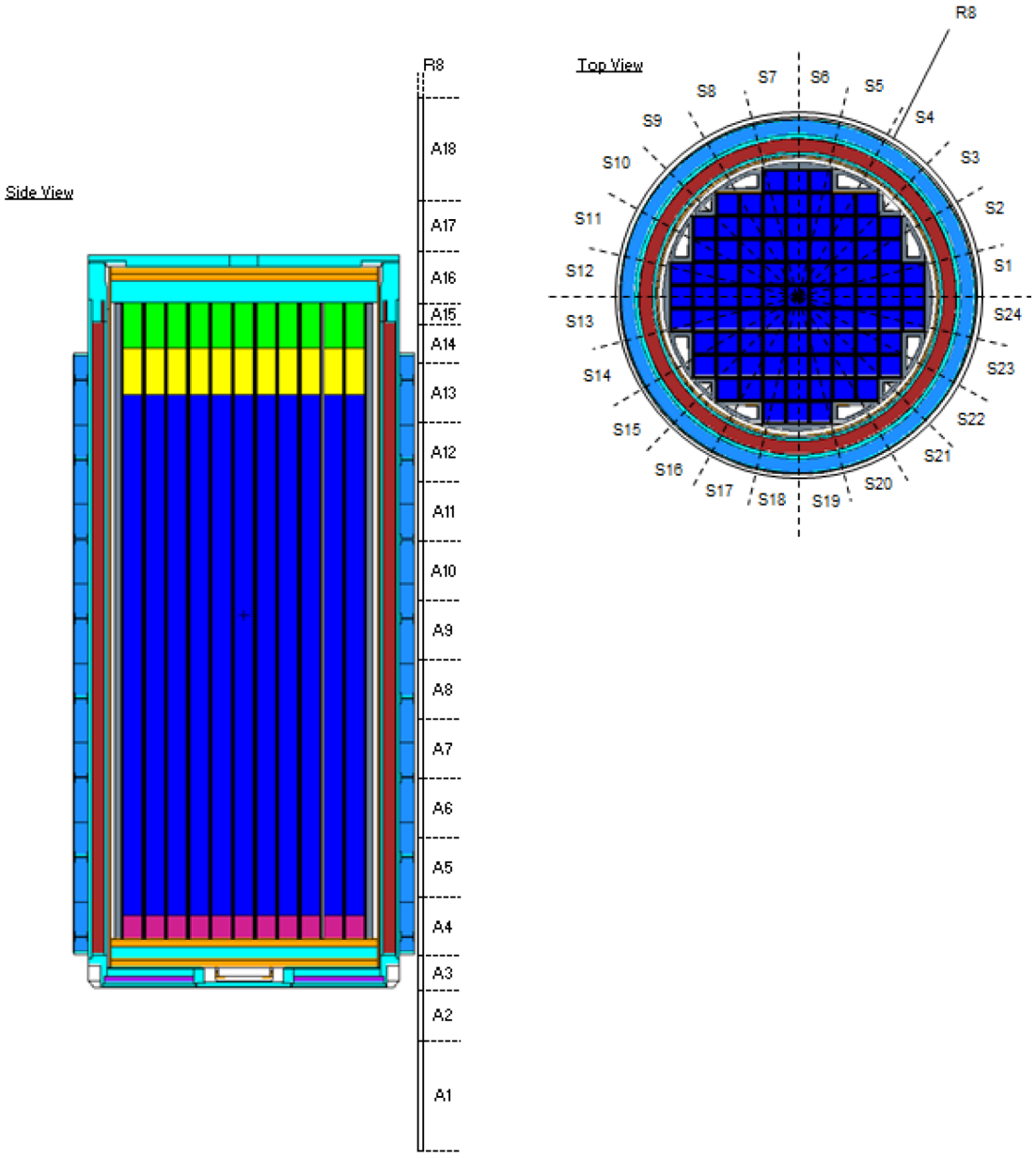

EOS-89BTH DSC in EOS-TC125/135 depicted; other configurations are similar.

Figure 6-10
EOS-TC Side Dose Rate Tally Locations, Transfer Configuration

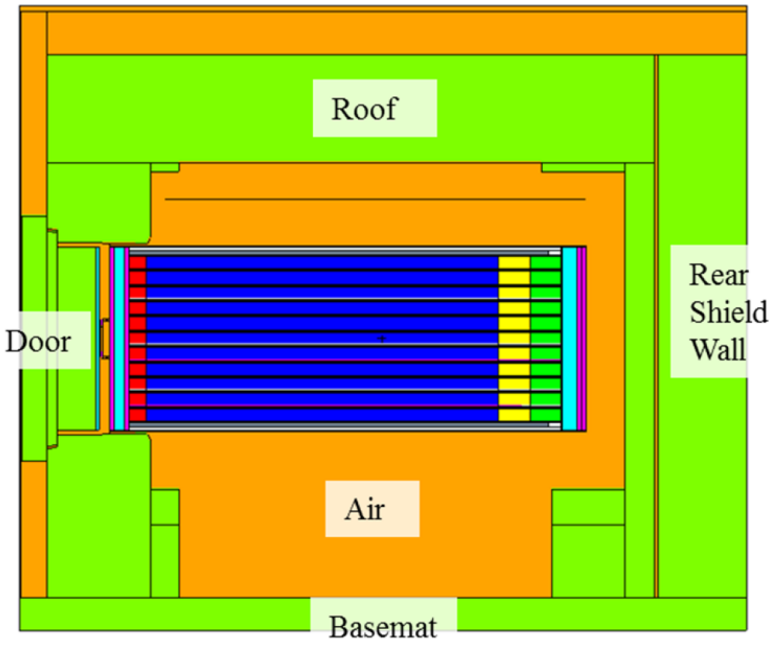

X = 0 cm

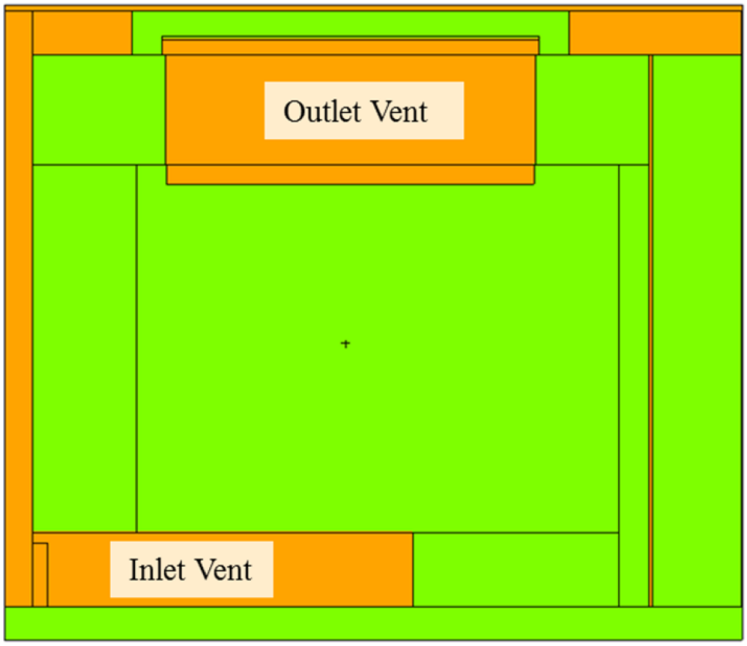

X = -143 cm

EOS-89BTH DSC in EOS-HSM-Medium depicted; other configurations are similar.

Figure 6-11
EOS-HSM MCNP Single-Reflection Model, z-y View

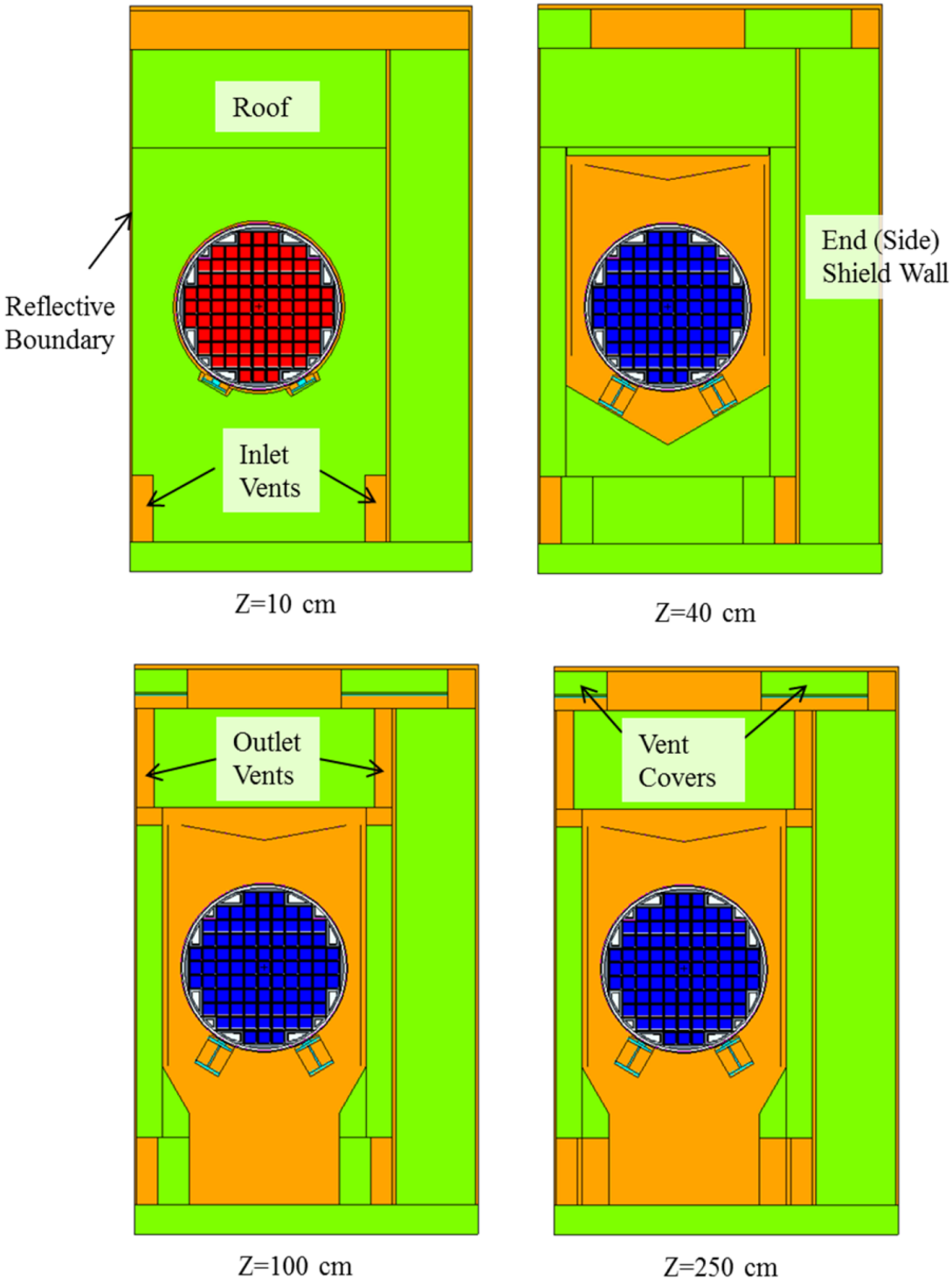

EOS-89BTH DSC in EOS-HSM-Medium depicted; other configurations are similar.

Figure 6-12
EOS-HSM MCNP Single-Reflection Model, x-y View

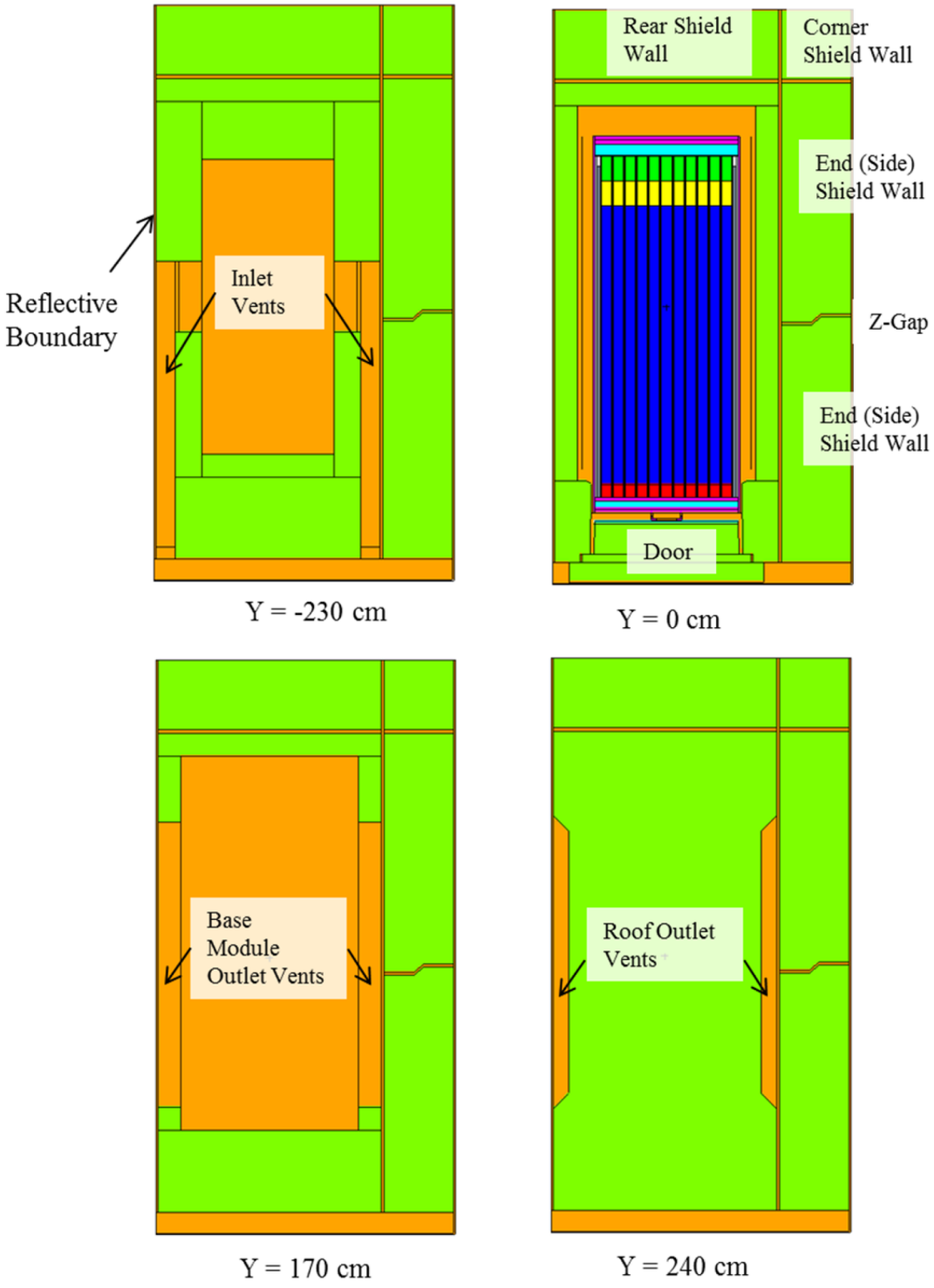

EOS-89BTH DSC in EOS-HSM-Medium depicted; other configurations are similar.

Figure 6-13
EOS-HSM MCNP Single-Reflection Model, x-z View

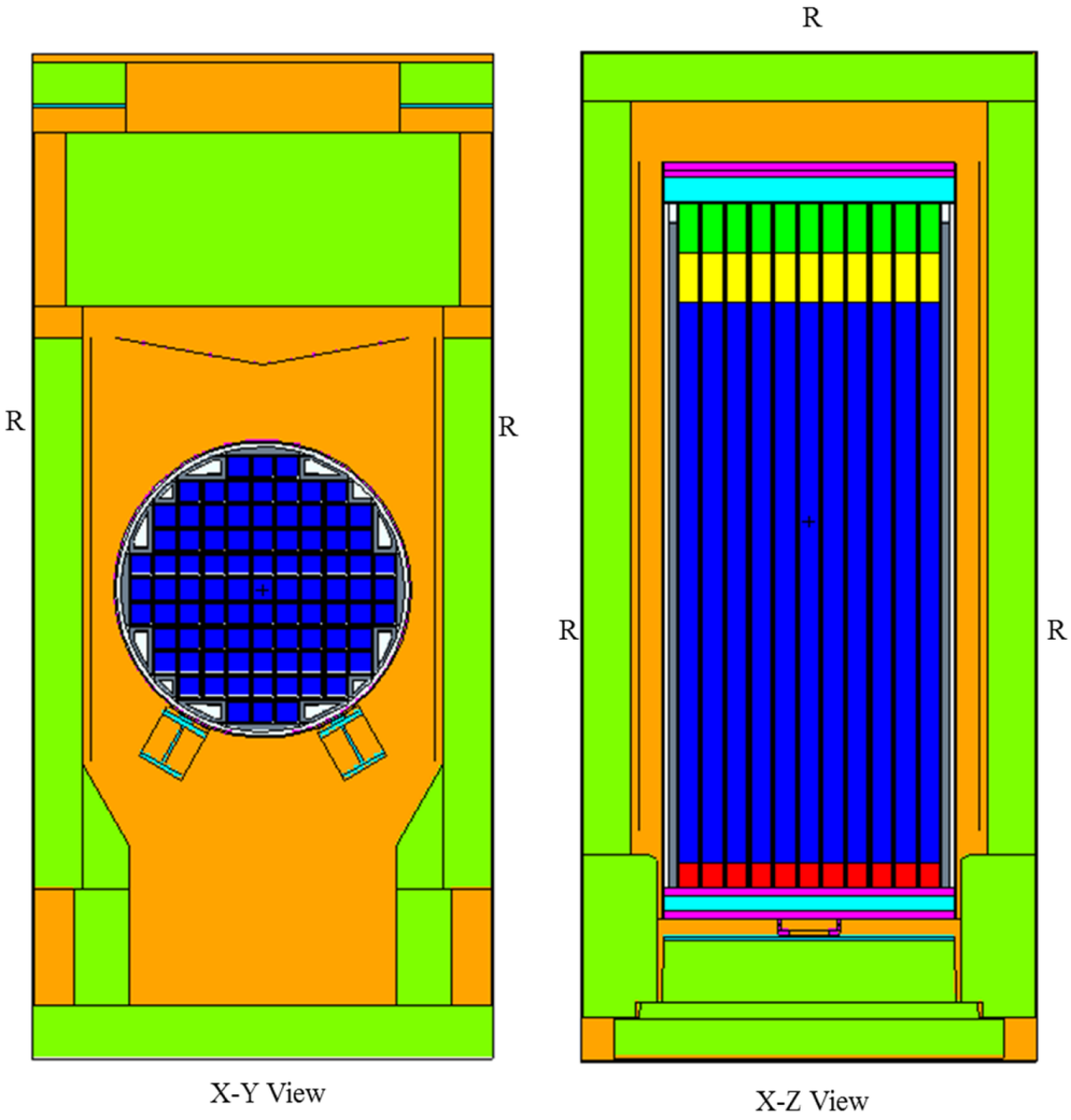

Reflective surfaces are denoted with an "R".

Figure 6-14
EOS-HSM MCNP Triple-Reflection Model

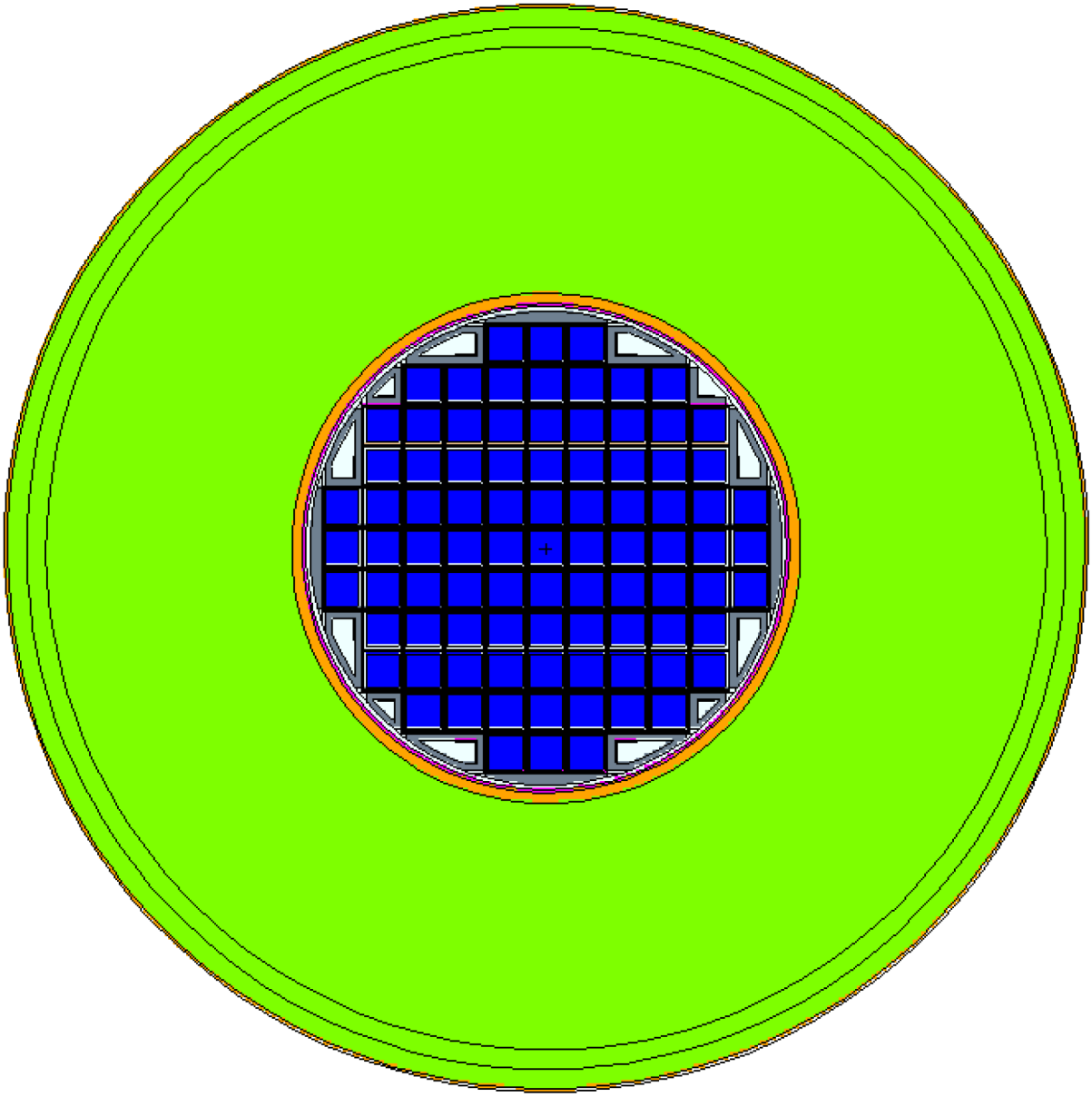

Figure 6-15
EOS-HSM MCNP Simplified Model for Grout Study

Proprietary Information on This Page
Withheld Pursuant to 10 CFR 2.390